Evaluation of LS-DYNA Soil Material Model 147

PUBLICATION NO. FHWA-HRT-04-094

NOVEMBER 2004

U.S. Department of Transportation
Federal Highway Administration

Research, Development, and Technology
Turner-Fairbank Highway Research Center
6300 Georgetown Pike
McLean, VA 22101-2296

Evaluation of LS-DYNA Soil Material Model 147

Report No. FHWA-HRT-04-094

November 2004

Federal Highway Administration
6300 Georgetown Pike
McLean, VA 22101-2296

Foreword

This report documents the evaluation of a soil material model that has been implemented into the dynamic finite element code, LS-DYNA, beginning with version 970. This material model was developed specifically to predict the dynamic performance of the foundation soil in which roadside safety structures are mounted when undergoing a collision by a motor vehicle. This model is applicable for all soil types when one surface is exposed if appropriate material coefficients are inserted. Default material coefficients for *National Cooperative Highway Research Program (NCHRP) Report 350, Strong Soil*, are stored in the model and can be accessed for use.

This report is one of two that completely documents this material model. The first report, *Manual for LS-DYNA Soil Material Model 147* (FHWA-HRT-04-095), completely documents this material model for the user. The second report, E*valuation of LS-DYNA Soil Material Model 147* (FHWA-HRT-04-094), completely documents the model's performance and the accuracy of the results. This performance evaluation was a collaboration between the model developer and the model evaluator. Regarding the model performance evaluation, the developer and evaluator were unable to come to a final agreement regarding the model's performance and accuracy. (The material coefficients for the default soil result in a soil foundation that may be stiffer than desired.) These disagreements are listed and thoroughly discussed in chapter 9 of the second report.

This report will be of interest to research engineers associated with the evaluation and crashworthy performance of roadside safety structures, particularly those engineers responsible for the prediction of the crash response of such structures when using the finite element code LS-DYNA.

Michael F. Trentacoste
Director, Office of Safety
Research and Development

Notice

Quality Assurance Statement

The Federal Highway Administration (FHWA) provides high-quality information to serve Government, industry, and the public in a manner that promotes public understanding. Standards and policies are used to ensure and maximize the quality, objectivity, utility, and integrity of its information. FHWA periodically reviews quality issues and adjusts its programs and processes to ensure continuous quality improvement.

Technical Report Documentation Page

1. Report No.	2. Government Accession No.	3. Recipient's Catalog No.
FHWA-HRT-04-094		

4. Title and Subtitle	5. Report Date
EVALUATION OF LS-DYNA SOIL MATERIAL MODEL 147	November 2004
	6. Performing Organization Code

7. Author(s)	8. Performing Organization Report No.
J.D. Reid and B.A. Coon, Midwest Roadside Safety Facility (MwRSF) B.A. Lewis, S.H. Sutherland, and Y.D. Murray, APTEK, Inc.	TRP-03-124-02

9. Performing Organization Name and Address	10. Work Unit No. (TRAIS)
MwRSF, University of Nebraska at Lincoln 1901 Y Street, Building C Lincoln, NE 68588-0601	
APTEK, Inc. 1257 Lake Plaza Drive Colorado Springs, CO 80906-3558	11. Contract or Grant No. DTFH61-98-C-00071

12. Sponsoring Agency's Name and Address	13. Type of Report and Period Covered
Federal Highway Administration 6300 Georgetown Pike McLean, VA 22101-2296	Final Report 09-28-1998 through 12-23-2003
	14. Sponsoring Agency's Code

15. Supplementary Notes

Contracting Officer's Technical Representative (COTR): Martin Hargrave, Federal Highway Administration, Turner-Fairbank Highway Research Center, 6300 Georgetown Pike, McLean, VA 22101-2296.

16. Abstract

This report documents the evaluation of a new soil material model intended for roadside safety simulation applications using the nonlinear finite element code LS-DYNA.

This report concentrates on the 18 parameters required for the soil material. The focus is on obtaining the appropriate parameter values (through testing or by analytical means), providing an engineering understanding of the parameters, and providing bounds for the effects of varying the parameters. Although extensive progress has been made on the soil material model, there is considerably more to be accomplished before the model would be effective in most roadside safety applications.

The companion manual to this report is:

Manual for LS-DYNA Soil Material Model 147 (FHWA-HRT-04-095)

17. Key Words	18. Distribution Statement
Soil material model, roadside safety simulation, LS-DYNA	No restrictions. This document is available to the public through the National Technical Information Service, Springfield, VA 22161.

19. Security Classif. (of this report)	20. Security Classif. (of this page)	21. No. of Pages	22. Price
Unclassified	Unclassified	85	

Form DOT F 1700.7 (8-72) **Reproduction of completed page authorized**

Preface

The goal of the work performed under this program, *Development of DYNA3D Analysis Tools for Roadside Safety Applications*, is to develop soil and wood material models, implement the models into the LS-DYNA finite element code,[1] and evaluate the performance of each model through correlations with available test data.

This work was performed under Federal Highway Administration (FHWA) Contract No. DTFH61-98-C-00071. The FHWA technical monitor was Martin Hargrave.

Two reports are available for each material model. One report is a user's manual, the second report is a performance evaluation. The user's manual, *Manual for LS-DYNA Soil Material Model 147*,[2] thoroughly documents the soil model theory, reviews the model input, and provides example problems for use as a learning tool. This report, *Evaluation of LS-DYNA Soil Material Model 147*, comprises the performance evaluation for the soil model. It documents LS-DYNA parametric studies and correlations with test data performed by a potential end user of the soil model, along with commentary from the developer. The reader is urged to review the user's manual before reading this evaluation report. A user's manual[3] and evaluation report[4] are also available for the wood model.

Development of the soil model was conducted by the prime contractor. The associated soil model evaluation effort to determine the model's performance and the accuracy of the results was a collaboration between the developer and evaluator. The developer created and partially evaluated the soil model. The evaluator performed a second, independent evaluation of the soil model, provided finite element meshes for the evaluation calculations, and provided shear test data for correlations with the model. Finally, the soil model was implemented into the LS-DYNA finite element code.

Regarding the second, independent evaluation of the soil model—the developer and evaluator were unable to come to a final agreement regarding several issues associated with the model's performance and accuracy. These issues are listed and thoroughly discussed in chapter 9 of this evaluation report. Throughout this report, the developer of the soil material model, is referred to as the *developer*. The evaluator, a potential end user of the soil material model, is referred to as the *user*. The user's calculations and final evaluation of the soil model are documented in chapters 1 through 8 of this evaluation report.

SI* (MODERN METRIC) CONVERSION FACTORS

APPROXIMATE CONVERSIONS TO SI UNITS

Symbol	When You Know	Multiply By	To Find	Symbol
		LENGTH		
in	inches	25.4	millimeters	mm
ft	feet	0.305	meters	m
yd	yards	0.914	meters	m
mi	miles	1.61	kilometers	km
		AREA		
in^2	square inches	645.2	square millimeters	mm^2
ft^2	square feet	0.093	square meters	m^2
yd^2	square yard	0.836	square meters	m^2
ac	acres	0.405	hectares	ha
mi^2	square miles	2.59	square kilometers	km^2
		VOLUME		
fl oz	fluid ounces	29.57	milliliters	mL
gal	gallons	3.785	liters	L
ft^3	cubic feet	0.028	cubic meters	m^3
yd^3	cubic yards	0.765	cubic meters	m^3
	NOTE: volumes greater than 1000 L shall be shown in m^3			
		MASS		
oz	ounces	28.35	grams	g
lb	pounds	0.454	kilograms	kg
T	short tons (2000 lb)	0.907	megagrams (or "metric ton")	Mg (or "t")
		TEMPERATURE (exact degrees)		
°F	Fahrenheit	5 (F-32)/9 or (F-32)/1.8	Celsius	°C
		ILLUMINATION		
fc	foot-candles	10.76	lux	lx
fl	foot-Lamberts	3.426	$candela/m^2$	cd/m^2
		FORCE and PRESSURE or STRESS		
lbf	poundforce	4.45	newtons	N
lbf/in^2	poundforce per square inch	6.89	kilopascals	kPa

APPROXIMATE CONVERSIONS FROM SI UNITS

Symbol	When You Know	Multiply By	To Find	Symbol
		LENGTH		
mm	millimeters	0.039	inches	in
m	meters	3.28	feet	ft
m	meters	1.09	yards	yd
km	kilometers	0.621	miles	mi
		AREA		
mm^2	square millimeters	0.0016	square inches	in^2
m^2	square meters	10.764	square feet	ft^2
m^2	square meters	1.195	square yards	yd^2
ha	hectares	2.47	acres	ac
km^2	square kilometers	0.386	square miles	mi^2
		VOLUME		
mL	milliliters	0.034	fluid ounces	fl oz
L	liters	0.264	gallons	gal
m^3	cubic meters	35.314	cubic feet	ft^3
m^3	cubic meters	1.307	cubic yards	yd^3
		MASS		
g	grams	0.035	ounces	oz
kg	kilograms	2.202	pounds	lb
Mg (or "t")	megagrams (or "metric ton")	1.103	short tons (2000 lb)	T
		TEMPERATURE (exact degrees)		
°C	Celsius	1.8C+32	Fahrenheit	°F
		ILLUMINATION		
lx	lux	0.0929	foot-candles	fc
cd/m^2	$candela/m^2$	0.2919	foot-Lamberts	fl
		FORCE and PRESSURE or STRESS		
N	newtons	0.225	poundforce	lbf
kPa	kilopascals	0.145	poundforce per square inch	lbf/in^2

*SI is the symbol for the International System of Units. Appropriate rounding should be made to comply with Section 4 of ASTM E380.
(Revised March 2003)

Table of Contents

List of Figures

List of Tables

CHAPTER 1. INTRODUCTION

The calculations and conclusions of chapters 2 through 8 of this report were written by a potential end user of the soil material model (herein referred to as the *user*). The commentary of chapter 9 was written by the developer of the soil material model (herein referred to as the *developer*). Chapter 9 reviews the soil model evaluation conducted by the user in chapters 2 through 8 and provides insight into issues raised by the user.

Several finite element models were developed by the user for the validation effort, including a direct shear test model, a modulus failure test model, and a shear failure test model. These models were intended to replicate soil testing performed at the user's facility. For several reasons, which are discussed throughout the report, this report concentrates on the direct shear test model and on providing an engineering-based understanding of the 18 parameters required for the soil material model.

Preliminary calculations generated during the validation effort are documented in appendixes A and B. These include initial experience with the soil model and verification of the results on different computer platforms.

All simulations performed by the user and reported in this document were performed using LS-DYNA, Version 970 Beta, Revision 1812, compiled by Livermore Software Technology Corporation (LSTC), June 7, 2002, on both Personal Computer (PC) Microsoft® Windows®- and Silicon Graphics, Inc. (SGI®) UNIX®-based machines.

CHAPTER 2. DIRECT SHEAR TESTING

To evaluate the soil material model, it is important that actual physical tests of the soil be simulated. This chapter describes one of the physical tests used for evaluating the soil model—the direct shear test. Two other tests—a soil modulus failure test and a soil shear failure test—are briefly described in appendix A and detailed by Coon.[5]

A large-scale direct shear testing device was developed at the user's facility.[6] This device was developed because it replicates one of the most common material tests performed on soil, except on a scale 10 times larger than the standard American Society for Testing and Materials (ASTM) specifications for direct shear testing. The larger scale was needed to accurately capture the direct shear behavior of National Cooperative Highway Research Program (NCHRP) Report 350 strong soil, which is the standard soil for roadside safety crash testing.[7] The 500-millimeter (mm)-diameter direct shear testing device is shown in figure 1 and detailed by Coon, et al.[6]

Nicholson, through testing, developed a general curve depicting soil performance during direct shear testing (see figure 2).[8] Results from direct shear testing performed on NCHRP 350 strong soil with an 18.5-kilopascal (kPa) overburden, using the user's large-scale direct shear testing device, are shown in figure 3. Physical test results from NCHRP 350 strong soil compared well with prior laboratory data.

Figure 1. Large-scale direct shear testing device.

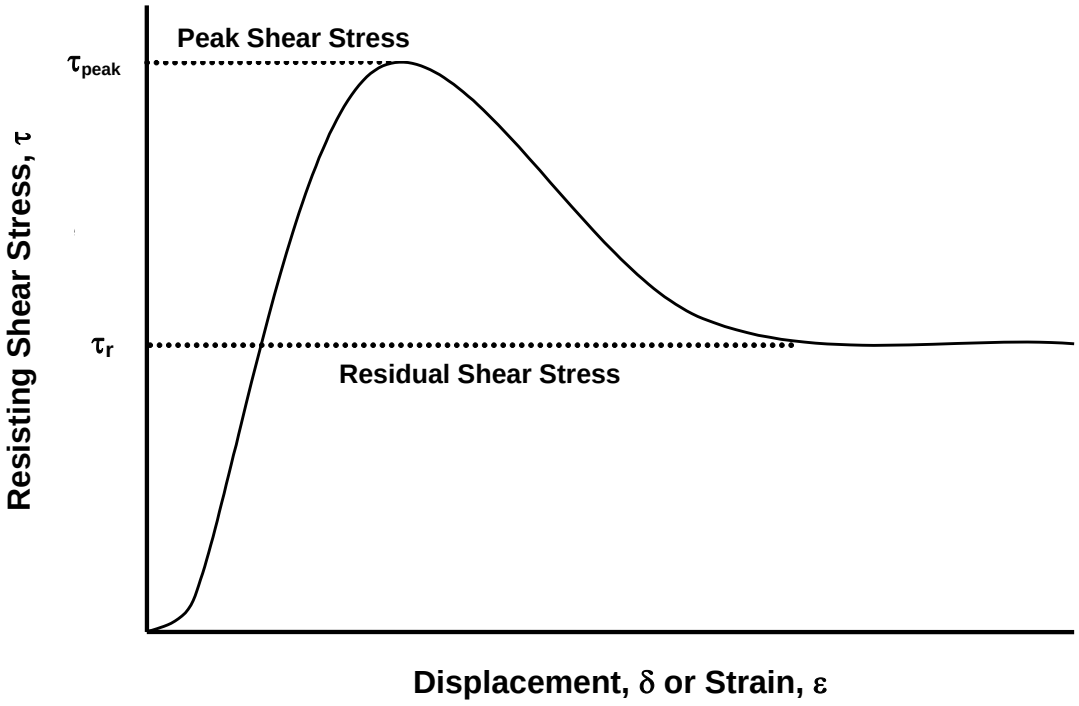

Figure 2. General direct shear testing performance.[8]

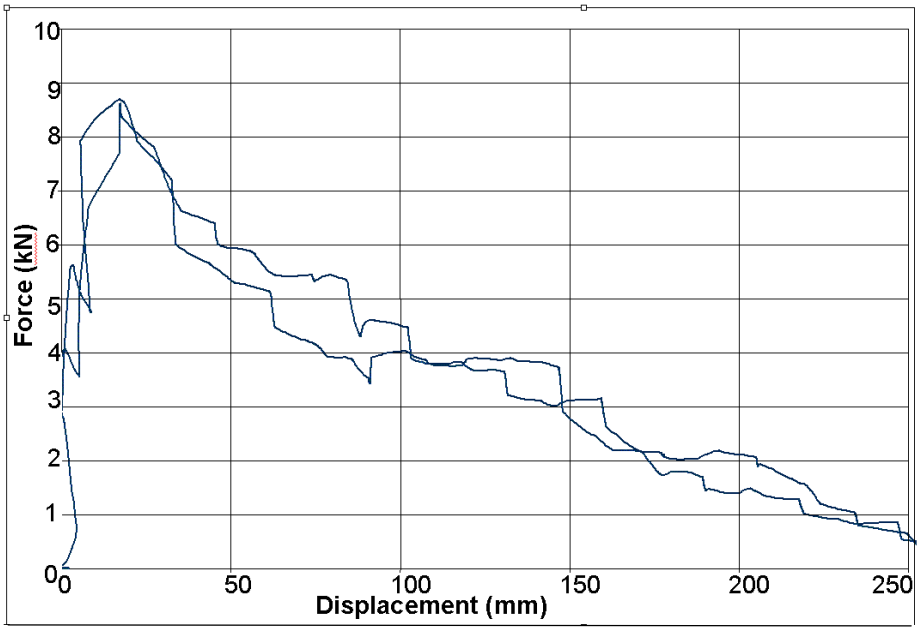

Figure 3. Results of two direct shear tests (performed at the user's facility).

CHAPTER 3. BASELINE MODEL: DIRECT SHEAR TEST SIMULATION

In this chapter, a baseline model of the direct shear test is established in order to investigate the effects of the various parameters associated with the soil model. A finite element model using 10,600 elements was developed based on the large-scale direct shear testing device (see figure 4). This model included solid rigid elements to model the steel, since no deformation had been seen during physical testing, and solid elements to implement the Federal Highway Administration (FHWA) soil model, material type 147.

An overburden pressure of 18.5 kPa was applied and dynamic relaxation was implemented before the soil was sheared in the finite element model. A prescribed motion condition of 1 millimeter per millisecond (mm/ms) was applied to the lower containing cylinder in the device, similar to the quasi-static testing motion condition. Loads and displacements were measured so that simulation results could be directly compared to the physical test results.

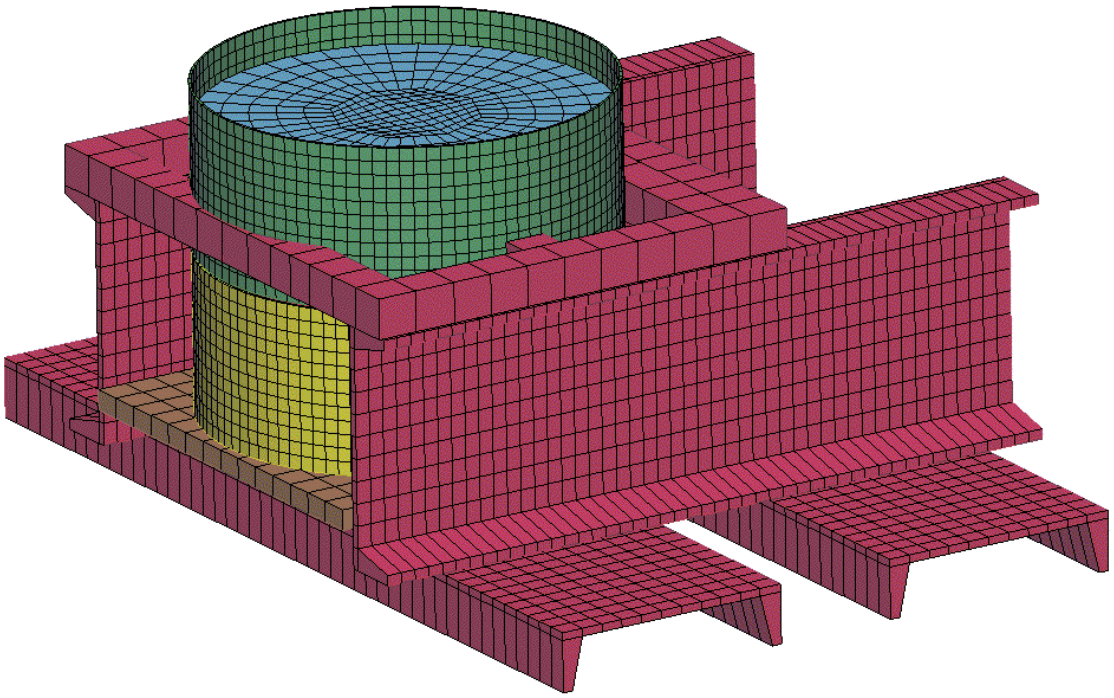

Figure 4. Finite element model of large-scale direct shear test.

BASELINE PARAMETERS

Initial parameters for material type 147 were selected from three LS-DYNA models provided by the developer. These models included two triaxial compression tests (cylin.k and txc3-4pr0c.k) and a hydrostatic tension test (hydten1.k). The initial parameters implemented in the developer's models and the comparison to the baseline model used in the parameter study are shown in table 1. The material input parameters in LS-DYNA keyword format are shown in table 2.

E-mail correspondence from the developer later recommended values for the shear modulus, *G*, and the bulk modulus, *K*, as 1.3 megapascals (MPa) and 3.25 MPa, respectively. Because of the lateness of obtaining these values, these changes were not reflected in the material parameter study of chapter 4. However, chapter 5 of this report, "Developer-Recommended Parameters," investigates these recommended values.

Table 1. Developer's and baseline material parameters.

	Material Parameter					
Input Deck	RO	Nplot	Spgrav	Rhowat	V_n	Gammar
cylin.k	2.350E-6	3	2.79	1.0E-6	1.1	0.0
txc3-4pr0c.k	2.350E-6	3	2.79	1.0E-6	1.1	0.0
hydten1.k	2.350E-6	3	2.79	1.0E-6	1.1	0.0
Baseline	2.350E-6	3	2.79	1.0E-6	1.1	0.0
Input Deck	Itermax	K	G	Phimax	Ahyp	Coh
cylin.k	10	0.465	0.186	1.1	1.0E-7	1.0E-6
txc3-4pr0c.k	10	0.465	0.186	1.1	1.0E-7	1.0E-6
hydten1.k	10	0.465	0.186	1.1	1.0E-7	6.2E-6
Baseline	10	0.465	0.186	1.1	1.0E-7	6.2E-6
Input Deck	Eccen	A_n	E_t	Mcont	Pwd1	PwKsk
cylin.k	0.7	0.4	10	0.034	0.0	0.0
txc3-4pr0c.k	0.7	0.0	10	0.034	0.0	0.0
hydten1.k	0.7	0.0	0	0.034	0.0	0.0
Baseline	0.7	0.0	0	0.034	0.0	0.0
Input Deck	Pwd2	Phires	Dint	Vdfm	Damlev	Epsmax
cylin.k	0.0	1.0E-3	5.0E-5	6.0E-7	0.98	1.00
txc3-4pr0c.k	0.0	0.0E-0	5.0E-5	1.0E-9	0.80	0.03
hydten1.k	0.0	0.0E-0	2.5E-3	5.0E-0	1.00	1.00
Baseline	0.0	0.0E-0	2.5E-3	5.0E-0	1.00	1.00

Table 2. LS-DYNA format: Baseline values for parameter study, model R3.

```
$$$$$$$$$$$$$$$$$$$$$$$$$$$$$$$$$$$$$$$$$$$$$$$$$$$$$$$$$$$$$$$$$$$$$$$$$$$$$$$$
$
$$$$ FHWA Soil Material
$
$$$$$$$$$$$$$$$$$$$$$$$$$$$$$$$$$$$$$$$$$$$$$$$$$$$$$$$$$$$$$$$$$$$$$$$$$$$$$$$$
$
$...>....1....>....2....>....3....>....4....>....5....>....6....>....7....>....8
$
$$$$ Material 147 Nebraska soil
$
*MAT_FHWA_SOIL
$      mid        ro     NPLOT    SPGRAV    RHOWAT        VN    GAMMAR   ITERMAX
         1  2.350E-6         3      2.79    1.0E-6       1.1       0.0        10
$        K         G    PHIMAX      AHYP       COH    ECCEN        AN        ET
  0.465000  0.186000       1.1    1.0E-7    6.2E-6       0.7       0.0       0.0
$    MCONT      PWD1    PWKSK      PWD2    PHIRES      DINT      VDFM    DAMLEV
     0.034      0.00       0.0       0.0       0.0  0.00250      5.00       1.0
$   Epsmax
       1.0
$
```

BASELINE RESULTS

Deformation of the baseline model results (without the frame structure) is shown in figure 5, the force to perform the direct shear simulation is shown in figure 6, and the internal energy absorbed by the soil during the simulation is shown in figure 7. Unfortunately, it appears that the soil model is only useable in this configuration for about 25 mm of deformation (as shown in figure 6). The force builds up nicely and peaks at 718 kilonewtons (kN) at 18.2 mm of displacement. The soil begins to soften, as it should, until it reaches the valley at 24.6 mm of displacement, with a corresponding force of 385 kN. After that time, the force begins to rise, which never occurs in physical tests. The force should either maintain a relative constant value or begin to drop, as previously shown in figures 2 and 3.

One reason for the rise in forces after 25 mm of displacement is because of the high damage level specification. However, if lower values of damage are used, the model becomes unstable and the code terminates. This will be discussed further in chapter 5. For the parameter study in this report (chapter 4), the main results of the comparison will be the peak force and the valley force, and their corresponding displacements and internal energy absorbed by the soil.

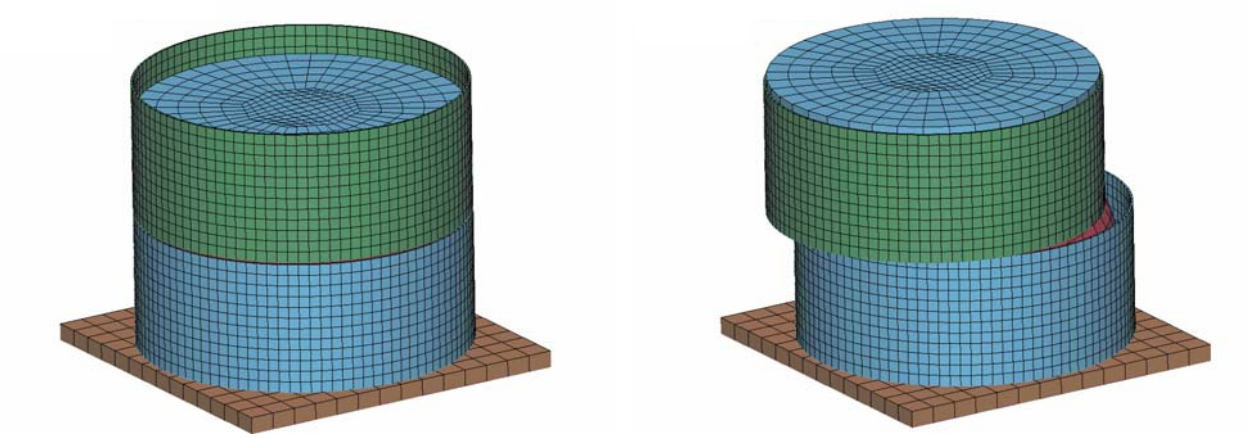

(a) 0 ms (b) 49.992 ms

Figure 5. Soil displacement: Baseline model.

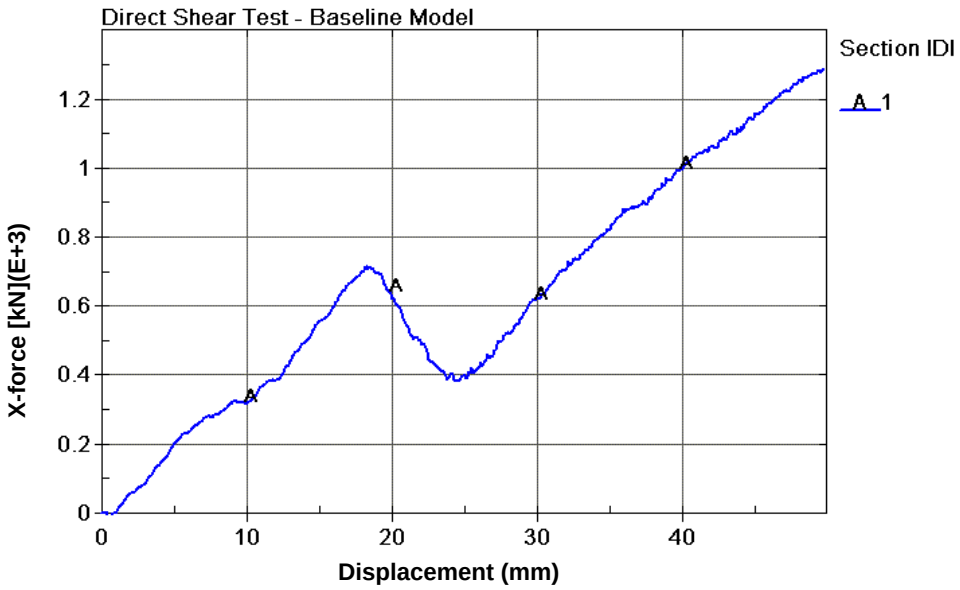

Figure 6. Direct shear force: Baseline model.

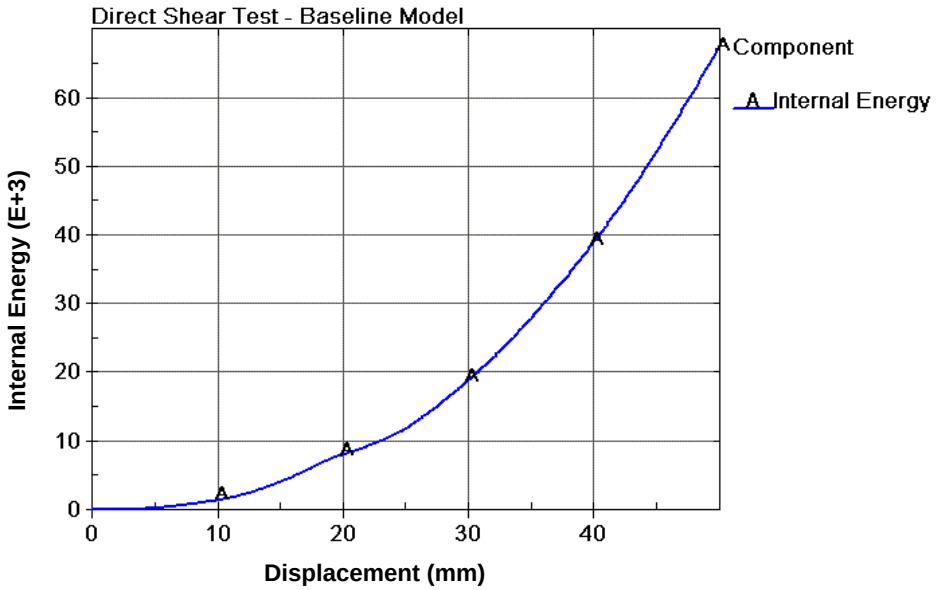

Figure 7. Direct shear soil internal energy: Baseline model.

CHAPTER 4. MATERIAL INPUT PARAMETER STUDY

One of the most difficult tasks associated with finite element modeling is the selection of appropriate material properties to accurately represent physical behavior. In many cases, this has led to the arbitrary tweaking of models by matching simulation results to a known physical test, sometimes without regard to the reasonableness of the material input variables.

Of course, it is desirable to be able to determine material input variables directly through physical testing. In order to determine the appropriate material input variables, the physical implications must be completely understood. Thus, a complete discussion of the variables and, when applicable, their physical meaning follows.

Many of the developer's initial soil parameters were based on triaxial testing performed by the U.S. Army Corps of Engineers (USACE) at the Waterways Experiment Station (WES). These data are contained in the Material Property Query (MPQ) database and are available only to documented government contractors.[9]

The objectives of this chapter are to: (1) provide an understanding of the soil parameters, (2) provide guidelines for appropriate parameter values, and (3) determine recommended parameter values for NCHRP 350 soil used at the user's facility. The following discussions attempt to provide an engineering interpretation of the material such that appropriate parameter values can be determined more readily.

SOIL DENSITY, RHO

RHO is the density of the soil material. It has the units of mass/volume (for this case, kilograms per cubic millimeter (kg/mm^3)). The developer's initial models included a density of 2.35E-6 kg/mm^3, almost the maximum dry density of the soil (ρ_{max} = 2.37E-6 kg/mm^3) found using a Modified Procter test. The soil tested by USACE had a density of ρ_{max} = 2.27E-6 kg/mm^3, which is more appropriate for densely compacted aggregate.

NCHRP 350 strong soil routinely has densities of about 2.114E-6 kg/mm^3. However, densities between 2.082E-6 kg/mm^3 and 2.242E-6 kg/mm^3 are reasonable.

Mass Verification

From the developer's hydraulic tension test file, hydten.k, a 1-mm cube of soil material was modeled. Calculating the mass of the sample from the density and volume:

$$M = \rho V = \left(2.35\text{E}-6\,\text{kg}/\text{mm}^3\right)\left(1.0\,\text{mm}^3\right) = 2.35\text{E}-6\ \text{kg} \qquad (1)$$

This was verified in the D3HSP output file from LS-DYNA. The FHWA soil model produces the correct mass from an inputted density. It is critical to verify the behavior of the density function of the soil model because significant inertial effects involving the soil-post interaction have been documented.[5]

PLOTTING OPTIONS, NPLOT

Nplot allows the plotting of information concerning the soil model. This includes information on the effective strain, damage criterion threshold, isentropic damage, current damage criterion, and current friction angle. The Nplot options are as follows:

1. Effective strain.
2. Damage criterion threshold.
3. Isentropic damage parameter, (diso).
4. Current damage criterion.
5. Not implemented.
6. Current friction angle.

For post-processing using LS-POST, the value specified in Nplot is stored as the Plastic Strain variable for plotting the fringe component stresses. When post-processing, the information stored for plastic strain will not contain the plastic strain data, but rather the data specified under Plotting Options, Nplot.

SPECIFIC GRAVITY, SPGRAV

The specific gravity of soil solids, usually designated by G_s, is the ratio of the soil solids to the density of water. While it is possible to have a range of values from 2.2 to 3.5, most soils have a specific gravity from 2.60 to 2.80. Any values outside of this latter range should be viewed skeptically, and the soil should be retested to verify the value. Where specific values are not available, the following can be assumed for local soils:[10]

Sand and gravels: $G_s = 2.65$
Silts and clay: $G_s = 2.78$

It should be noted that the specific gravity, G_s, is not the bulk specific gravity, G_{blk}, of the material, but rather the specific gravity of only the soil solids. This is to say that air voids internal to and between soil particles are not considered when calculating the specific gravity. Since NCHRP 350 strong soil is designated as a gravel, a specific gravity of $G_s = 2.65$ is appropriate. However, laboratory testing should be performed to accurately identify the exact specific gravity associated with the Nebraska crushed limestone used at the user's facility.

In the FHWA soil model, the specific gravity of the soil is used to calculate the porosity. Soil porosity is the ratio of the total volume of voids, V_v, to the total volume, V_t, of a sediment.

A discrepancy exists in the calculation of the Spgrav input variable as it is read by LS-DYNA. In the baseline model, a value of Spgrav = 2.79 was used. This value came from the USACE WES testing. In the D3HSP output file, produced by LS-DYNA, SPGRAV was reported as 0.1854, a variation of a factor of 15. These values are shown in bold in Table 3. The other values of the input deck matched exactly, as shown in table 3. The D3HSP output from LS-DYNA is shown in table 4. This discrepancy was observed through the normal verification of input decks with output parameters.

The ramifications of this discrepancy are not fully understood. It is impossible to determine whether the material model is reading the correct values and merely outputting incorrect values only to the D3HSP file or whether the material model is, in fact, altering Spgrav incorrectly. This can only be verified through a careful examination of the source code.

Table 3. Comparison between LS-DYNA input deck and D3HSP output reveals the Spgrav discrepancy (shown in bold).

Parameter	RO	Nplot	Spgrav	Rhowat	V_n	Gammar
Input Deck	2.350E-6	3	**2.79**	1.0E-6	1.1	0.0
D3HSP File	2.350E-6	3	**0.1854**	1.0E-6	1.1	0.0
Parameter	Itermax	K	G	Phimax	Ahyp	Coh
Input Deck	10	0.465	0.186	1.1	1.0E-7	6.2E-6
D3HSP File	10	0.465	0.186	1.1	1.0E-7	6.2E-6
Parameter	Eccen	A_n	E_t	Mcont	Pwd1	PwKsk
Input Deck	0.7	0.0	0.0	0.034	0.0	0.0
D3HSP File	0.7	0.0	0.0	0.034	0.0	0.0
Parameter	Pwd2	Phires	Dint	Vdfm	Damlev	Epsmax
Input Deck	0.0	0.0E-0	2.5E-3	5.0	1.00	1.00
D3HSP File	0.0	0.0E-0	2.5E-3	5.0	1.00	1.00

Table 4. D3HSP output file (truncated).

```
SOIL

 Part ID .......................   1
    material type ............... 147
    equation-of-state type .....   0
    hourglass type .............   1
    bulk viscosity type ........   1

  den ............................... = 2.35000E-06
  hourglass coefficient ............. = 1.00000E-01
  quadratic bulk viscosity ......... = 1.50000E+00
  linear bulk viscosity ............. = 6.00000E-02
  element type ...................... = 0
     eq.0: 8-node solid element
     eq.1: 2-node beam/truss element
     eq.2: 4-node membrane/shell element
     eq.3: 8-node thick shell element

  flag for bulk viscosity in shells  = 0
  flag for RBDOUT/MATSUM output .... = 0
     eq.0: RBDOUT and MATSUM
     eq.1: RBDOUT only
     eq.2: MATSUM only
     eq.3: no output

  static coefficient of friction ... = 0.00000E+00
  kinetic coefficient of friction .. = 0.00000E+00
  exponential decay coefficient .... = 0.00000E+00
  viscous friction coefficient ..... = 0.00000E+00
  optional contact thickness ....... = 0.00000E+00
  optional thickness scale factor .. = 0.00000E+00
  local penalty scale factor ....... = 0.00000E+00
  flag for adaptive remeshing ...... = 0
     eq.0: inactive
     eq.1: h-adaptive only
     eq.2: r-adaptive only

  rayleigh damping coefficient ..... = 0.00000E+00
  nplot ............................. = 3.0000E+00
  spgrav ............................ = 1.8540E-01
  rhowat ............................ = 1.0000E-06
  v_n ............................... = 1.1000E+00
  gammar ............................ = 0.0000E+00
  itermax ........................... = 1.0000E+01
  bulk modulus ...................... = 4.6500E-01
  shear modulus ..................... = 1.8600E-01
  phimax ............................ = 1.1000E+00
  ahyp .............................. = 1.0000E-07
  coh ............................... = 6.2000E-06
  eccen ............................. = 7.0000E-01
  a_n ............................... = 0.0000E+00
  e_t ............................... = 0.0000E+00
  mcont ............................. = 3.4000E-02
  pwd1 .............................. = 0.0000E+00
  pwksk ............................. = 0.0000E+00
  pwd2 .............................. = 0.0000E+00
  phires ............................ = 0.0000E+00
  dint .............................. = 2.5000E-03
  vdfm .............................. = 5.0000E+00
  damlev ............................ = 1.0000E+00
  epsmax ............................ = 1.0000E+00
```

DENSITY OF WATER, RHOWAT

RHOWAT is the density of water (1.0 x 10^{-6} kg/mm^3 (62.4 lb/ft^3)). This is used to determine the air void strain when calculating pore-water effects.

VISCOSITY PARAMETERS, V_n AND GAMMAR

GAMMAR (γ_r) and V_n are viscosity parameters used to develop the strain-rate-enhanced strength of the material model. The algorithm interpolates between the elastic trial stress (beyond the yield surface) and the inviscid stress (stresses where the material viscosity effects are so small that they can be neglected). The inviscid stresses are on the yield surface. In equation form, this is written:

$$\bar{\sigma}_{\mathrm{vp}} = (1-\zeta)\bar{\sigma} + \bar{\sigma}_{\mathrm{trial}} \tag{2}$$

where:

$$\zeta = \frac{\eta}{\Delta t + \eta} \tag{3}$$

and

$$\eta = \left(\frac{\gamma_r}{\dot{\varepsilon}}\right)^{\frac{V_n - 1}{V_n}} \tag{4}$$

Setting GAMMAR to 0.0 eliminates any strain-rate-enhanced strength effects, regardless of any values that remain for V_n. Additional work must be performed to determine the appropriate values for these strain-rate parameters.

BULK MODULUS, *K*

The bulk modulus, *K*, is an elastic constant that reflects the resistance of the material to an overall gain or loss of volume under conditions of hydrostatic stress. If the hydrostatic stress increases, then the volume will decrease and the volume change will be negative. If the hydrostatic stress decreases, then the volume will increase.

The relationship between the elastic modulus, *E*, and the bulk modulus, *K*, is:

$$E = 3K(1-2\nu) \tag{5}$$

The determination of the elastic modulus, *E*, is difficult because volume changes in the soil require the precise determination of pore pressures. Moreover, the value of Poisson's ratio may influence the results. Poisson's ratio, ν, has the following approximate values in soils:[11]

ν = 0.5 (saturated impervious soils)
ν = 0.25 (pervious coarse materials)

For NCHRP 350 strong soil, it is appropriate to use ν = 0.25. On this basis, the equation above simplifies to:

$$E = 1.5K \tag{6}$$

Rewritten,

$$K = \frac{2E}{3} \tag{7}$$

In 1975, Penman performed tests on gravel, finding an elastic modulus of *E* = 15.8 MPa.[12] Penman also found a Poisson's ratio of ν = 0.27. This corresponds well with known data as shown above. This would imply a bulk modulus of *K* = 10.5 MPa. The initial developer's models used a value of *K* = 465 MPa. As mentioned previously, the developer's revised suggested value for the bulk modulus was *K* = 3.25 MPa.

SHEAR MODULUS, *G*

Just as the modulus of elasticity, *E*, is a measure of the relationship of the stress to the strain below the proportional limit, the shear modulus of elasticity, *G*, relates shear stress to shear strain. The shear modulus is also referred to as one of the two Lamé constants, *G* and λ. Using conventional engineering mechanics, the shear modulus can be expressed as a function of the modulus of elasticity, *E*, and Poisson's ratio, ν:

$$G = \frac{E}{2(1+\nu)} \tag{8}$$

Using the values found by Penman,[12] a shear modulus of *G* = 6.22 MPa is found. The initial developer's models used a value of *G* = 186 MPa. As mentioned previously, the developer's revised suggested value for the shear modulus was 1.3 MPa.

Poisson's Ratio

In 1987, Trautmann and Kulhawy found general ranges of Poisson's ratio for granular soils.[13] These values are shown in table 5. It is important to ensure that appropriate values of Poisson's ratio are used in the FHWA soil material model.

Table 5. General range of Poisson's ratio for granular soils.

Soil Type	Range of Poisson's Ratio
Loose Sand	0.20-0.40
Medium Dense Sand	0.25-0.40
Dense Sand	0.30-0.45
Silty Sand	0.20-0.40
Sand and Gravel	0.15-0.35

NCHRP 350 strong soil is most similar to the "sand and gravel" listed in table 5. It is believed that the most reasonable values would lie at approximately ν = 0.25, as noted previously.

The bulk modulus, *K*; the shear modulus, *G*; Poisson's ratio, ν; and the modulus of elasticity, *E*, are all interrelated. These relationships can be used to determine the value of Poisson's ratio, υ, that the developer used in both the initial models and the subsequent recommended values. This is accomplished by solving for the elastic modulus, *E*, and combining equations 5 and 8 as follows:

$$2G(1+\nu)=3K(1-\nu) \tag{9}$$

Rearranging, it is seen that:

$$G=K\frac{3(1-2\nu)}{2(1+\nu)} \tag{10}$$

Substituting with υ = 0.25 yields:

$$G=K\frac{3(1-2(0.25))}{2(1+0.25)} \tag{11}$$

Solving through, this yields:

$$G = K\frac{3(1-0.50)}{2(1.25)}$$

$$G = K\frac{1.50}{2.50} \tag{12}$$

$$G = 0.6K$$

Equation 9 can also be solved for Poisson's ratio as a function of the bulk and shear modulus. For the developer's initial values of K = 465 MPa and G = 186 MPa, a Poisson's ratio of 0.32 can be calculated. Similarly, with the developer's subsequent recommendations via email, with K = 3.25 MPa and G = 1.3 MPa, a Poisson's ratio of 0.32 can also be calculated. This is not an unreasonable value.

It is important that the end user understand the relationship between the shear modulus and the bulk modulus. In order to maintain consistency with the laws of physics and conventional engineering mechanics, reasonable and appropriate values of Poisson's ratio must exist.

Appropriate Values for Bulk and Shear Moduli

It is critical to associate material model parameters with physical test results that can be performed in the field. The modulus of elasticity has been correlated to the standard penetration number, N, and also the cone penetration resistance, q_c, by various investigators.[14] These values and their corresponding bulk and shear moduli are shown in table 6.

Table 6. General range of bulk and shear moduli for υ = 0.25.

Soil Type	Modulus of Elasticity, *E* (MPa)	Bulk Modulus, *K* (MPa)	Shear Modulus, *G* (MPa)
Loose Sand	10.35-24.15	6.90-16.10	4.14-9.66
Medium Dense Sand	10.35-17.25	6.90-11.50	4.14-6.90
Dense Sand	17.25-27.60	11.50-18.40	6.90-11.04
Silty Sand	34.50-55.20	23.00-36.80	13.80-22.08
Sand and Gravel	69.00-172.50	46.00-115.00	27.60-69.00

Nuclear densometer readings from field testing of roadbed materials have given values for the modulus of elasticity between 26.2 MPa and 193 MPa.[15] These values correspond well to values found by Das [10] and do not seem unreasonable compared to Penman.[12]

With these values, it would seem that selecting the median value for a "sand and gravel" soil would be appropriate. Median values would be K = 80.5 MPa and G = 48.3 MPa for the bulk and shear moduli, respectively. However, these values produced too stiff of a soil response in the direct shear test simulation, relative to physical testing. Using Penman's recommended values of 10.5 MPa and 6.22 MPa for the bulk and shear moduli, respectively, the direct shear test simulation still produced an unreasonably stiff soil response. When the bulk and shear moduli were adjusted to the developer's recommended values of 3.25 MPa and 1.3 MPa, respectively, the model appeared to provide a more reasonable prediction of soil stiffness.

ANGLE OF INTERNAL FRICTION, PHIMAX, AND COHESION, COH

In 1900, Mohr presented a theory for rupture in materials that contended that a material fails because of a critical combination of normal stress and shearing stress, not from either maximum normal or shear stress alone.[16] For most soil mechanics problems, it is sufficient to approximate the shear stress on the failure plane as a linear function of the normal stress.[17] Hence, the linear function can be written as:

$$\tau_{\phi} = c + \sigma \tan\phi \tag{13}$$

where:

c = Cohesion
σ = Normal stress
ϕ = Angle of internal friction

The preceding relationship is called the Mohr-Coulomb failure criteria. Values for cohesion, *c*, and the angle of internal friction, ϕ, can be determined through direct shear testing or triaxial compression tests. A graphical representation of the Mohr-Coulomb failure criteria is shown in figure 8.

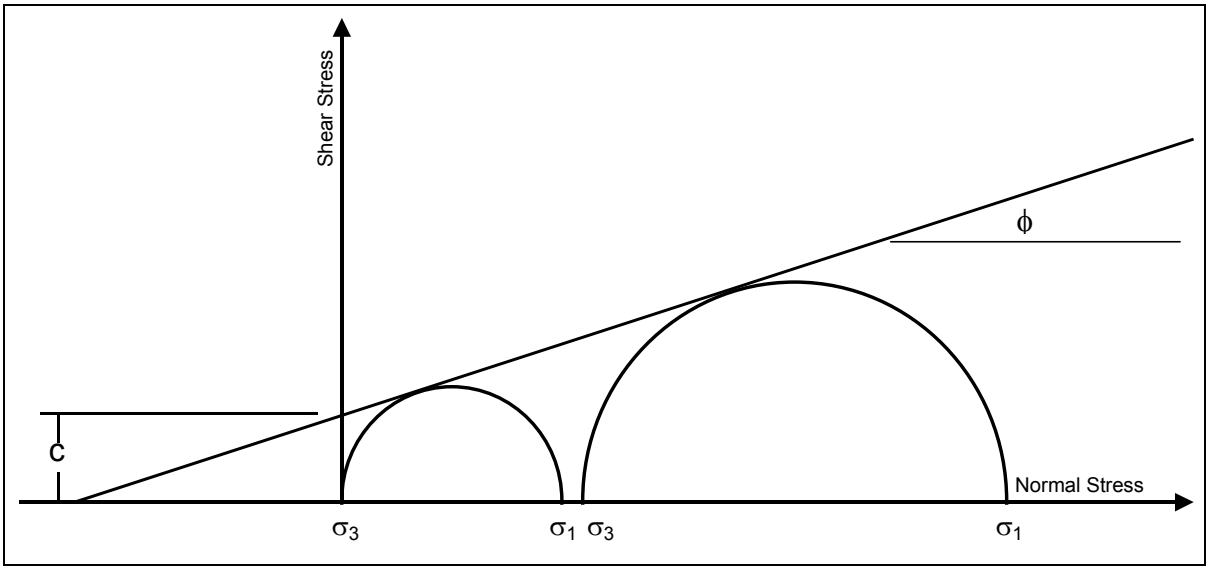

Figure 8. Graphical representation of the Mohr-Coulomb failure criteria.

Cohesion

When soil is removed from a bed of dry or completely immersed sand, the material at the sides of the excavation slides toward the bottom. This behavior indicates the complete absence of a bond between the individual sand particles. The sliding material does not come to rest until the angle of inclination of the slopes becomes equal to a certain angle known as the angle of repose (the angle of friction, which is the angle of

repose in a cohesionless material such as sand).[18] The angle of repose of dry sand is independent of the height of the slope.

On the other hand, a trench 6.1 to 9.1 meters (m) (20 to 30 feet (ft)) deep with unsupported vertical sides can be excavated in stiff plastic clay. This fact indicates the existence of a firm bond between the clay particles. However, as soon as the depth of the trench exceeds a certain value, dependant on the intensity of the bond between the clay particles, the sides of the trench fail and the slope of the debris that covers the bottom of the cut after failure is far from vertical. The bond between the soil particles is called *cohesion*. No definite angle of repose can be assigned to a soil with cohesion, because the steepest slope at which such a soil can stand decreases with the increasing height of the slope. However, even sand, if it is moist, has *apparent cohesion* because of matrix suction between the grains of sand.

Coulomb's paper (1773) quoted Musschenbroek's idea (1729) that for construction materials, tensile strength (adhesion) is about equal to shear strength with no overburden (cohesion).[19] Coulomb found that, for physical tests on 1290-square millimeter (mm^2) (2-square inch ($inch^2$)) cross section specimens of limestone, the tensile failure load was 1.91 kN (430 pounds force (lbf)) and the shear failure load was 1.96 kN (440 lbf). These and other tests on brick and wood confirmed Musschenbroek's idea. Hence, if adhesion is known to be small or negligible for some material, then the cohesion of that material must also be taken to be zero.

For Coulomb, the fracture of intact bodies of undisturbed soil and rock involved both friction and cohesion; the flow of ground that has been broken up and is newly disturbed does not involve cohesion. Placement of fill behind a wall involves breaking up ground with picks, shoveling soil or broken rock into barrows, wheeling it to the site, and tipping it behind the wall. Coulomb states three times in his design calculations for such fill that there is no adhesion in newly disturbed soil.

For soil consistent with crushed limestone, such as NCHRP 350 strong soil, cohesion is, by definition, zero, because it is a cohesionless soil. This can be verified by relating the adhesion of the soil to the cohesion—tensile tests on the strong soil would show that there is no adhesion since there is no bond between the individual pieces of aggregate.

Rather than introduce an apparent cohesion of soil that is itself a function of strain, it is better to characterize peak strength as the sum of the critical state angle of repose plus a dilation angle. This interlocking strain rate depends on effective pressure and relative density.[20]

However, direct shear testing shows the presence of some cohesion—the failure envelope has a positive value as it passes through the pressure axis. It is noted, however, that the strong soil has no cohesion. This is caused by the dilation of the soil specimen during testing. The work caused by this effect, designated as *interlocking* by Taylor, is a distinctly different phenomenon than the work caused by friction.[21] While

interlocking can be treated, in a general sense, as particle cohesion, it is important to differentiate between the two physical phenomena.

The concept of Taylor's aggregate interlock explains how soil can exhibit apparent cohesion as it flows, exhibit apparent cohesion at peak strength, and still satisfy Coulomb's law. From a mechanics standpoint, it would be best to represent the material with aggregate interlock; from a simplicity standpoint, it may be best to have artificial cohesion to represent the aggregate interlock.

Cohesion in the soil model was varied in a parameter study to determine the appropriate values. The results are provided in table 7 and figure 9. As a reminder, the results throughout this chapter are limited to the point where the force required to shear the soil reached a minimum force (referred to as "Valley" in the tables). Simulations continued after that point; however, forces began to rise unrealistically (as discussed in chapter 3).

It did not appear that significant differences existed between "small" (i.e., any value less than 6.2e-7 gigapascals (GPa)) and smaller values, as shown in table 7. The model successfully ran even with cohesion set to zero; however, the plasticity routines were limited by the parameter Itermax, the maximum number of iterations that allow the plasticity algorithm to converge.

Table 7. Cohesion parameter study.

Test Identifier	Angle of Internal Friction, ϕ	Cohesion, Coh (GPa)	Itermax	CPU* Time (seconds (s))	Peak			Valley		
					Disp (mm)	Force (kN)	Internal Energy	Disp (mm)	Force (kN)	Internal Energy
T4	0.3°	+6.2E-7	10	2,183	18.8	805	8529	24.5	473	13,044
T5	0.3°	+6.2E-6	10	2,177	18.8	805	8529	24.5	473	13,044
T33	63°	+6.2E-5	10	1,962	19.4	741	7257	25.7	395	11,907
Baseline	63°	+6.2E-6	10	2,644	18.2	718	6795	24.6	385	11,450
T6	63°	+6.2E-7	10	3,608	17.1	689	6358	23.9	387	11,289
T7	63°	+6.2E-8	10	4,038	17.0	708	6450	23.4	389	11,049
T8	63°	+6.2E-9	10	4,018	16.9	703	6335	24.4	396	11,975
T9	63°	+6.2E-10	10	3,775	16.9	708	6350	23.3	376	10,865
T10	63°	+0.0E+0	10	3,727	16.9	704	6351	24.0	393	11,609
T11	63°	+0.0E+0	50	12,717	16.7	685	5972	24.0	378	11,241
T12	63°	+0.0E+0	100	21,647	17.1	691	6205	24.1	382	11,286

* All CPU (central processing unit) times reported in this report are for simulation runs of approximately 30 ms on an SGI® Origin® 300, R14000™ 500 megahertz (MHz).

1 degree = 0.1592 radians

As shown in figure 9, decreasing the cohesion past 6.2E-7 GPa did not appear to have any significant effects. However, at values above this, the curve was shifted to the right, indicating a delay in the initial yielding of the soil material. This agrees with conventional soil mechanics. The cohesion of the soil would delay the failure caused by chemical attraction at the molecular level.

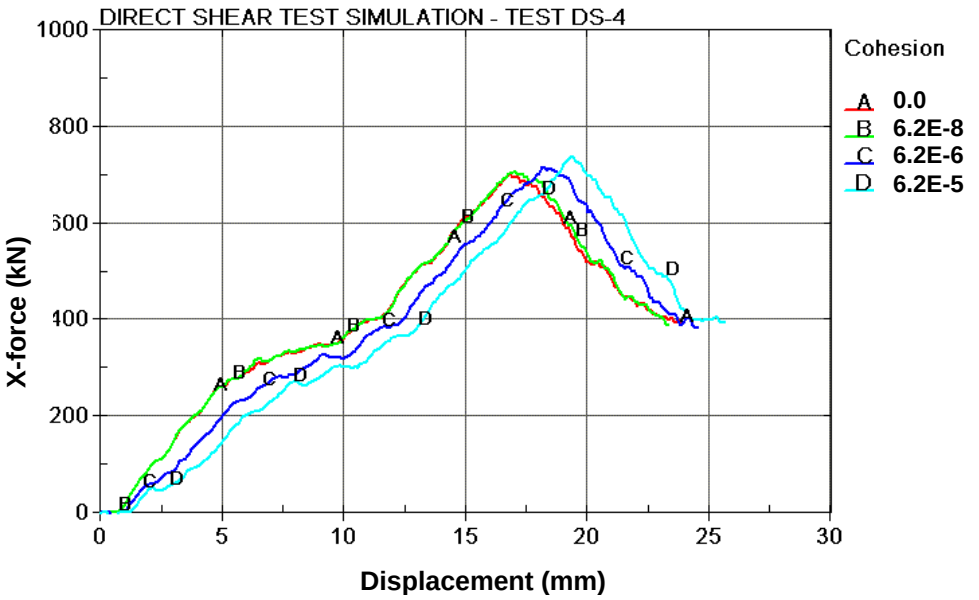

(a) Force.

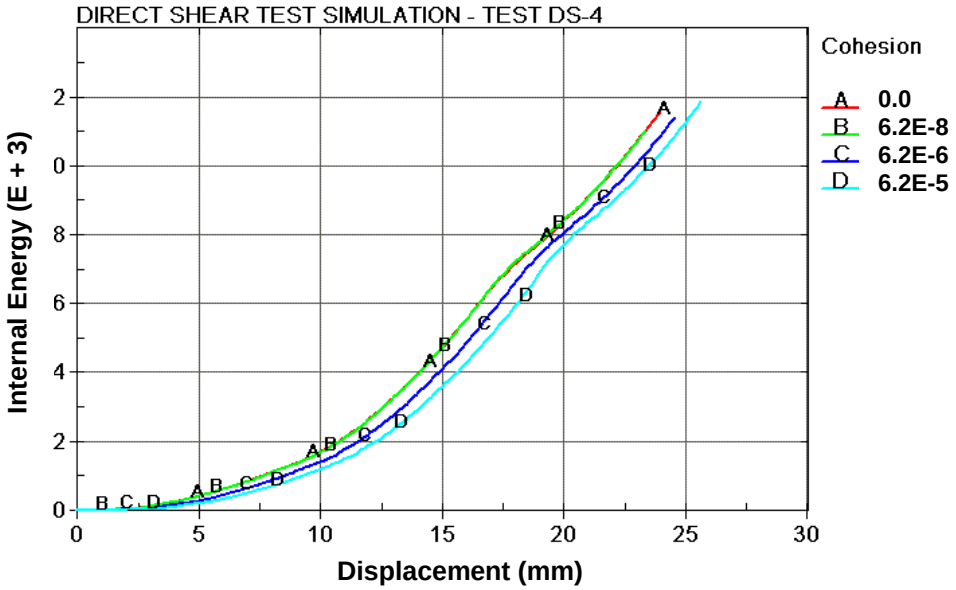

(b) Internal Energy

Figure 9. Cohesion parameter (Coh) variations.

It is recommended that the values of cohesion for *cohesionless* soil be placed at approximately 6.2E-6 GPa. This value appears to be close enough to zero, but still allows the plasticity routines to converge relatively rapidly. Larger values of cohesion rapidly digress from the zero value for cohesion. However, larger values do allow for

more rapid convergence in the plasticity algorithms. It should also be examined whether the value of cohesion should be increased to compensate for the soil dilation caused by Taylor's aggregate interlock.

Angle of Internal Friction

The angle of internal friction, ϕ, is also the slope of the shear strength envelope and, therefore, represents the effect that increasing effective normal stress has on the shear strength of the soil. For a given soil, holding all other parameters constant, an increase in the angle of internal friction should increase the shear force required to fail the soil.

For a cohesionless soil, the angle of internal friction is equal to the angle of repose—the angle at which the soil will settle into naturally. Visually, if one pours dry sand into a pile, there is a maximum angle that is achieved. This angle is the angle of repose.

A parameter study was performed varying the angle of internal friction. These values are shown in table 8. Cohesion was maintained at a constant throughout the variations of the angle of internal friction. It is critical to note that this parameter is input into LS-DYNA in radians, not degrees.

As shown in figure 10, shear forces increase for decreasing angles of internal friction. This result is counter to conventional soil mechanics theories, where shear forces are known to decrease with decreasing angles of internal friction. The user was unable to determine why increasing the angle of internal friction decreased the force levels.

The baseline value of 63 degrees (1.1 radians) for an angle of internal friction was determined through physical testing performed by the user.[6] This value is recommended for NCHRP 350 soil of crushed limestone. Other types of soil that meet NCHRP 350 specifications should be tested separately.

Table 8. Internal angle of friction parameter study.

Test Identifier	Angle of Internal Friction, ϕ	CPU Time (s)	Peak			Valley		
			Disp (mm)	Force (kN)	Internal Energy	Disp (mm)	Force (kN)	Internal Energy
Baseline	63°	2644	18.2	718	6795	24.6	385	11,450
T1	43°	2692	18.6	768	7131	24.8	420	11,597
T2	23°	3077	18.9	769	7605	24.6	455	11,757
T3	3°	2179	18.8	805	8529	24.5	473	13,044

1 degree = 0.1592 radians

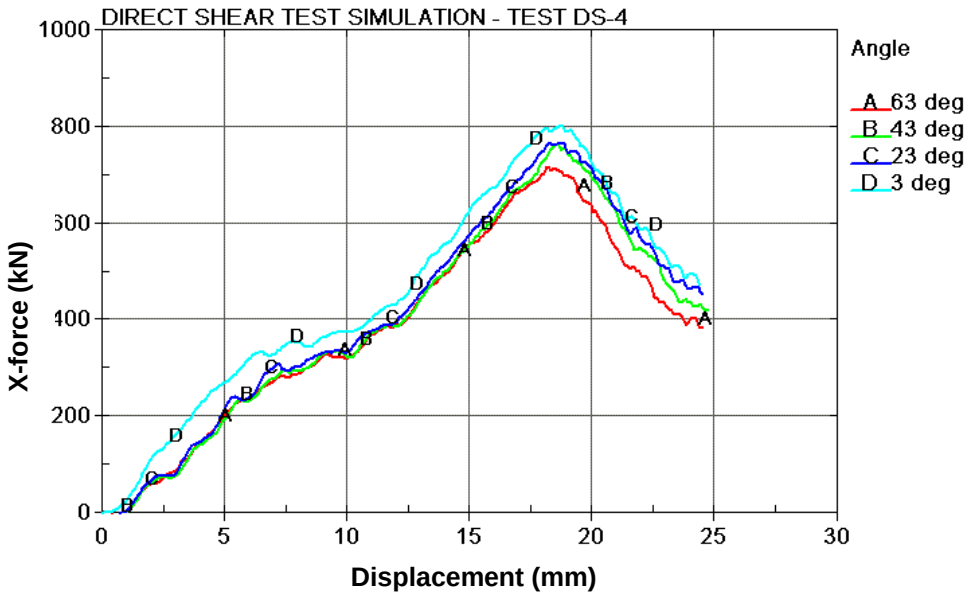

(a) Force.

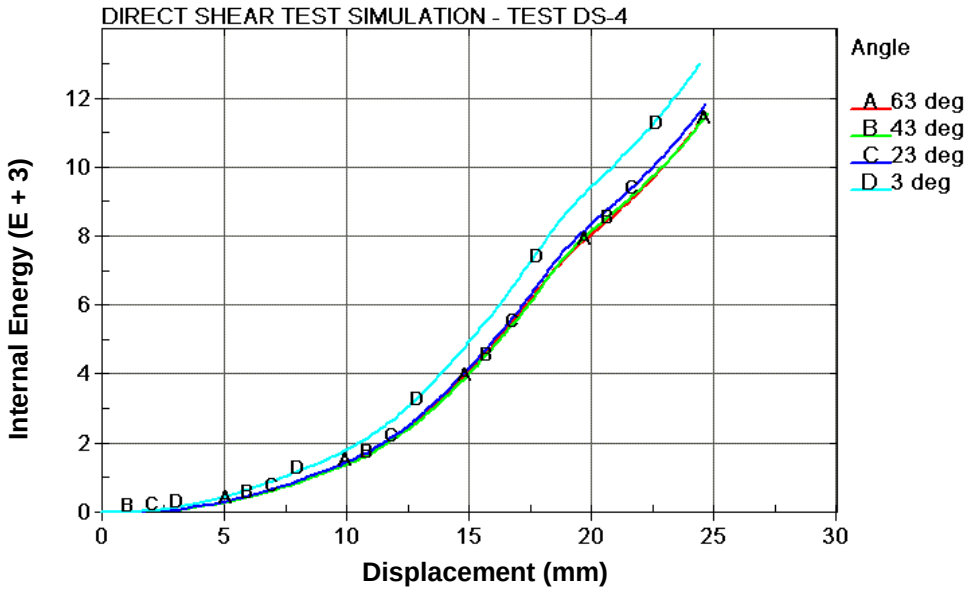

(b) Internal Energy.

Figure 10. Angle of internal friction variations.

DRUCKER-PRAGER COEFFICIENT, *AHYP*

The Mohr-Coulomb failure criterion can be represented as a straight line in space (σ_m, $-\bar{\sigma}$), as shown in figure 11. The point where the line cuts the σ_m-axis corresponds

to the tip of the hexagonal Mohr-Coulomb pyramid; it is here that the gradient of the yield surface is undefined.

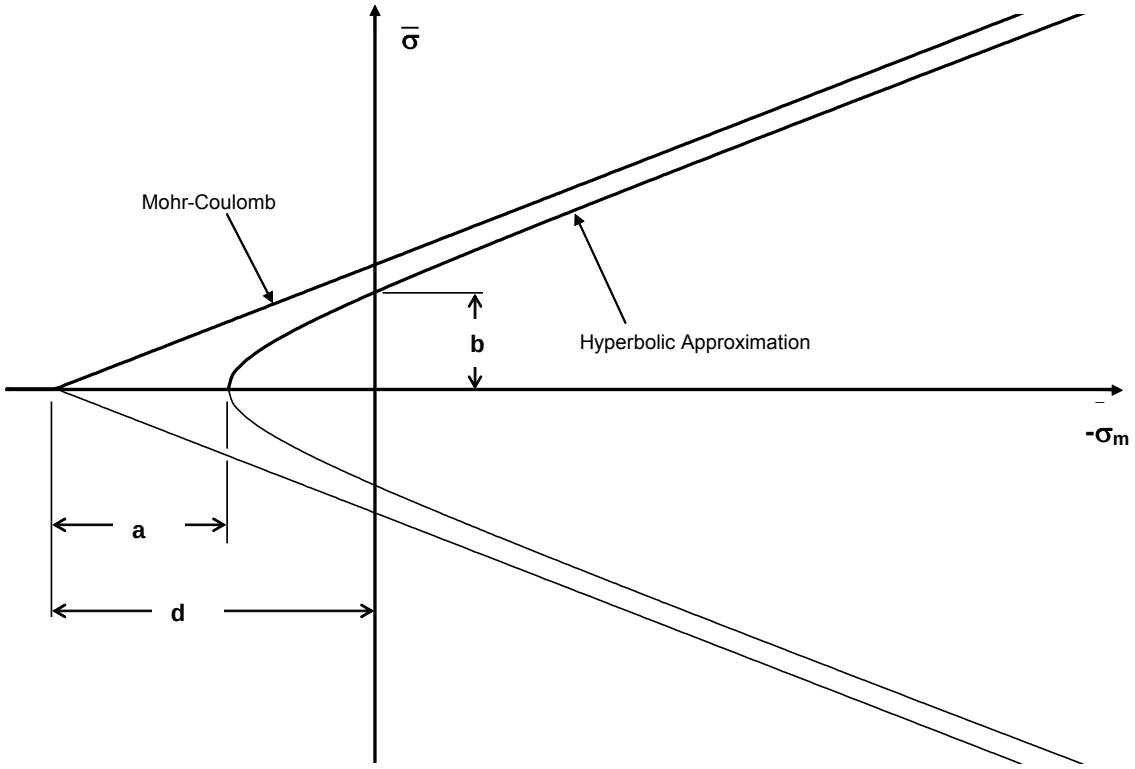

Figure 11. Hyperbolic approximation of Mohr-Coulomb.

To avoid such angularity, Drucker-Prager introduced an inscribed cone that still possesses a vertex, but in which the "ridge" corners have been smoothed.[22] Combinations of the Mohr-Coulomb and Drucker-Prager yield surfaces can give better approximations of real failure conditions than the Drucker-Prager alone (while still avoiding the singularity of the Mohr-Coulomb yield criterion).

The developer implemented a hyperbolic approximation of the plasticity surface based on the work of Abbo and Sloan.[23] The modified yield surface is given as:

$$\sigma_y = -P\sin\phi + \sqrt{J_2 K(\theta)^2 + Ahyp^2 \sin^2\phi} - c\cos = 0 \qquad (14)$$

where:

σ_y = Yield surface
P = Pressure
ϕ = Angle of internal friction

J_2 = Second invariant of the stress deviator
$K(\theta)$ = Function of the angle in the deviatoric plane
Ahyp = Drucker-Prager coefficient
c = Cohesion

The elimination of the vertex singularity is also extremely useful in speeding the convergence of numerical computation, particularly where large angles of internal friction, ϕ, and small cohesion conditions exist. This is predominantly the case with respect to NCHRP 350 crash criteria, since American Association of State Highway and Transportation Officials (AASHTO) soil specifications stipulate exactly this variety of soil.

Selecting an appropriate value for the hyperbolic coefficient, *Ahyp*, is important for stability in the simulation. The Drucker-Prager coefficient can be chosen as a function of the angle of internal friction and cohesion.[24] A reasonable approximation that has been found to yield good results is:

$$Ahyp = \frac{c}{20} \cot(\phi) \tag{15}$$

For values of $Ahyp \leq \frac{c}{4} \cot(\phi)$, the hyperbolic surface closely represents the Mohr-Coulomb surface. At *Ahyp* = 0, the original Mohr-Coulomb surface is recovered. This also restores the vertex singularity. At larger values of *Ahyp*, the hyperbolic surface becomes increasingly disparate from the Mohr-Coulomb surface. For numerical considerations, *Ahyp* should be set to values of less than *c* cot (ϕ). A graphical representation of the influence that *Ahyp* has on the yield surface is shown in figure 12.

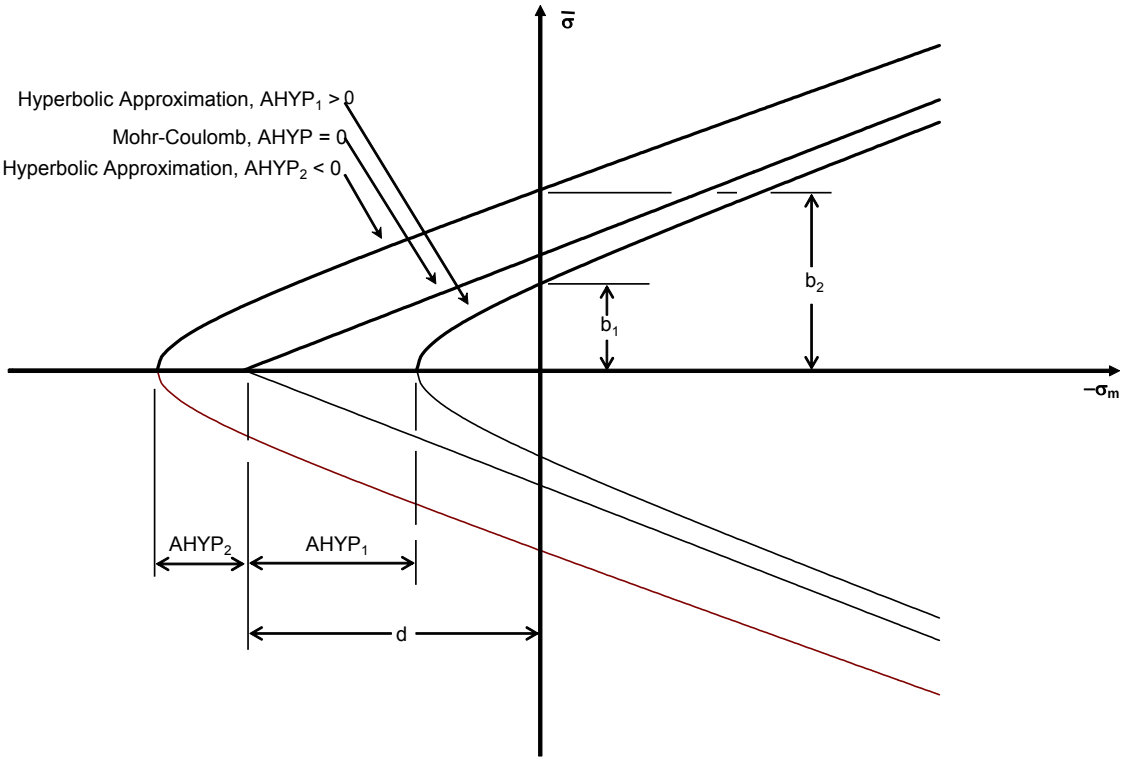

Figure 12. *Ahyp* influence on yield surface.

For the initial simulations, *Ahyp* was not changed in relation to the changing cohesion and angle of internal friction parameters. It was desirable to vary each parameter separately, thus *Ahyp* remained constant during the cohesion and angle of internal friction parameter studies.

It was found that significant increases in forces were found when *Ahyp* was increased, as shown in table 9 and figure 13. The parameter *Ahyp* does not have significant variations from Mohr-Coulomb when it is set to very small values (1.0E-7). Keep in mind, however, that increasing *Ahyp* to larger values significantly deviates from the Mohr-Coulomb failure envelope.

In order to maintain similarity to the original Mohr-Coulomb failure envelope, values on the order of 1.0E-7 are recommended. For an internal angle of friction, Phimax, equal to 63 degrees (1.1 radians) and a cohesion of 6.2E-6 GPa, equation 15 yields a value of *Ahyp* = 1.58E-7 GPa.

Table 9. Effects of material parameter *Ahyp*.

Test Identifier	*Ahyp* (GPa)	CPU Time (s)	Peak			Valley		
			Disp (mm)	Force (kN)	Internal Energy	Disp (mm)	Force (kN)	Internal Energy
T16	-1.0E-7	2636	18.2	718	6795	24.6	385	11,450
T15	0.0	2636	18.6	730	7148	24.5	392	11,369
Baseline	1.0E-7	2644	18.2	718	6795	24.6	385	11,450
T14	1.0E-3	3017	17.3	839	8181	28.6	653	20,416

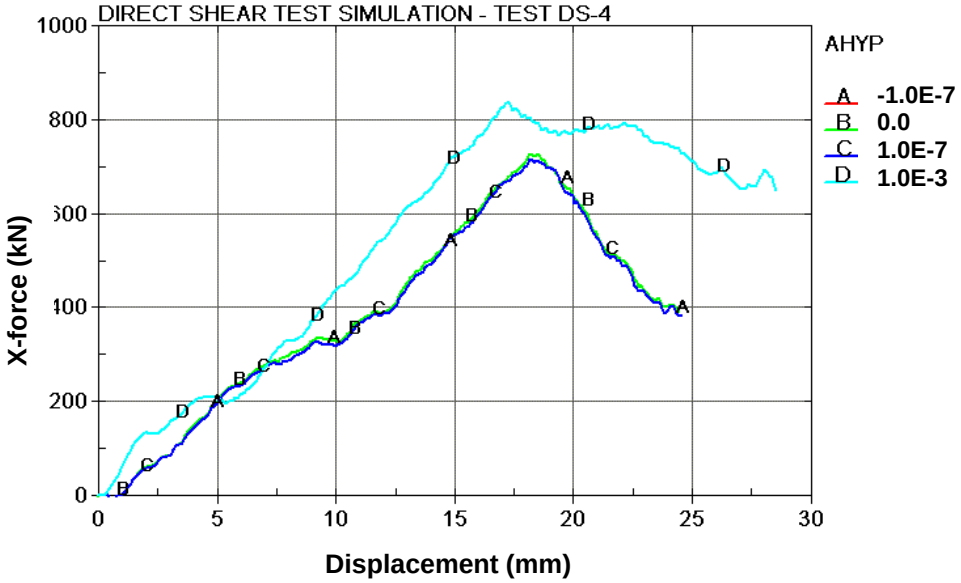

(a) Force.

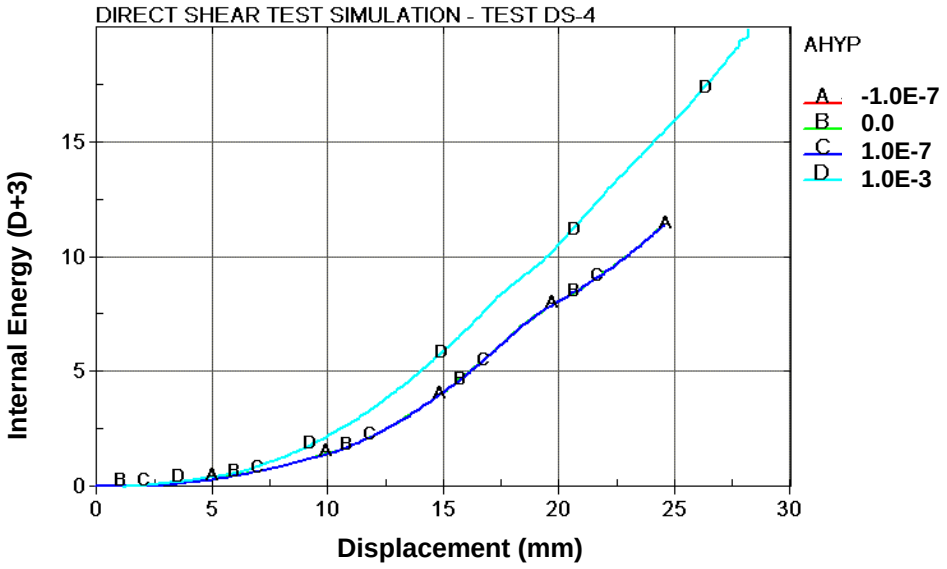

(b) Internal Energy.

Figure 13. *Ahyp* parameter variations.

PLASTICITY ITERATIONS, ITERMAX

To solve the global system of nonlinear plasticity equations, an iterative approach is frequently required. Although non-iterative methods exist, such as radial return, these algorithms may lead to inaccurate results. The FHWA soil model implements an iterative plasticity scheme to solve the plasticity equations.

Iterative approaches are required because the solution to the nonlinear system is not necessarily in an equilibrium state. Strain hardening or softening may have placed the current stress state beyond the yield surface and iterative schemes, such as the Newton-Ralphson or other methods, must be used to ensure that the plasticity model converges to the true plasticity surface.

Itermax controls the number of iterations for the plasticity routine. In cases where the cohesion, Coh, is extremely small, obtaining convergence can take several iterations. This is a quality inherent in most plasticity routines and can significantly affect the accuracy and precision of a simulation.

A parameter study was performed manipulating the cohesion, Coh, and the maximum number of iterations for the plasticity routines, Itermax. The results are shown in table 10 and figure 14.

Table 10. Examination of Itermax.

Test Identifier	Cohesion, Coh	Itermax	CPU Time (s)	Peak			Valley		
				Disp (mm)	Force (kN)	Internal Energy	Disp (mm)	Force (kN)	Internal Energy
T10	0.0	10	3,727	16.9	704	6351	24.0	393	11,609
T11	0.0	50	12,717	16.7	685	5972	24.0	378	11,241
T12	0.0	100	21,647	17.1	691	6205	24.1	382	11,286
T29	6.2E-6	1	814	18.5	737	7412	24.3	397	11,856
T30	6.2E-6	3	1,050	18.8	743	7449	24.5	388	11,652
T31	6.2E-6	5	1,679	18.5	732	7135	24.7	386	11,695
T32	6.2E-6	7	1,772	18.7	739	7255	25.6	403	12,677
Baseline	6.2E-6	10	2,644	18.2	718	6795	24.6	385	11,450
T27	6.2E-6	15	4,507	17.7	696	6331	24.2	376	10,984
T28	6.2E-6	100	20,770	17.4	677	5818	24.2	368	10,473

(a) Cohesion = 6.2E-06.

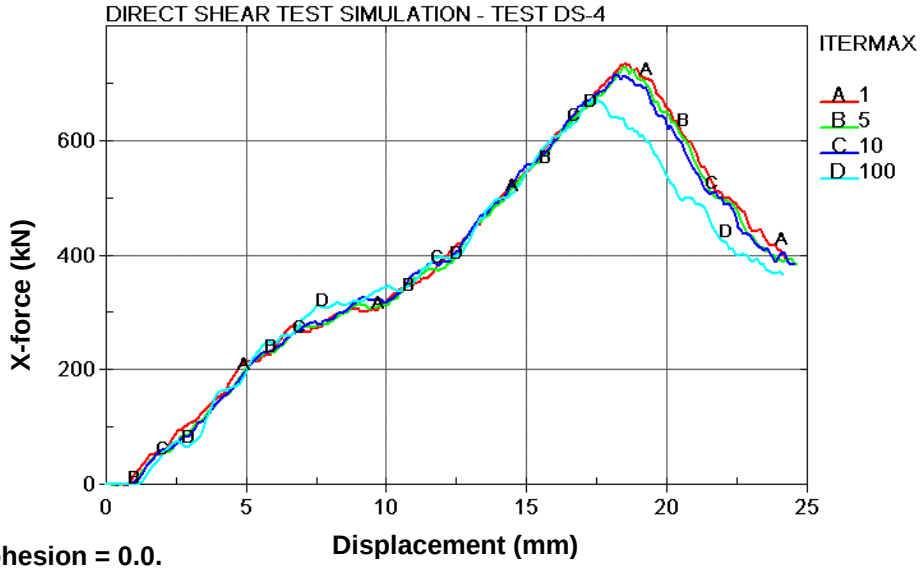

(b) Cohesion = 0.0.

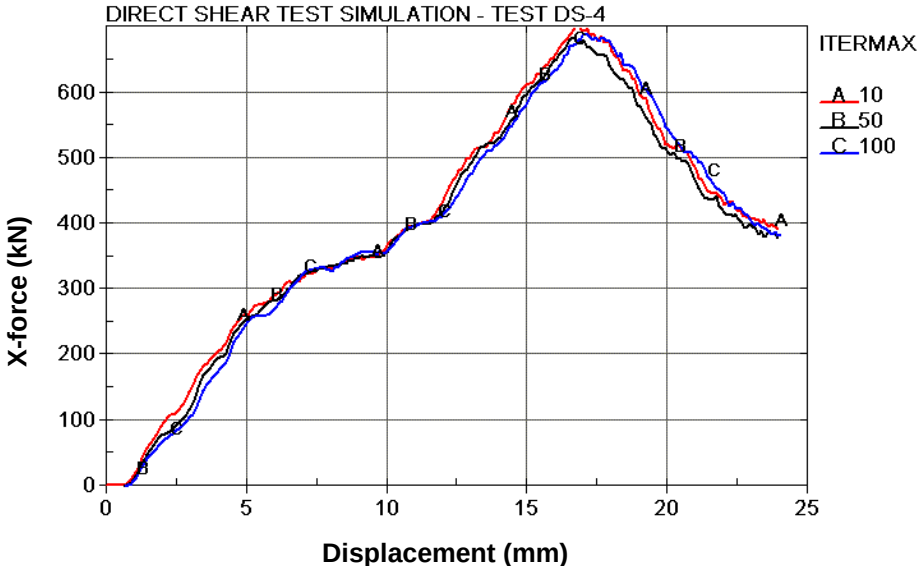

Figure 14. Itermax parameter variations.

The user was unable to determine whether there was a convergence criteria within the soil material model (increasing Itermax always generated a longer run time, with no apparent check for some type of convergence criteria being satisfied).

When cohesion is set to the recommended value of 6.2E-6, low Itermax numbers (1 through 20) give roughly the same response. Although the developer has recommended using Itermax = 10, it appears that significant CPU time can be saved with lower values of Itermax without a loss of accuracy. However, with Itermax = 100, a significant difference is seen in the results. This parameter definitely needs revisiting when the soil model is able to handle larger deformation situations (such as being able to correctly handle the direct shear test up to 100 or 200 mm of deflection, rather than only 25 mm in the current implementation).

ECCENTRICITY PARAMETER, ECCEN

Eccen is the eccentricity parameter for the third stress invariant effects. To generalize the shape of the yield surface in the deviatoric plane, the developer changed the standard Mohr-Coulomb *K(t)* function to one developed by Klisinski.[25-26] Klisinski's yield function takes the form:

$$K(\theta) = \frac{4\left(1-e^2\right)\cos^2\theta + (2e-1)^2}{2\left(1-e^2\right)\cos\theta + (2e-1)\sqrt{4(1-e^2)\cos^2\theta + 5e^2 - 4e}} \tag{16}$$

where:

$$\cos 3\theta = \frac{3\sqrt{3}\ J_3}{2\sqrt{J_2{}^3}} \tag{17}$$

J_3 = Third invariant of the stress deviator
e = Ratio of extension strength to compression strength (Eccen)

The ratio of the extension strength to the compression strength, Eccen, is the eccentricity parameter responsible for third invariant (J_3) effects. If Eccen is set to 1.0, then a circular cone surface is formed. If Eccen is set to 0.55, then a triangular surface is formed. The function $K(\theta)$ is defined for values of Eccen ranging as follows: $0.5 < e \leq 1.0$.

Initial models included a value of Eccen = 0.7. This creates a relatively smooth yield surface without over-smoothing the corners of the yield surface. The authors are unaware of any physical testing or theoretical means for determining the recommended values for Eccen.

STRAIN HARDENING PARAMETERS, A_n AND E_t

To simulate nonlinear strain hardening behavior, the angle of internal friction, ϕ, is increased as a function of effective plastic strain, $\varepsilon_{eff\ plastic}$. It is increased as a function of E_t, the amount of the nonlinear strain hardening effects desired, and A_n, the percentage of Phimax where nonlinear behavior begins. The increase in the angle of internal friction is given by the equation:

$$\Delta\phi = E_t\left(1 - \frac{\phi - \phi_{init}}{A_n\ \phi_{max}}\right)\Delta\varepsilon_{eff\ plastic} \tag{18}$$

For input in LS-DYNA, A_n is expressed as a decimal, with values between 0 and 1.0 (0 percent and 100 percent). E_t affects the rate at which nonlinear hardening occurs. The authors are unaware of any physical testing or theoretical means for determining the recommended values for A_n or E_t.

MOISTURE CONTENT, MCONT

Increasing moisture content significantly reduces soil shear strength.[27] Additionally, it has been reported that marked reductions in Poisson's ratios occur because of increases in moisture content.[28] The developer addresses this by reducing the second stress invariant, J_2, to produce the resulting loss in shear strength. It is critical to note that for Mcont to have any effect, the parameters Pwd1, Pwd2, and PwKsk must also be active.

Although NCHRP 350 does not give a specific moisture content criterion, for the performance of crash tests, material specification requires compaction at or near optimum moisture content. In general, optimum moisture content is around 4 percent to 5 percent, based on dry weight. Generally, the moisture content after compaction and prior to crash testing does not vary significantly. For the direct shear testing discussed in this report, moisture content was 0 percent.

As of this writing, the moisture effects are not operable within the FHWA soil model.

PORE-WATER EFFECTS ON THE BULK MODULUS, PWD1

To simulate the effects of moisture and air voids, the FHWA soil material model modifies the nonporous bulk modulus by using a constant relating the stiffness of the soil material before the air voids are collapsed. In equation form, this is:

$$K = \frac{K_{\mathrm{i}}}{1 + K_{\mathrm{i}} D_1 n_{\mathrm{cur}}} \tag{19}$$

where:

K_i = Nonporous bulk modulus

n_{cur} = Current porosity (the maximum of either 0 or ($w - \varepsilon_v$))

w = Volumetric strain corresponding to the volume of the air voids = $n(1 - S)$

ε_v = Total volumetric strain

D_1 = Parameter controlling the stiffness before the air voids are collapsed (Pwd1)

n = Porosity of the soil = $\frac{e}{1 + e}$

e = Void ratio = $\frac{\gamma_{sp}\rho_w(1+m_c)}{\rho} - 1$

S = Degree of saturation = $\frac{\rho m_c}{n\rho_w(1+m_c)}$

ρ, γ_{sp}, m_c , ρ_w = soil density, specific gravity, moisture content, and soil density.

Appropriate values for Pwd1 must be larger than zero, but no appropriate upper limit is known. At Pwd1 = 0, the standard linear bulk modulus, K_i, is used. If Pwd1 is not set to 0.0, the bulk modulus, K, should be the fully collapsed bulk modulus. Increasing this value reduces the stiffness of the response of the soil. Information provided by the developer included the values of Pwd1, ranging from 0.0 to 10.0.

The development of excess pore pressure in a soil matrix is dependent on the portion of the pore space occupied by fluid, the rate at which the fluid can move through the soil matrix, and the driving force moving the fluid. The dissipation of excess pore pressure is a key parameter in understanding the dynamic performance of soils. In partially saturated situations, consideration of both the movement of air and fluid is necessary to define the effects of excess pore pressure on soil strength properties. In order to determine the rate of pore-pressure dissipation, the permeability of the soil matrix (both in terms of fluid and air) is a key parameter. Excess pore pressure is created by consolidation of the soil pore space, leading to localized increases in fluid/air pressure. This pressure dissipates at a time rate dependent on pressure magnitude and resistance to fluid/air flow in the soil matrix. In NCHRP 350 strong soil, the relative permeability is high, meaning that excess pore-pressure effects tend to be localized and short lived. The criteria for the decay of pore pressure relative to the soil fabric are not clear from the summary of the developer's engineering report. Without consideration of permeability, there would be no way to rationally address excess pore pressure.

PORE-WATER EFFECTS ON PORE-WATER PRESSURE, PWD2

Excess pore-water pressure reduces the total pressure and will lower the shear strength of the soil. Large pore-water pressures can cause the effective stress to disappear, causing liquefaction of the soil. To simulate the effects of excess pore-water pressure, the FHWA soil material model calculates the pore-water pressure, u, in a similar manner to that of the moisture effects on the bulk modulus:

$$u = \frac{K_{\text{sk}}}{1 + K_{\text{sk}}\, D_2\, n_{\text{cur}}}\, \varepsilon_v \tag{20}$$

where:

K_{sk} = Nonporous bulk modulus

n_{cur} = Current porosity (the maximum of either 0 or ($w - \varepsilon_v$))

w = Volumetric strain corresponding to the volume of the air voids = $n(1 - S)$

ε_v = Total volumetric strain

D_2 = Parameter for pore-water pressure before the air voids are collapsed (Pwd2)

n = Porosity of the soil = $\frac{e}{1 + e}$

e = Void ratio = $\frac{\gamma_{sp}\rho_w(1+m_c)}{\rho}-1$

S = Degree of saturation = $\frac{\rho m_c}{n\rho_w(1+m_c)}$

ρ, γ_{sp}, m_c, ρ_w = soil density, specific gravity, moisture content, and water density.

Pore-water pressure is not allowed to become negative. If Pwd2 is set relatively high compared to K_{sk}, there is no pore-water pressure developed until the volumetric strain is greater than the strains associated with the air voids. As Pwd2 is lowered, the pore pressure starts to increase before the air voids are fully collapsed.

For an initial porosity and bulk moduli, the parameter Pwd2 can be calculated using the Skempton pore-water pressure parameter, *B*, as defined below:

$$B = \frac{1}{1 + \mathrm{n}\frac{K_{\mathrm{sk}}}{K_v}} \tag{21}$$

This allows for the calculation of the pore-water parameter Pwd2 directly, as follows:

$$Pwd2 = D_2 = \frac{K_{\mathrm{sk}}}{1 + K_{\mathrm{sk}}\, D_2\, n_{\mathrm{cur}}}\varepsilon_v \tag{22}$$

Again, the comments of the previous section apply to this input. Additionally, it is assumed that excess pore pressure is used to reduce effective stress, with the commensurate influence on shear strength. In terms of shear strength, negative pore pressures, generated from the capillary rise evidenced in many soil matrixes (NCHRP 350 strong soil would not be included on this list), are important to consider in developing reasonable failure criteria. Negative pore pressure, the source of apparent cohesion in sands, can influence the peak shear strength. In practice, however, the authors are unaware of any physical testing or theoretical means for determining specific recommended values for Pwd2.

SKELETON BULK MODULUS, PWKSK

The skeleton bulk modulus is a parameter that also determines the amount of the effect that pore-water pressure has on the bulk modulus. To eliminate pore-water effects, this parameter is set to zero.

For sands, Stephen found that the dry skeleton bulk modulus was two orders of magnitude lower than the grain bulk modulus. The units of measurement (stress) for the bulk modulus are gigapascals. In practice, however, the authors are unaware of any physical testing or theoretical means for determining specific recommended values for PwKsk.

RESIDUAL SHEAR STRENGTH, PHIRES

This is the angle, in radians, of the slope of the failure envelope, ϕ_{ult}. This failure envelope defines the residual strength after the initiation of shear failure. The implementation of this value is material-dependent. In other words, there is no fixed strain at which this value is appropriate. As evidenced in the direct shear tests performed by the user, there is a gradual decrease in shear strength after the peak. The slope of this decrease is dependent on particle shape and, particularly, on density. The dilatancy and confinement of the material play important roles in this value. The residual shear strength is defined as:

$$S_{\text{residual}} = \sigma' \tan \phi_{\text{ult}} \tag{23}$$

where:

$s_{residual}$ = Residual shear strength

σ' = Effective stress

ϕ_{ult} = Residual angle of internal friction

This strength is easily defined for most materials; however, the current limitation of the model to calculate beyond peak shear strength in the trials makes the evaluation of this parameter impossible. The rate of change from ϕ to ϕ_{ult} is less available, but could be determined for soils of interest and appropriate confining conditions.

VOID FORMATION ENERGY, VDFM, AND VOLUMETRIC STRAIN, DINT

When material models include strain softening, special techniques must be used to prevent mesh sensitivity. Mesh sensitivity is the tendency of a finite element model to produce significantly different results as the element size is reduced. Mesh sensitivity occurs because the softening in the model becomes concentrated in one or in a few elements.

To reduce the effects of strain softening on mesh sensitivity, the softening parameter, α (the strain at full damage), must be modified as the element size changes. The FHWA soil model uses an input parameter, Vdfm (G_f), that is analogous to fracture energy in metals. The void formation parameter is the area under the softening region of the pressure-volumetric strain curve times the cube root of the element volume, $V^{1/3}$:

$$\alpha = \frac{2G_f}{K\xi_o V^{\frac{1}{3}}} + \xi_o \tag{24}$$

where:

ξ_o = Initial damage threshold strain, Dint

If G_f is made increasingly small relative to $K\xi_0 V^{\frac{1}{3}}$, the softening will become progressively more brittle. Conversely, larger ratios of G_f to $K\xi_0 V^{\frac{1}{3}}$ will cause the softening to become more ductile.

Dint is the volumetric strain at the peak pressure. Physically, this is the point where damage effects begin to occur, such that Dint can be conceived as the strain at the initial damage.

The authors are unaware of any physical testing or theoretical means for determining the recommended values for Vdfm or Dint.

DELETION DAMAGE, DAMLEV, AND PRINCIPAL FAILURE STRAIN, EPSMAX

As strain softening (damage) increases, the effective stiffness of the element can get very small, causing severe element distortion. One solution to this problem is deleting these distorted elements. Damlev is the percentage of damage, expressed as a decimal, that causes the deletion of an element. Epsmax is the maximum principal failure strain at which the element is deleted. It is important to note that both Damlev and Epsmax must be exceeded in order for element deletion to occur. If it is desired to turn off element deletion, Damlev should be set to zero.

In the current application, erosion of the soil elements is an unstable process and is not recommended. This is discussed further in chapter 5.

The authors are unaware of any physical testing or theoretical means for determining the recommended values for Damlev or Epsmax.

CHAPTER 5. DEVELOPER'S RECOMMENDED PARAMETERS

The developer modeled direct shear test 4 (DS-4) using LS-DYNA and prepared a graph of the physical test data compared to the shear stress-deflection curve from LS-DYNA. This figure and the corresponding input parameters from the developer are shown in figure 15 and table 11, respectively. The LS-DYNA format for these parameters is shown in table 12.

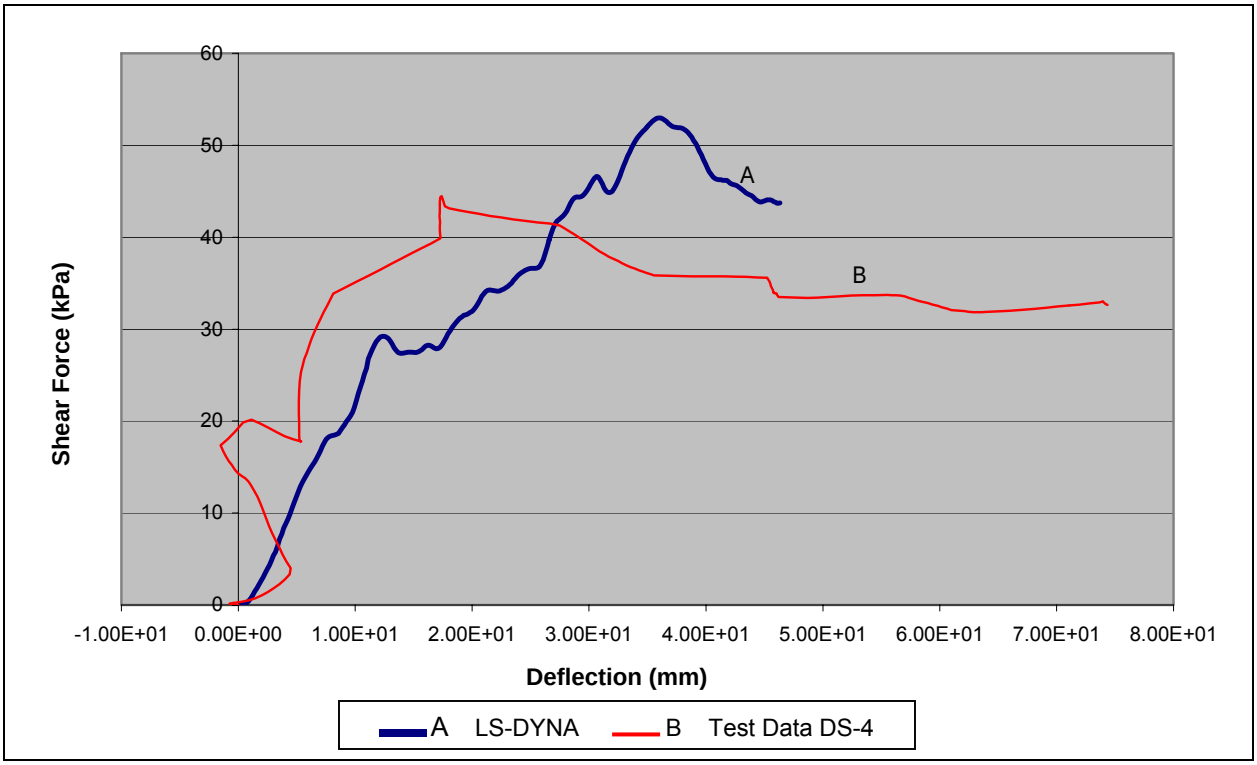

Figure 15. DS-4 simulation results from the developer.

Note: Figure 15 is labeled "shear force"; however, it is really shear stress. It is assumed that the shear stress was made by dividing the shear force (the x-direction cross section force defined in the model) by the original cross-sectional area of the sample (0.2 square meters (m^2)).

Table 11. Revised developer's and baseline material parameters.

	Material Parameter					
Input Deck	RO	Nplot	Spgrav	Rhowat	V_n	Gammar
Baseline	2.350E-6	3	2.79	1.0E-6	1.1	0.0
Developer's e-mail	2.350E-6	3	2.79	1.0E-6	1.1	0.0
Input Deck	Itermax	K	G	Phimax	Ahyp	Coh
Baseline	10	0.465	0.186	1.1	1.0E-7	6.2e-6
Developer's e-mail	10	0.00325	0.0013	1.1	1.0E-7	6.2e-6
Input Deck	Eccen	A_n	E_t	Mcont	Pwd1	PwKsk
Baseline	0.7	0.0	0	0.034	0.0	0.0
Developer's e-mail	0.7	0.0	0	0.034	0.0	0.0
Input Deck	Pwd2	Phires	Dint	Vdfm	Damlev	Epsmax
Baseline	0.0	0.0E-0	2.5E-3	5.0E-0	1.00	1.00
Developer's e-mail	0.0	1.0E-3	1.0E-5	6.0E-8	0.99	0.80

Table 12. Input deck as per developer's e-mail.

```
$
*MAT_FHWA_SOIL
$      mid        ro      NPLOT     SPGRAV     RHOWAT        V_N   GAMMAR   ITERMAX
         1  2.350E-6          3       2.79     1.0e-6        1.1      0.0        10
$        K         G     PHIMAX       AHYP        COH     ECCEN        A_N        E_T
   0.00325   0.00130        1.1     1.0E-7     6.2E-6       0.7        0.0        0.0
$     MCONT      PWD1     PWKSK       PWD2     PHIRES      DINT      VDFM    DAMLEV
      0.034      0.00       0.0        0.0      0.001   0.00001  6.0E-08       0.99
$ EPSMAX
      0.80
$
```

These parameters were put into the direct shear model at the user's facility and were simulated. The model became unstable at 38 ms and terminated, as shown in figure 16. The shear stress versus displacement for this run is shown in figure 17. The shear stress calculated on the user's SGI computer was significantly lower than the shear stress calculated by the developer's PC computer.

It was then noted that the developer's graph, as shown in figure 15, terminated at approximately 46 mm. Because the loading was at 1 mm/ms and the specified termination time was 50 ms, the direct shear model should have displaced 50 mm. This suggests that the developer's graph is representative of instability occurring in the soil material model as well.

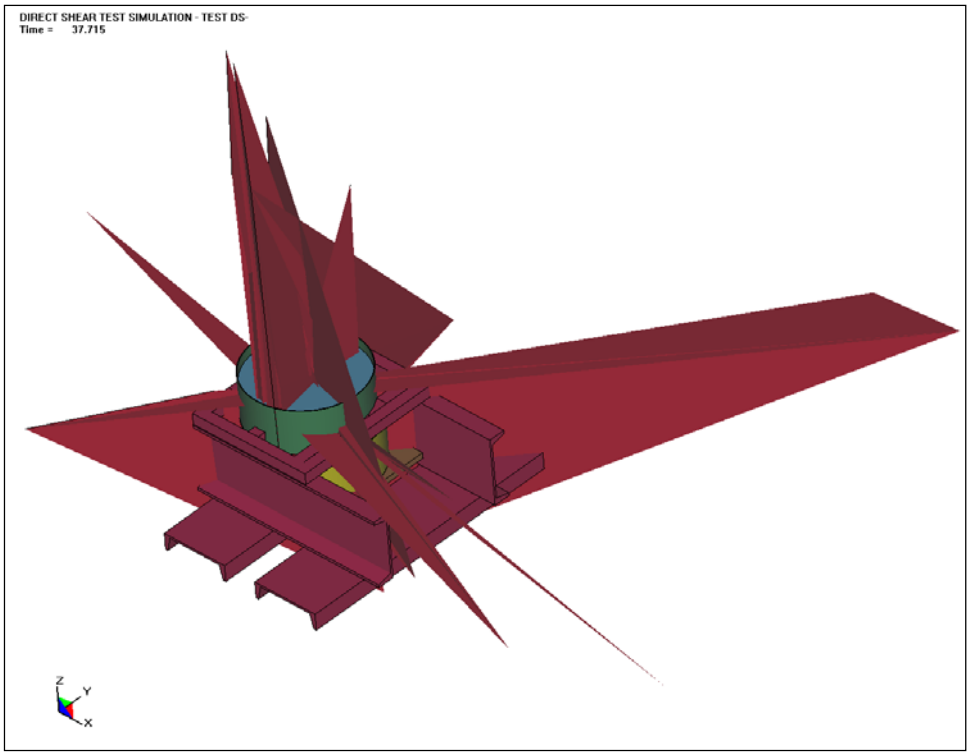

Figure 16. Instability of developer's soil model.

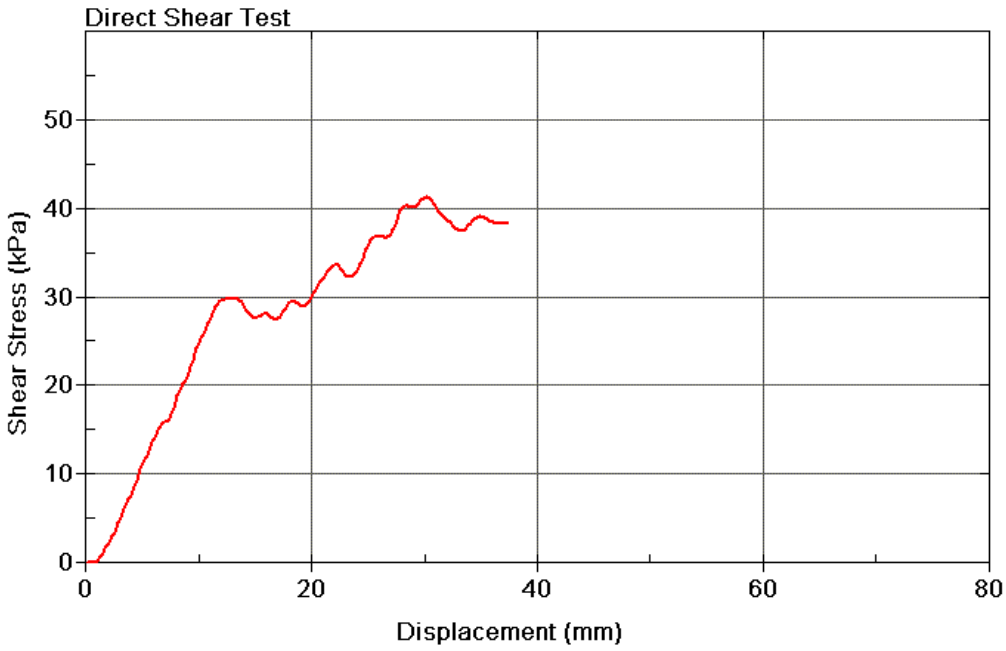

Figure 17. Direct shear results with the developer's soil parameters.

CAUSE OF INSTABILITY

As is shown in figure 16, shooting nodes can be seen in the model. It was desired to see which material parameters induced this failure mode. The parameters used are shown in tables 13 and 14. Additionally, the four parameters that were believed to be the source of the instability were altered individually to determine the source of the instability. These parameters and their corresponding LS-DYNA runs are listed in table 15.

It appears that the damage routines caused the instability. When Damlev was changed from 1.00 to 0.99, the model became unstable. Since both Damlev and Epsmax must be exceeded in order to delete elements, the instability lies somewhere in the damage algorithms and probably not in the variable input routines. Therefore, it must be the instability with other material parameters, the damage algorithms, and/or the element formulation.

Subsequently, the developer proposed a probable cause for the instability as follows. In LS-DYNA, an element fails when one of the gauss points reaches the failure criteria. For fully integrated elements (8 gauss points), this causes an early failure. This early failure does not let the internal forces go to zero before the failed elements are eliminated from the calculation. In turn, this leads to very large unbalanced forces at the nodes, causing unstable behavior (shooting nodes). In addition, this analysis is difficult for LS-DYNA to complete with fully integrated elements because of the well-known problems with shear locking of fully integrated elements.

Unfortunately, under-integrated elements are not an option because of excessive hourglassing as discussed in chapter 6.

Table 13. Material parameters used to determine instability.

$	- K =	2.162E-6 kg/mm3	Field experience
$	- SPGRAV =	2.65	Prior studies
$	- RHOWAT =	1.0E-6 kg/mm3	Theoretical
$	- V_N =	1.1	Developer's original value
$	- GAMMAR =	0.0	Developer's original value
$	- ITERMAX =	10	Developer's original value
$	- K =	0.00325 GPa	Developer's e-mail value
$	- G =	0.00130 GPa	Developer's e-mail value
$	- PHIMAX =	1.1	Direct shear physical testing
$	- AHYP =	1.6E-7 GPa	Calculated from COH and PHIMAX
$	- COH =	6.2E-6 GPa	Parameter study
$	- ECCEN =	0.7	Theoretical/reasonability
$	- A_N =	0.0	Developer's original value
$	- E_T =	0.0	Developer's original value
$	- MCONT =	0.034	Irrelevant with PWD = 0
$	- PWD1 =	0.0	No pore-water effects
$	- PWKSK =	0.0	No pore-water effects

Table 14. Parameters varied to identify instability source.

	Material Parameter	
Input Deck	**Baseline Value**	**New Recommendations From Developer**
Phires	0.0	0.001
Dint	0.0025	0.00001
Vdfm	5.0	6.0E-8
Damlev	1.0	0.99
Epsmax	0.80	0.80

Table 15. LS-DYNA models for instability determination.

	Material Parameter					
Input Deck	**Phires**	**Dint**	**Vdfm**	**Damlev**	**Epsmax**	**Complete Run?**
T35	New	Baseline	Baseline	Baseline	Baseline	Yes
T36	New	New	Baseline	Baseline	Baseline	Yes
T37	New	New	New	Baseline	Baseline	Yes
T38	New	New	New	New	Baseline	No
T34	New	New	New	New	New	No

CHAPTER 6. ELEMENT FORMULATION: HOURGLASSING

There are three applicable solid element formulations available within LS-DYNA:

1. Constant stress.
2. Fully integrated selective reduced (S/R) solid.
3. Fully integrated quadratic eight-node element with nodal rotations.

These are listed in order of increasing accuracy and in order of increasing computational costs. Element formulation no. 1 can exhibit hourglassing, while formulation nos. 2 and 3 have no hourglassing. Details of hourglassing and the various hourglass control algorithms will not be provided here. The reader is referred to the LS-DYNA user's and theoretical manuals for details.

When using element formulation no. 1, an hourglass control algorithm is mandatory. The default hourglass control is referred to as control type 1. An important parameter associated with hourglass control is called the *hourglass coefficient* and is given the label *qm*. The default value for *qm* is 0.1.

The new soil material model has exhibited hourglassing when element formulation no. 1 was used in the direct shear model. Default hourglass control (type 1, *qm* = 0.1) results are shown in figure 18, while the results from hourglass control type 4, *qm* = 0.005, are shown in figure 19.

Under certain conditions, hourglassing was brought under control for the majority of the simulation time, with hourglassing appearing late in the calculation. However, the results were very sensitive to both the hourglass control and the values used for the soil parameters. Quantifying this behavior was not possible in the limited amount of time available for this study.

Additionally, a limited mesh refinement study was performed in order to investigate whether a finer mesh exhibited lower hourglassing (as is often the case in LS-DYNA modeling). However, with a refined mesh, the contact between the soil and the direct shear testing device became unstable, and no firm results were obtained. A detailed investigation into the contact difficulties was not possible in the limited amount of time available for this study.

Thus, in the current implementation, it is recommended that element formulation no. 2 be used with the soil material model. Note that for all other chapters in this report, element formulation no. 2 was employed.

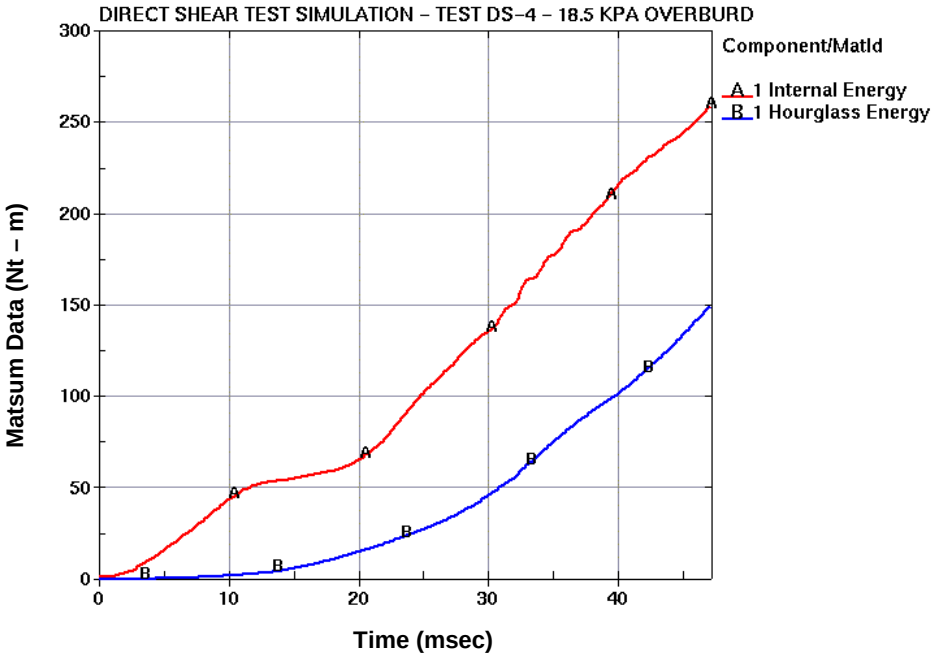

Figure 18. Hourglass control type 1, *qm* = 0.1.

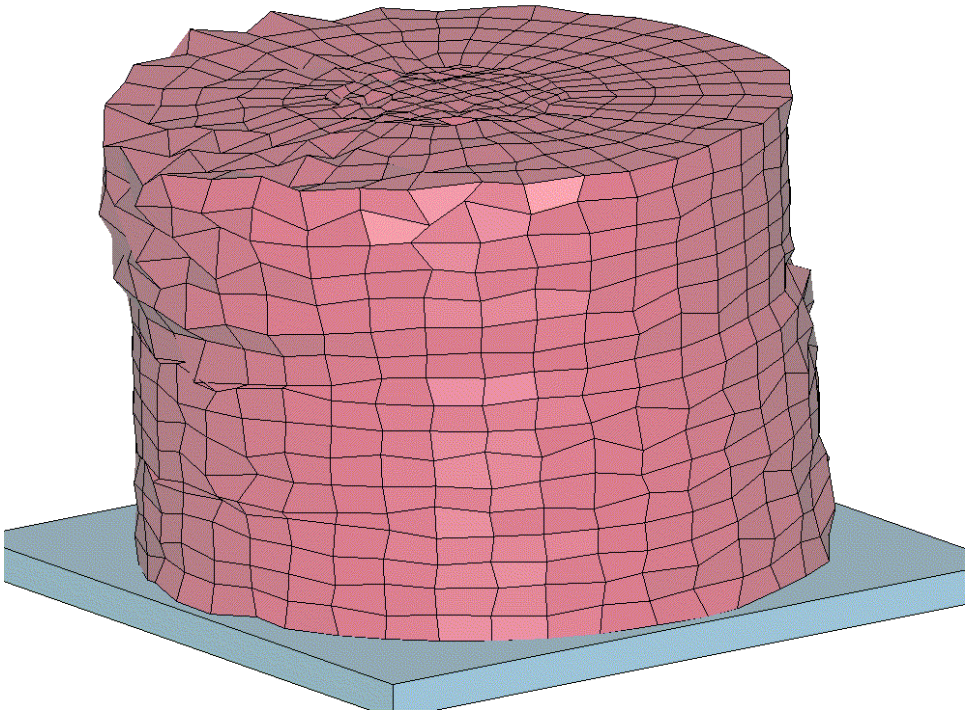

Figure 19. Hourglass control type 4, *qm* = 0.005.

CHAPTER 7. LARGE DEFORMATION TECHNIQUES

Soils, in many roadside safety applications, require large deformation capabilities. This requirement is difficult to meet for Lagrangian-based codes. However, it is possible to implement a material that would allow large deformations while maintaining stability. For example, consider material type 126, a modified honeycomb material. This material was specifically developed to handle extremely large deformations for modeling the honeycomb typically used on moving deformable barriers (MDBs). MDBs are used by the automotive industry for side-impact testing. An example of the stable large deformation capability of material type 126 is shown in figure 20.

Another possibility within LS-DYNA is to use the Eulerian capabilities for modeling materials that undergo large deformations. There are several possibilities available, two of which are: (1) using the Arbitrary Lagrangian-Eulerian (ALE) formulation or (2) using the multimaterial Eulerian formulation with Lagrangian coupling.

The ALE formulation basically works by re-meshing the material throughout the simulation so that the mesh stays relatively uniform. A uniform mesh can prevent local instabilities caused by highly distorted elements. A classical problem used to demonstrate the ALE formulation is the Taylor problem, shown in figure 21.

Multimaterial Eulerian formulation is an approach that allows multiple materials to exist within each solid element and lets the material flow from element to element. The solid element mesh is fixed in space in this approach. Lagrangian coupling allows structural elements to be placed within the Eulerian mesh. Interaction between the fluid-like elements (Eulerian) and the structural elements (Lagrangian) is handled by contact algorithms. A contrived example of a post in soil using this method is shown in figure 22.

Unfortunately, time did not permit investigation of these methods with the FHWA soil material model.

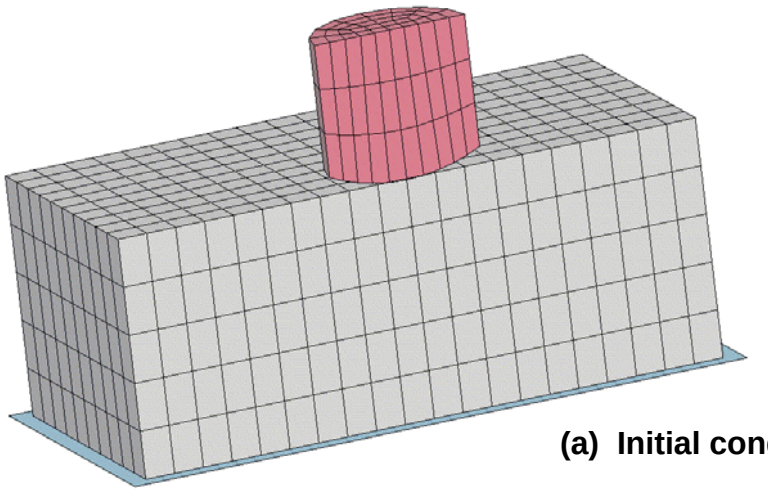

(a) Initial condition.

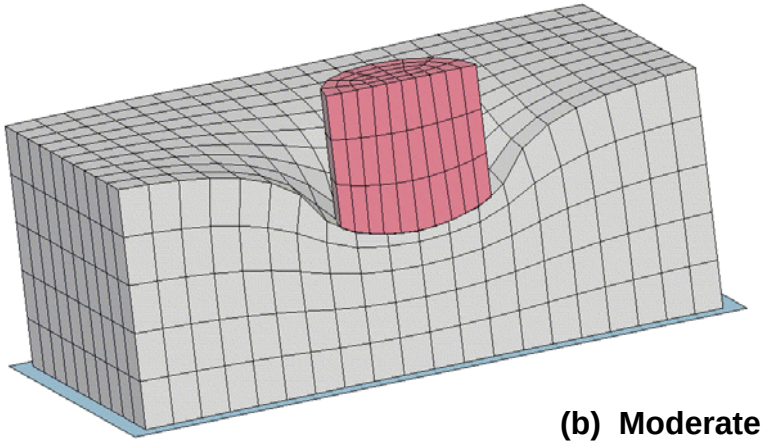

(b) Moderate deformation.

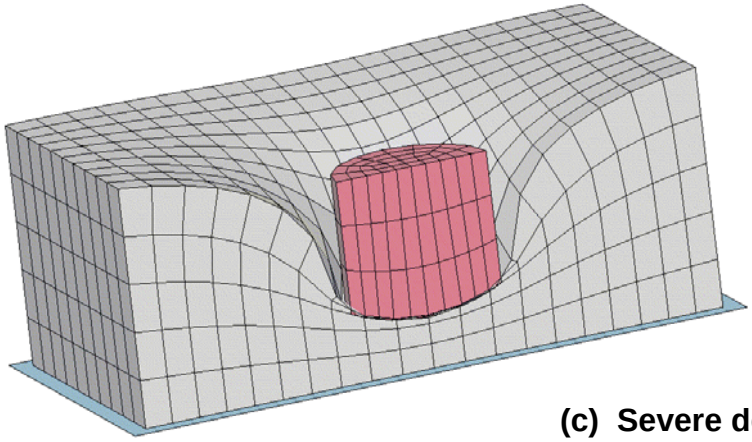

(c) Severe deformation.

Figure 20. Lagrangian approach: Stable large deformations, modified honeycomb material.

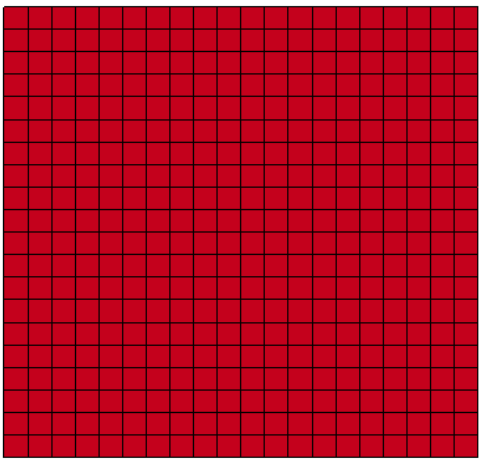

(a) Initial Condition:

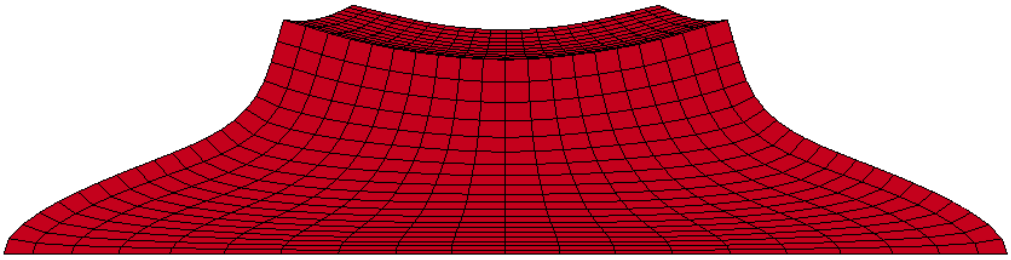

(b) Lagrangian Approach:
Highly distorted elements lead to inaccuracies

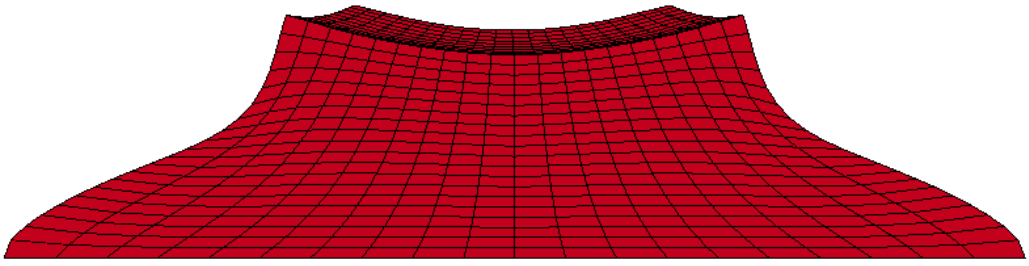

(c) ALE Formulation:
Uniform mesh maintained.

Figure 21. Taylor problem.

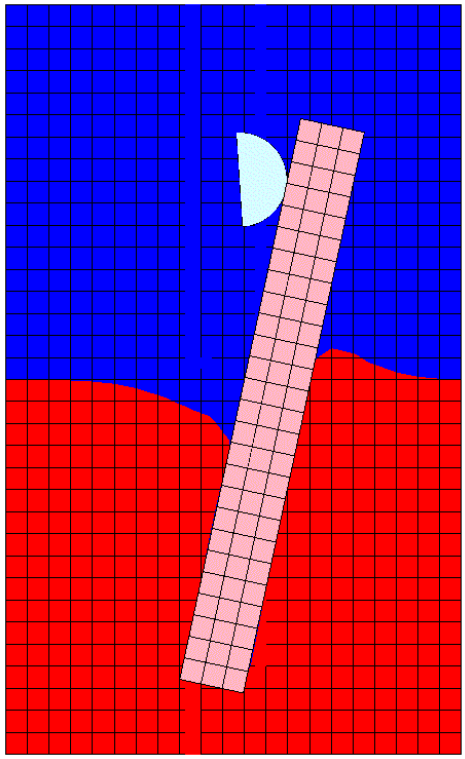

(a) Side view.

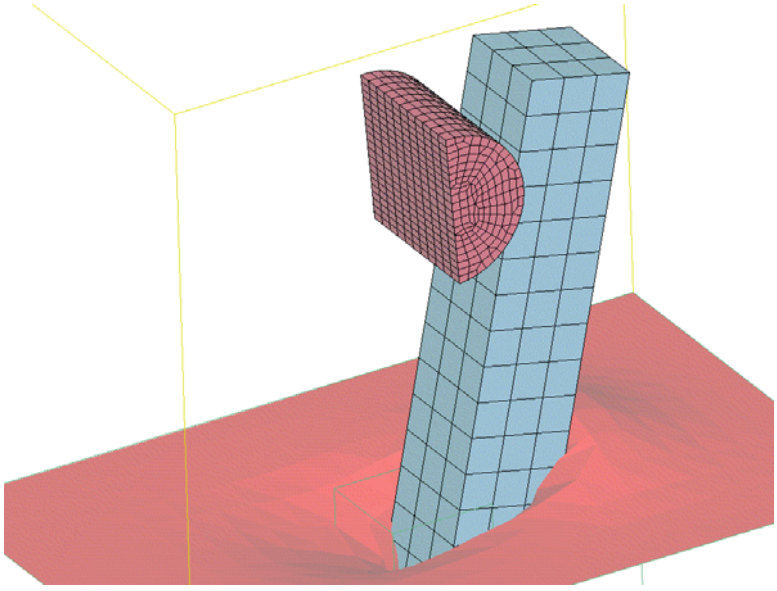

(b) Close up.

Figure 22. Multimaterial Eulerian formulation with Lagrangian coupling.

CHAPTER 8. USER'S CONCLUSIONS AND RECOMMENDATIONS

Significant progress was made examining the effects of material input parameters for the FHWA soil material model developed for LS-DYNA. Appropriate values for some material parameters were found and are presented in this chapter.

From in situ density testing performed in the user's facility, soil densities between 2.082E-6 kg/m^3 and 2.242E-6 kg/m^3 are reasonable. Soil density is critical when examining the dynamic effects of soil behavior.

For the NCHRP 350 strong soil, reasonable bulk and shear moduli values for a "sand and gravel" soil would be K = 80.5 MPa (0.0805 GPa) and G = 48.3 MPa (0.0480 GPa), respectively. However, these values yield an overly stiff response with the FHWA soil model. Suggested values are significantly lower. Values that appear to yield the appropriate stiffness are on the order of 3.25 MPa and 1.3 MPa for the bulk and shear moduli, respectively.

The baseline value of 63 degrees (1.1 radians), as determined through physical testing performed by the user, is recommended for Phimax, the angle of internal friction. This value is reasonable for the NCHRP 350 strong soil of crushed limestone as used at the user's facility.

An appropriate value for the hyperbolic coefficient, *Ahyp*, is $\frac{c}{20}\cot(\phi)$. This value was shown to provide stable performance both theoretically and through parameter studies. Unfortunately, this value is dependent on cohesion, Coh, and the angle of internal friction, Phimax. This requires manual calculation to determine the value that adds a human error factor to the simulation.

Therefore, it is recommended that the default value of $\frac{c}{20}\cot(\phi)$ be used when the *Ahyp* field is left blank. This will allow for fewer parameters that may need to be adjusted, while still giving the option of altering the value, if necessary. Additionally, a check should be performed to ensure that the *Ahyp* parameter is not less than zero. This creates a yield surface that is outside that of the original Mohr-Coulomb yield surface.

In order to maintain similarity to the original Mohr-Coulomb failure envelope, values on the order of 1.0E-7 are recommended for *Ahyp*. For an internal angle of friction, Phimax, equal to 63 degrees (1.1 radians) and a cohesion of 6.2E-6 GPa, the recommended criteria yields a value of *Ahyp* = 1.58E-7 GPa.

It is recommended that the values of cohesion for "cohesionless" soil be placed at approximately 6.2E-6 GPa. This value appears close enough to zero, but still allows the plasticity routines to converge relatively rapidly. It should also be determined whether

the value of cohesion should be increased to compensate for the soil dilation caused by Taylor's aggregate interlock.

The parameter Itermax is a difficult parameter to specify. This parameter determines the number of iterations for the plasticity routines. This would be much better as a tolerance. As it currently stands, a parameter study of Itermax must be performed for every simulation that is run. Specifying a value for convergence would be more straightforward and would not require the end user to perform comparisons of varying numbers of iterations to determine the appropriate quantity.

For various reasons, several features of the new soil model were not available for complete analysis, including strain-rate effects, moisture content, and pore-water pressure. Additionally, researchers were unable to find physical testing methods or analytical methods for determining the appropriate values for several of the soil parameters.

Although extensive progress has been made on the soil material model, there is considerably more to be accomplished before the model would be effective in most roadside safety applications. The current implementation of the soil material model appears to be applicable for only small displacement problems (on the order of 25 to 50 mm). Techniques for modeling large soil displacement problems were discussed; however, there was not enough time to apply these concepts to the new soil material model.

CHAPTER 9. DEVELOPER'S COMMENTS

This chapter was written by the developer of the soil material model. It begins with an itemization of topics (previously discussed by the user in chapters 2 through 8) that the developer concluded were worthy of additional discussion and explanation. These topics and the developer's comments are briefly itemized in table 16. Following all of the topics is a more indepth discussion of pertinent modeling issues and answers to some of the questions posed by the user.

The developer wishes to thank the user for providing a detailed report on the initial use of the FHWA soil material model. The insights provided by a novice user of the soil model enabled the developer to incorporate needed improvements. However, it is the developer's opinion that the user's soil model evaluation revealed no substantial problems with the model. Instead, the evaluation exposed mainly what appears to be a misunderstanding of continuum mechanics material models and their use in finite element analysis.

TABLE OF SOIL MODELING TOPICS

Table 16. Developer's response to user's soil model evaluation.				
Issue	**User's Comment**	**Developer's Response**		
			Soil Model Problem?	Adjust Soil Input?
Force Rising in the Direct Shear Test Simulation	In the direct shear test simulation, after initial softening, the force begins to rise, which never happens in tests.	- Developer thinks that this behavior results from the well-known shear-locking problem of the fully integrated S/R element. (See figure 28 in user's manual.[(2)]) - Developer also believes the user tried to analyze their direct shear test simulation for displacements larger than for which their current model is valid. (See developer's comments under Range of Applicability below.)	No	No
Spgrav Value Incorrect	An incorrect value of Spgrav is reported by LS-DYNA as compared to the value input.	- LSTC was notified of this problem and it was corrected in a later release of LS-DYNA.	No	No
Strain-Rate Parameters	Associated parameter values are not set and strain-rate effects are not available for evaluation.	- A strain-rate model *is* available for evaluation; however, default values are not set. - Soil strain-rate effects are expected to be of minimal importance in roadside safety applications. Treatment of strain-rate effects was implemented in the soil model at this time because it was straightforward to do so.	No	Yes
Shear and Bulk Moduli Values	Values from physical tests produce too stiff of a response with the soil model. Penman's much lower recommended values for gravel also produce too stiff of a response.	- This is partly a result of the use of the fully integrated S/R element in shear. (See figure 28 in user's manual.[(2)]) - Since there is no measurement of the basic elastic properties in the direct shear test, this statement cannot be addressed completely until such data are available.	No	No

Table 16. Developer's response to user's soil model evaluation (continued).				
Issue	**User's Comment**	**Developer's Response**		
			Soil Model Problem?	Adjust Soil Input?
Hourglass Control	The user recommends the use of the S/R solid element to avoid having to deal with hourglass control. They state that the use of the constant stress element is not an option. They also state that the S/R element is more accurate than the constant stress element.	- The constant stress element *is* an option. - 25-years of experience with the constant stress element in analyses as demanding as roadside safety applications proves that it is an option. - The S/R element has the well-known shear-locking problem and is not even recommended by LSTC. - The S/R element is not more accurate. - In any event, this is not a soil model issue.	No	No
Shooting Nodes	The direct shear test simulation stops (fails) because of shooting nodes. The user believes that the instability is associated with the material parameters, damage algorithm, and/or element formulation.	- The developer believes that the instability results from conditions for element deletion occurring at only one of the 8 gauss points of the S/R element. Sudden deletion of a loaded element causes dynamic oscillations that overload elements. If element deletion resulting from failure conditions at 1 gauss point is the problem, LSTC must consider how element deletion in LS-DYNA should be treated for the S/R element. - This instability does not occur if the constant stress (a single gauss point) element is used.	No	No
Mesh Refinement	The user tried the constant stress element and mesh refinement in the direct shear test simulation. Upon using mesh refinement, they encountered a soil-test fixture contact surface instability.	- The developer guesses that the instability is probably the same as that observed in the wood model studies that found that the controlling time step for a stable analysis was sometimes determined by contact surface stability requirements instead of the smallest element wave transit time. An analyst must be aware that several factors contribute to stable time-step selection.	No	No

Table 16. Developer's response to user's soil model evaluation (continued).				
Issue	**User's Comment**	**Developer's Response**		
			Soil Model Problem?	Adjust Soil Input?
Large Deformation Techniques	The user states that it is possible to implement a material model that handles very large deformations. They show an analysis with material type 126 (a modified honeycomb model) to illustrate their point.	- The large deformation honeycomb model analysis presented is entirely irrelevant with respect to the soil direct shear test simulation. The latter involves material failure, separation, and development of a sliding interface, while the honeycomb example only illustrates crushing of a material block without generation of new material surfaces or significant shearing. Material type 126 is essentially just large springs (see note 4 in the SECTION_SOLID chapter of the LS-DYNA manual). ALE could be available for the soil material model if LSTC elects to allow it.	No	No
Angle of Internal Friction	Counter to conventional soil mechanics theories, the soil model predicts an increase in shear force with a decreasing angle of internal friction.	- This is not true for soil mechanics theories that involve strain softening. The amount of dilation (volume expansion) increases for a constant strain increment as the angle of internal friction increases. Strain softening (damage) is dependent on the dilation (i.e., as the dilation increases, so does the damage). Therefore, more damage occurs as the angle of internal friction increases. This increase in damage causes the apparent decrease in shear force as the angle of internal friction increases. The implication of these dependencies is that the damage input parameters must be changed in conjunction with the value of the internal angle of friction.	No	No

Table 16. Developer's response to user's soil model evaluation (continued).				
Issue	**User's Comment**	**Developer's Response**		
			Soil Model Problem?	Adjust Soil Input?
Range of Applicability	The user maintains that the soil material model is only applicable for small displacement problems.	- Not true. The soil model handles large deformations. Single element runs in shear show that the soil model accommodates shear strains greater than 100 percent. Shear deformations in the user's direct shear test simulation *are* large deformations (about 100-percent shear strain). - The user apparently believes that their direct shear test simulations show that the soil model works only for small displacements. The fundamental problem is that their finite element model of the direct shear test is faulty since it makes no provisions for the development of a sliding surface between the two soil volumes. This interface controls 80 percent of the measured response that the user says it wishes to simulate. - The soil model is a continuum model that should predict material failure and separation. It should not be expected to create sliding surfaces as well.	No	No
Measuring Model Parameter Values	The user is unaware of physical testing or theoretical means for determining values for model parameters Eccen, A_n, E_t, Pwd2, Pwksk, Vdfm, Dint, Damlev, Epsmax.	- There are data for some of the mentioned parameters in the literature (Eccen, Pwksk). As mentioned in the soil model manual, the author is not aware of any damage theory or damage data for soils. The parameters for damage (Vdfm, Dint, Damlev, epsmax) must be set based on user experience. The other parameters are obtained using laboratory test data (e.g., the triaxial compression test (see figure 6) provides data from which parameters A_n and E_t can be obtained).	No	No

Table 16. Developer's response to user's soil model evaluation (concluded).				
Issue	**User's Comment**	**Developer's Response**		
			Soil Model Problem?	Adjust Soil Input?
Plasticity Iterations	The user is unable to determine if there is a convergence criterion for plasticity iterations.	- There is no user-accessible convergence criterion. There is an internal convergence criterion similar to that used by other LS-DYNA material models (e.g., see models 25, 78, 79, etc.).	No	No
Moisture Effects	Treatment of these is not operating correctly.	- Treatment of moisture content *is* operating correctly. The moisture content determines how pressure and shear strength are calculated. (This formulation was fixed when the problem with the value of the Spgrav parameter was fixed.)	No	No
Pore-Water Effects	These are not really available for evaluation. What are the criteria for the decay of pore pressure relative to the pressure in the soil fabric? Pore-water pressure should be allowed to become negative. How is dissipation dealt with?	- Pore-water effects *are* available; however, test data are lacking for setting parameter values. - Decay of pore-water pressure relative to the soil fabric requires the modeling of fluid flow. Fluid flow (dissipation or mass transfer of water from element to element) is not implemented. No data is available for road base soil to develop a model for fluid flow. - Pore-water pressure can become negative. (The statement in the soil model manual that prompted this comment was restated.) - The excess pore-pressure method in the soil model does not include dissipation of excess pore pressure as a function of time. The rate of dissipation can be a function of loading rate and soil parameters, such as permeability. However, lack of experimental data for the road base material on typical roadside tests makes such a dissipative model useless. However, if data and required parameters for roadside tests become available, then a dissipative model could be easily inserted.	No	No

ITEMIZED SOIL MODEL TOPICS

In this section, the developer discusses two of the more substantive issues raised by the user.

Issue 1: Model Will Not Run to Completion

The developer believes that the user made this statement because they found that their simulation of a direct shear soil test did not run for the entire range of displacement observed in the test.

It is the opinion of the developer that the soil model performed correctly in this direct shear test simulation and no considerable action is required to "fix" the soil model.

In the direct shear test, two metal cylinder halves containing a continuous soil volume are moved diametrically with respect to each other. Initially, the soil in one cylinder half interacts with that in the other at the continuous soil interface between the two. At first, the force needed to move the two halves of the test apparatus increases steadily up to a peak (as seen in figure 3 of this soil evaluation report). Then, as the soil in the interface region undergoes significant straining, it begins to sustain damage (causing it to soften) and its ability to resist continued displacement of the two cylinder halves decreases, leading to a significant decline from the peak value in the force needed to drive the displacement. Finally, once strain (or damage) is sufficiently great, the soil in the interface region separates (or fractures). From then on, the two soil halves interact only by sliding with friction against each other over the newly formed interface between them. In this part of the direct shear test, the force required to continue driving the displacement gradually decreases as the contact area between the two soil halves decreases. This last phase of the response can be seen in figure 3, starting at around 40 mm of displacement.

The soil model is a continuum mechanics material model. It is designed to model the material response of the continuous soil material. Upon being used in the direct shear test simulation, it should predict the initial increase of the driving force in the experiment to peak value and the decrease of the force as the soil sustains damage. The soil model did this in the user's simulation (as seen in figure 6). It should also indicate material damage and separation (fracture) at the same force-displacement point observed in the experiment. The developer thinks that the soil model would have done this in the direct shear test simulation if the damage parameters had been properly adjusted.

It is the job of the soil model to handle the portion of the simulation up to the point of material separation. The soil model is not responsible for treating the phase of the test (involving most of the force-displacement history in figure 3) in which two soil volumes interact principally through frictional contact as they slide with respect to each other. Such interaction typically is simulated in finite element analyses using sliding interfaces, or sliding surfaces, with friction. The user's finite element model simulation of the direct

shear test does not provide for this sliding interface; so, fundamentally, the user's simulation is completely incapable of representing the force-displacement response once soil fracture occurs and the sliding interface between the two soil halves is created.

Ideally, the soil model would create new finite elements or, at least, element faces at the newly created fracture surface that could be used during computational run time to add a sliding interface to the direct shear test analysis model. It does not. To the developer's knowledge, no existing material model does this for three-dimensional applications.

Issue 2: Hourglass, ALE, and Element Choice

The user's soil model evaluation touches upon several issues that we collectively refer to here as the issue of "Hourglass, ALE, and Element Choice." Claiming that it is more accurate than the constant stress (1 gauss point) element, the user recommends the use of the fully integrated (8 gauss point) element in conjunction with the soil model. The user recommends using artificially reduced soil stiffness values to counter the well-known excessive stiffness of the fully integrated element. The user also suggests that use of ALE might be helpful in alleviating perceived soil model performance shortcomings.

It is the developer's opinion that these issues have nothing to do with evaluation of the soil model, nor are any of these issues material model issues. No action with respect to the soil model is required to address these issues.

The bold statement that the fully integrated element is more accurate than the constant stress element is unsubstantiated and, in fact, incorrect. The user likes the fully integrated element because it enables them to avoid dealing with hourglass control. However, to use the fully integrated element, the user recommends arbitrarily decreasing (i.e., "tweaking") soil stiffness properties to improve correlations obtained when using the element type. Hence, the recommendation is to use non-physical material properties in all analyses with the soil model. In contrast, the developer recommends the use of actual material properties, the constant stress element, and hourglass control.

Neither the developer nor the user had an opportunity to evaluate the soil material model in conjunction with ALE. By bringing up ALE in their soil evaluation study, the user seems to be suggesting that it might help their direct shear test simulation to run to completion. Since the principal deficiency with the simulation model is its failure to offer any provisions for handling a newly created sliding interface between the soil halves, ALE, of course, is not a solution.

ADDITIONAL EVALUATION TOPICS

Material Input Parameter Study

The error with Spgrav has been fixed. This parameter is used to determine the initial volumetric strain associated with the air voids. The output for the material input variable spgrav has been changed to show "initial air voids" (the volumetric strain of the initial air voids), which is calculated from the input variables Spgrav, Rhowat, Rho, and Mcont. This calculated parameter is used in the simulation of pore-water pressure effects (moisture content effects). At this time, there is no data available for road base materials to determine the input parameters needed to simulate the pore-pressure effects. They may be determined by the testing of drained and undrained test specimens.

Angle of Internal Friction: Damage and Dilation

On page 23, the comment, "This result is counter to conventional soil mechanics theories" is *only correct* if there is no strain softening (damage). The amount of dilation (volume expansion) increases for a constant strain increment as the angle of internal friction increases. The strain softening (damage) is dependent on the dilation (i.e., as the dilation increases, so does the damage). Therefore, more damage occurs as the angle of internal friction increases. This increase in damage causes the apparent decrease in shear force as the angle of internal friction increases. The implication of these dependencies is that the damage input parameters must be changed in conjunction with the value of the internal angle of friction.

Modified Yield Surface

Figure 12 is somewhat misleading. The modified yield surface (hyperbolic approximation) cannot be set outside the Mohr-Coulomb yield surface. Since the parameter *Ahyp* is squared in the yield function (see equation 14), it is always the absolute value. This behavior is shown in table 9 between test T16 and the baseline. Hence, there is no need to place a check on *Ahyp* to make sure that it is always equal to or greater than zero (see the conclusions on page 49). A caution possibly should be added to this section: "The input parameter *Ahyp* should not be set so large that the initial stress state lies outside the modified Drucker-Prager surface (hyperbolic approximation surface)."

Iterations Parameter

On page 29, in the discussion of the itermax parameter, it should be noted that the radial return method is used if itermax is set to 1. However, the radial return method is not accurate when strain softening is invoked or the yield surface is not smooth. There is a convergence tolerance for determining if the plastic stress state is close to the yield surface.

DS-4 Simulation Instabilities

The instabilities in the DS-4 simulation are caused by a combination of the strain softening/erosion used in the material model and the element formulation. The FHWA soil material model includes strain softening (damage); once the element has been fully damaged, the model sets a flag to erode (eliminate) the element. This must be done because, at full damage, the element has no stiffness (internal forces). In the current version of LS-DYNA, the S/R solid element (8 gauss integration points) is eroded when the first gauss point is fully damaged. However, there are still internal forces associated with the eroded element because the other gauss points are not fully damaged. When the element is eroded, these internal forces are suddenly eliminated. This causes large unbalanced forces at the nodes of the eroded element, which, in turn, cause the shooting nodes behavior mentioned in this report. If damage/erosion of elements is not used because of this problem in the current version of LS-DYNA, then the well-known shear locking behavior dominates the simulation. The shear locking behavior manifests itself when the elements have large distortions (see note 4 for the *SECTION card in the LS-DYNA user's manual). The use of ALE may be used to overcome these problems. However, at long simulation times, the analysis becomes a simulation of almost two separate bodies separated by a slide surface with friction, which is not really a test of the FHWA soil material model.

Determining Input Parameter Values

In many areas of the report, it is mentioned that the authors where unaware of any physical testing or theoretical means for determining the input parameters. In some of these cases, there are direct means (e.g., the Eccen parameter (see figure 2 of the soil model user's manual)).[(2)] For other cases, indirect methods, such as parameter fits, will need to be made using the material model. An example of this would be to use drained and undrained triaxial compression tests to determine the pore-water effects. In a few cases, there exists no theory. This is the case for the parameters involving strain softening (damage). With other materials, such as steel, concrete, and wood, there are parameters based on theory (fracture energy). To the developer's knowledge, such a theory does not exist at this time for soil. As mentioned in the soil model user's manual,[(2)] a method was developed for the FHWA soil material model that is similar to the fracture energy theory used for other materials. A second example of limited theory is pore-water (moisture) effects. To fully take into account the effects of pore water, a coupled fluid flow, solid mechanics analysis method is needed. However, the FHWA soil model makes an assumption that the soil deformation times are much shorter than fluid flow though the soil. Therefore, the moisture content (and other input parameters) is assumed to be constant for the simulation times used in vehicle impacts.

DIRECT SHEAR TEST SIMULATION

The user claims that the soil material model does not perform correctly in their direct shear simulation. This is a test in which two metal cylinder halves filled with soil are slid with respect to each other, resulting in shearing of the soil volume. Looking at the force

predicted in their simulation as required to drive the deformation, the user states “the force builds up nicely” (peaking at a value close to the experimental data); next, “the soil begins to soften, as it should, until it reaches a valley at 24.6 mm of displacement”; and then, “the force begins to rise, which never occurs in physical tests.” They claim that this means that the soil material model does not perform correctly. It is believed that this is the example analysis leading to the statement that the soil model “will not run to completion.”

The user’s assessment of the performance of the soil material model in their direct shear simulation is erroneous. They appear either to have not thought out in detail the nature of the soil response in the direct shear test (and how to prepare a simulation capable of capturing that response) or are exhibiting a considerable misunderstanding of what is to be expected from continuum mechanics material models (of which the soil model is a member). Justification of these observations is provided in the following paragraphs.

Soil response in the direct shear test occurs in two phases. During the first phase, even though half the soil tends to move in one direction and the balance in the opposite direction, the block of soil maintains its continuity. The material experiencing the greatest stress and strain is localized chiefly in a narrow region of the soil volume between the oppositely moving soil halves. The material in this narrow region sustains increasing strain as the direct shear test proceeds until material separation occurs and an interface develops between the two soil halves. Once this happens, the second phase of the direct shear test response begins. In this phase, the physical situation is best described as one-half of the original soil volume interacting with the other half only by sliding over the newly formed soil interface. However, the key point is that, in the second response phase, soil volumetric material response is no longer a controlling factor in how much force is required to continue displacement in the direct shear test. Instead, it is the frictional force acting over the interface between the two soil halves that correlates to the force needed to continue the shearing process.

What does all this mean with respect to the FHWA soil model and how it performs in the direct shear simulation? There are two parts to the answer to this question. First, since the soil material model is a continuum model, for it to be useful, it must be able to correctly model the first phase of the direct shear test response. That is, it should accurately predict stresses developed throughout the entire soil volume, particularly in the transitional region between the two halves of the oppositely moving soil. It should predict the increase of stress up to some maximum and then the decrease of stress as the material softens because of damage. Finally, it should support separation or failure of the material if the strain exceeds levels for which the soil can remain in one piece. Second, again, since the soil model is a continuum model, it should not and cannot be viewed as the only part of the direct shear test simulation responsible for predicting the second phase of the response. As described above, this is dominated by the interaction across the interface of the two oppositely moving soil volumes. In analysis codes such as LS-DYNA, this sort of interaction is modeled using what are known as sliding

interfaces. In this case, a sliding interface with friction would seem to be most appropriate. Such interaction is not handled by a material model.

Based on a comparison of the direct shear simulation results obtained by the user using the FHWA soil model (figure 6) with the direct shear test results that they were attempting to model (figure 3), it appears that the FHWA soil model accurately correlates with the peak force and the displacement associated with that force as measured in the tests. The model also appears to soften accurately over an appropriate displacement range before it erroneously begins to harden again. Thus, it appears that the soil material model did not predict the fracture as it should have, although it otherwise correctly treated the first response phase of the direct shear test. Its failure to predict "failure" in this simulation is probably attributable to the inappropriate specification of material damage parameters. It is not evidence that there is a problem with the soil material theory or its computational implementation.

Even if the soil material model (with the parameters used by the user in their direct shear test simulation) had correctly predicted material failure, the user would have failed to obtain good correlation with the test results for large displacements. This is because the analysis model (i.e., the entire finite element model) that they used is incapable of simulating the second phase of the direct shear test response. A sliding interface or surface is needed to do this. The soil material model is not designed to create one. (No material models in LS-DYNA are designed to do so!)

The user states (page 30) that they would like "to correctly handle the direct shear test up to 100 or 200 mm of deflection, rather than only 25 mm in the current implementation." That being the case, the user will need to develop a better simulation model (i.e., the entire finite element model) of the test and obtain a far better understanding of what to expect from and how to use continuum material response models before they are likely to reach their goal. The user presents LS-DYNA material type 126 (modified honeycomb material) as an example of a material model that can handle very large deformations. They show an analysis example (figure 20) in which this model simulates extreme crushing of a material without presenting any analysis difficulties. They infer that a useful soil model must be able to do the same. While this is interesting, it is entirely irrelevant since the material crushing example involves only the deformation of a continuous material without the complication of material separation such as must occur in the direct shear test. To make the material crushing example relevant to the direct shear test simulation, punch-crushing the material in the former example would have to shear a hole into the crushing material rather than just crush it without causing development of new material surfaces.

MATERIAL MODEL PARAMETERS, HOURGLASSING, AND ELEMENT CHOICE

The user performed an interesting evaluation of the material parameters used by the soil model. They pointed out some problems with a few of the developer's recommendations for parameter values; confirmed some of the other values by references to the literature; offered some good insight as to the care needed in

obtaining values for other model parameters; and accurately noted that it is difficult, or impossible, to specify a particular test to measure some of the parameters. Sophisticated material models often contain some parameters whose values are not directly measurable, but may be inferred through correlations with test data.

The user also states: "One of the most difficult tasks associated with finite element modeling is the selection of appropriate material properties to accurately represent physical behavior. This has led to, in many cases, the arbitrary 'tweaking' of models by matching simulation results to a known physical test, sometimes without regard to the reasonableness of the material input variables." The reason that this quotation is of note becomes apparent when considering the user's recommendation (page 43) that "it is recommended that element formulation 2" (fully integrated) "be used with the soil material model." The principal alternative to using the fully integrated element is the under-integrated element.

The user's objection to the under-integrated element is that it can suffer from hourglassing. There are perfectly legitimate ways for controlling hourglassing, and the defense community has used them and the under-integrated element almost exclusively for more than 20 years. Hourglassing is understood and the control methods work. Of course, more than a beginner's understanding of finite element technology is required to correctly use hourglass control.

The obvious problem with fully integrated elements is that they are too stiff. What is the user's recommendation for counteracting this deficiency? Consider what they write in the Conclusions and Recommendations section (page 49): "reasonable bulk and shear moduli for a 'sand and gravel' would be *K* = 80.5 MPa (0.0805 GPa) and *G* = 48.3 MPa (0.0480 GPa), respectively." Then, "However, these values yield an overly stiff response with the FHWA soil model. Suggested values are significantly lower" (by more than a factor of 10). This recommendation flies in the face of the implied condemnation of "arbitrary 'tweaking'" noted above. Obviously, the excess stiffness is a problem brought to the table by the element choice and not a consequence of the material model.

USER'S MANUAL QUESTIONS AND ANSWERS

The following questions were posed by an expert in soil mechanics from the user's team and were answered by the developer. The questions were posed by the user following a review of the developer's *Manual for LS-DYNA Soil Material Model 147*.[2] The questions resulted in changes to the soil model where appropriate.

Question 1:

In assessing damage, you set $d_{\max}$ as a function of the angle of internal friction (φ) of the soil and the residual angle of internal friction (φ_{res}). Typically, this residual angle of friction is a quantity representing the relationship between the normal force and the shear strength on a plane after a significant amount of shear displacement. For

noncohesive materials, this angle can be significantly lower than the initial φ. Soil in shear can maintain the residual strength for very large displacements (i.e., 0.8 kilometer (km) (0.5 mile (mi))). It is not clear to me how this limiting value of damage affects the large strain situations. Is it that we use φ_{res} after this damage parameter is reached? As soils experience higher triaxial stresses, the effective φ can become quite small, but the shear strength remains constant relative to the deviator stress. How does this fit into the current damage scheme?

Answer 1:

The maximum damage allowed is related to the internal friction angle of residual strength by:

$$d_{\max} = \frac{\sin\varphi - \sin\varphi_{res}}{\sin\varphi} \tag{25}$$

If $\varphi_{res} > 0$, then $d_{\max}$, the maximum damage, will not reach 1, and the soil will have residual strength.

The damage parameter is used to reduce the effective internal stress $\sigma = (1-d)\overline{\sigma}$. If the damage parameter d is allowed to go to 1, then the internal stress is zero, which for a finite element code such as LS-DYNA (explicit) causes the internal forces (element stiffness) to become zero. By not allowing the damage parameter d to become 1, this keeps a residual stiffness in the element. Setting $\varphi_{res} > 0$, $d_{\max}$, the maximum damage, will not reach 1, and the soil will have some residual strength (the strength will not go to zero). If the strains continue with approximately the same behavior, the effective internal stresses will be almost constant. However, if the strains drastically increase or decrease, then the effective internal stresses can change, because $\overline{\sigma}$, the undamaged stresses, are changing drastically. Or stated differently, if the strains stay well behaved and the normal forces stay constant, the residual shear strength will stay almost constant.

Question 2:

You state in your report that dilation of the soil signals a loss in friction between the particles that you represent by reduction of effective modulus. Any noncohesive soil undergoing shear needs to dilate to allow the particles to move around each other. It is not clear to me how this represents a loss of friction.

Answer 2:

This statement is somewhat confusing. The statement is based on data shown in *Geotechnical Engineering* by Holtz and Kovacs. They show data for dense sand (in a triaxial test) where the void ratio sharply increases as the peak stress is reached and continues to increase to a maximum value as the stress declines. For this data, the

void ratio was determined by the increase or decrease of the volume of the sand specimen. Therefore, an increase in the void ratio can be interpreted as dilation (i.e., the dilation sharply increases as the peak stress is reached). We needed to use a strain value (volumetric strain) to implement the damage criterion algorithm because strain increments are the basic measurement in LS-DYNA. To avoid confusion, the statement has been changed to:

> "When $\varepsilon_{pv} < 0$, the soil is dilating, which in turn signals a loss of strength. The loss of strength is represented by the reduction of the effective moduli."

Question 3:

In determining excess pore pressure, I do not understand how the dissipation is dealt with in your model. Generation of excess pore pressure in noncohesive soils is a very load- and dissipation rate-dependent phenomena. I do not see any permeability or tortuosity measures indicating parameters for dissipation.

Answer 3:

The excess pore-pressure method in the soil model does not include the dissipation of excess pore pressure as a function of time. The rate of dissipation can be a function of loading rate and soil parameters, such as permeability. However, at this time, the lack of experimental data on road base material on typical roadside tests would make this type of dissipative model useless. However, if experimental data and required parameters for roadside tests become available, then a dissipative model could be easily inserted.

We believe that in most test reports of roadside safety tests that we have seen, moisture content and in situ void ratio are not reported. The void ratio can greatly change the basic strength of a given soil. Also, the void ratio is highly dependent on the amount of compaction. The parameters, such as permeability and tortuosity, are greatly dependent on the void ratio. We have tried to restrain the number of input parameters in the model that are difficult or impossible to obtain.

Question 4:

You state that the pore pressure is not allowed to become negative. In noncohesive soils, negative pore pressure can have profound effects on effective stress because of both capillarity and dilation during shear. I do not think that it is appropriate to set this constraint.

Answer 4:

The statement has been changed to:

> "The increment of pore-water pressure is zero if the incremental mean strain is negative (tensile)."

This new statement is more descriptive of the actual coding used in the routine. See the equation for the pore-pressure effects on the bulk modulus on page 9 of the soil model user's manual.[2]

Question 5:

Your simulation of a direct shear test ends after about 40 to 50 mm of shear deflection. From the standpoint of deflections that we need to model, this is just getting to the interesting range. Is there a reason that you terminated the run at this short duration?

Answer 5:

LS-DYNA terminated the run at this time because of a known problem with how the element deletion algorithm is implemented for 8 gauss point brick elements. This was explained in the soil model user's manual[2] on page 42.

We believe that the analysis after about 50 mm of deflection is not a test of the soil model, but requires a slide surface to correctly model discontinuous behavior of the two halves of the cylinder. As shown in figure 5, there are surfaces of the soil that start in contact with the soil, and at the end time of the analysis, are in contact with metal or air. Also, the interface between the two cylinder halves has become a noncontinuous surface (i.e., a slide surface). A continuum mechanics material model cannot accurately model this behavior; it may be modeled by a combination of tied/slide surfaces.

APPENDIX A. INITIAL SOIL EXPERIENCE OF USER

The soil material model using the Nebraska soil parameters provided by the developer do not accurately simulate the physical testing (as shown in the following figures).

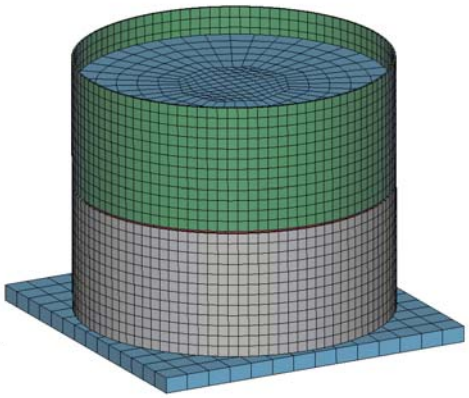

(a) Initial condition.

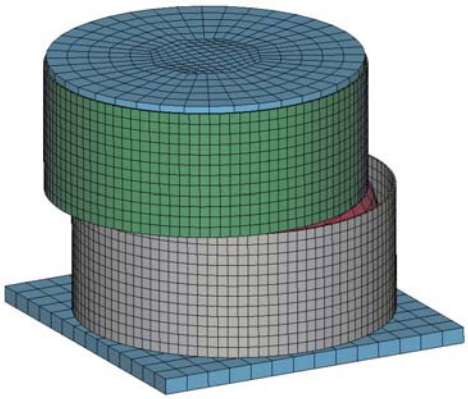

(b) Soil deforms uncharacteristically.

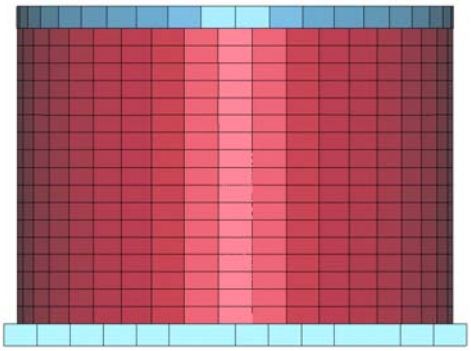

(c) Side view.

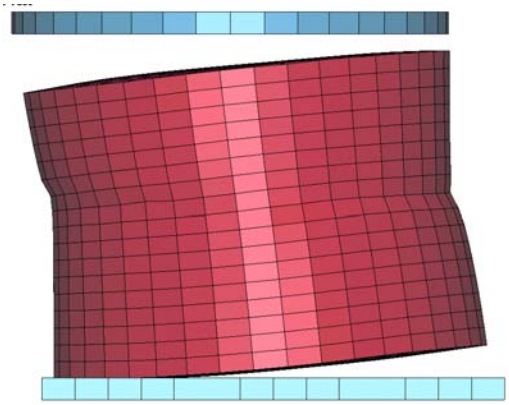

(d) No "shear" across soil as seen in physical testing.

Figure 23. Direct shear test.

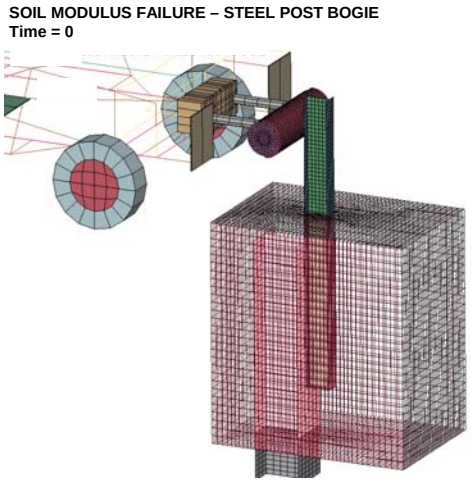

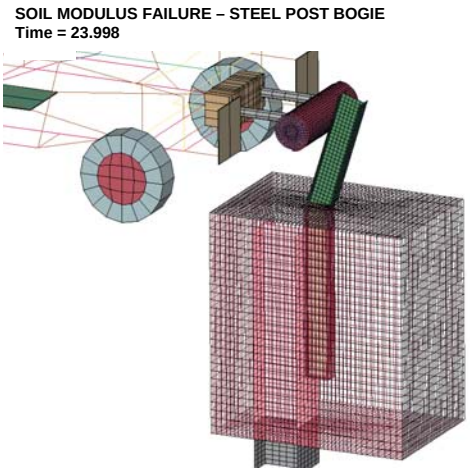

Simulation: Post bends in soil.

(a) 0 msec.

Physical testing: Post rotates in soil.

(b) 24 msec.

Figure 24. Soil modulus failure test.

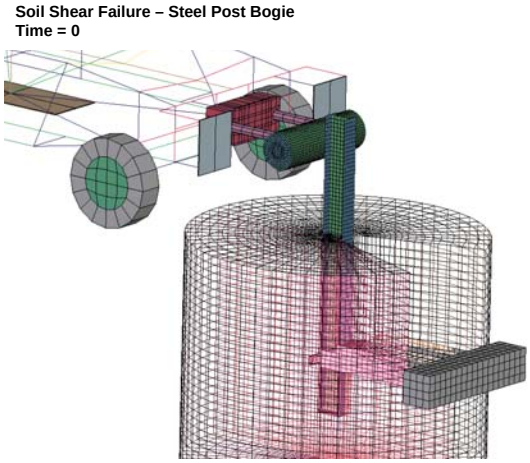

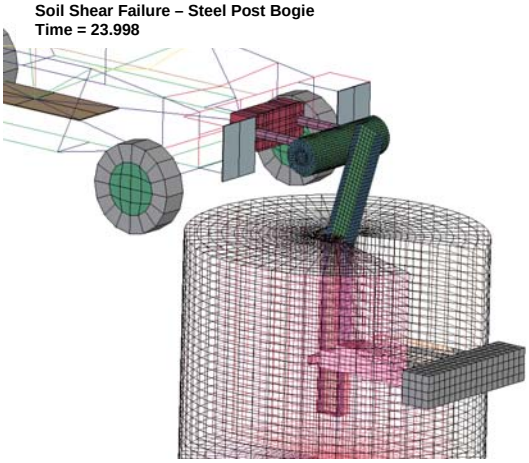

Simulation: Post bends in soil.

(c) 0 msec.

Physical testing: Post rotates in soil.

(d) 24 msec.

Figure 25. Soil shear failure test.

APPENDIX B. VERIFICATION OF RESULTS ON DIFFERENT COMPUTER PLATFORMS

Using different computer platforms, a comparison of three different models using the FHWA soil model in LS-DYNA is made. Results from an Intel®-based PC (using Windows) are provided by both the developer and the user, while UNIX-based results from an SGI Octane® (using UNIX) are provided by the user.

The user's SGI results were obtained using LS-DYNA, Version 970 Beta, Revision 1812, June 7, 2002, for an SGI Workstation IRIX64 6.5.

The developer's PC results were obtained using LS-DYNA, Version 970 Beta, Revision 1812, June 7, 2002, for a PC (Intel) Windows 2000.

Although the results are shown to be different in the latter stages of the simulations on the different computer platforms, they appear to be within an acceptable range based on previous experience with using different computers.

SINGLE ELEMENT MODELS

Two single element models were run to check the consistency between the PC (Intel)-based computers and the SGI-based computers. Specific results for each model are described below. The developer supplied only the d3plot files from these runs; thus, the comparison is limited to the information stored in those files.

The deformed geometry of the single element models appeared to be the same and, thus, are not shown.

Model hydten1: Hydrostatic Tension

The internal energy for the hydrostatic tension runs are shown in figure 26. The results are nearly identical until 35 ms. After 35 ms, the results for the SGI and PC begin to diverge. There was no discernible difference between the developer's PC and the user's PC results. The difference between the SGI and PC results after 35 ms is attributed to the significant plasticity that the element has undergone after that time. Once plasticity becomes great enough, round-off errors between the computer platforms begin to influence the results. This, however, is only conjecture.

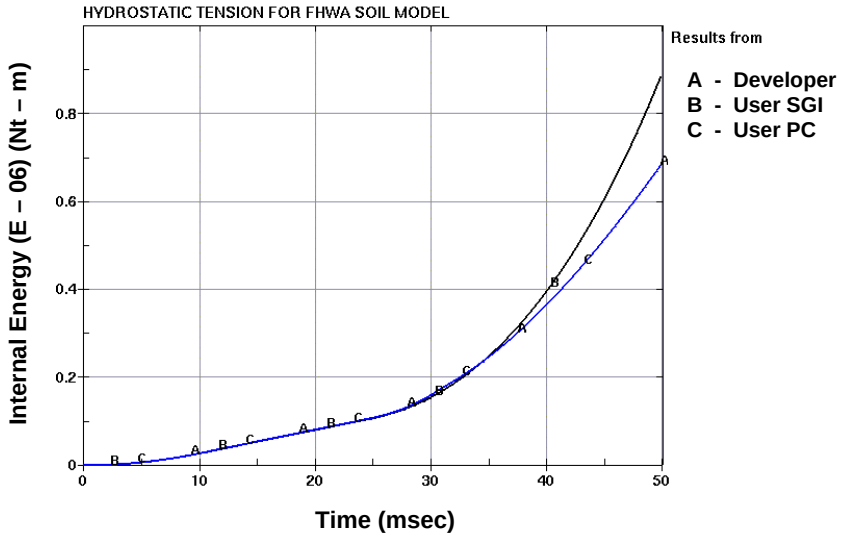

Figure 26. Hydrostatic tension: Internal energy.

Model txc3-4pr0c.k: Triaxial Compression

The internal energy and effective stress for the triaxial compression runs are shown in figures 27 and 28. The results are nearly identical, with the exception that the single element in the user's SGI run fails a few cycles before the PC runs.

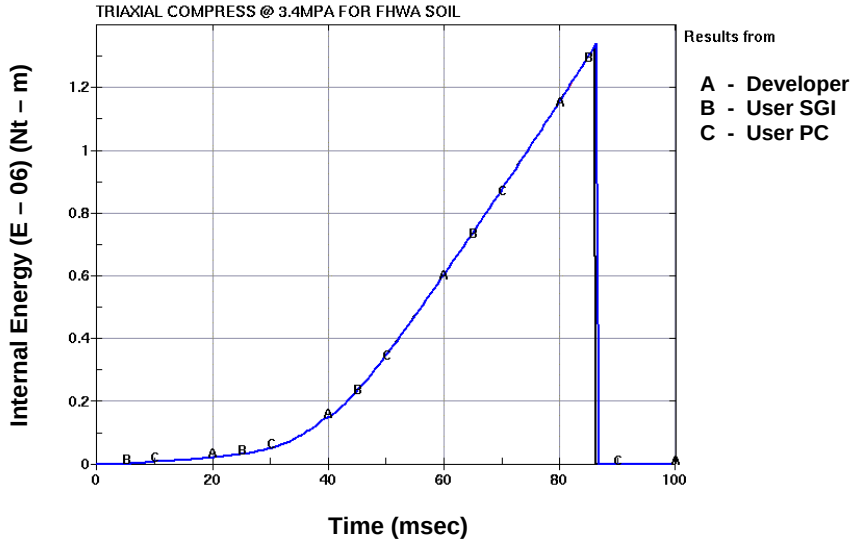

Figure 27. Triaxial compression results: Internal energy.

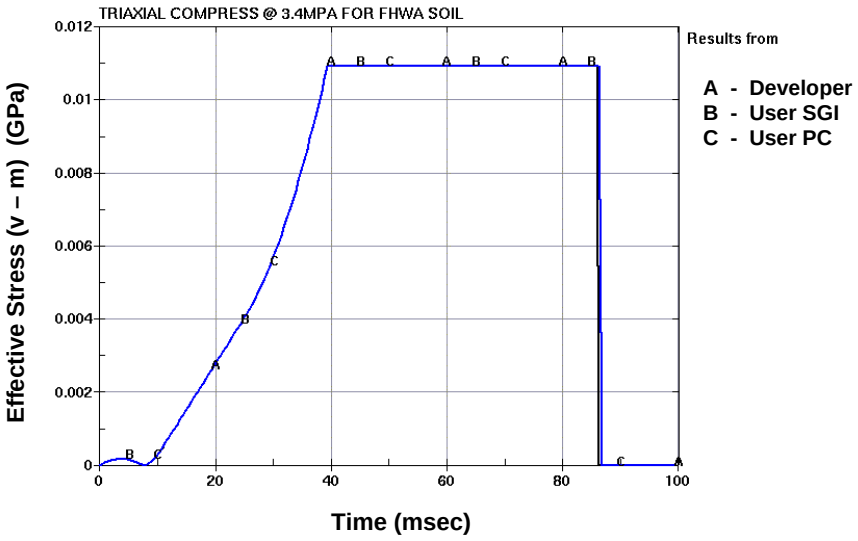

Figure 28. Triaxial compression results: Effective stress.

MULTI-ELEMENT CYLINDER: TRIAXIAL COMPRESSION TEST

This model is a multi-element cylindrical model of a triaxial compression test. The constant-stress solid element formulation is used in this model. As evidenced in figures 29 through 31, the results from the developer's computers match the results from the user's computers very well for the first 260 ms of simulation. After that time, elements begin to fail and the results start to diverge. The elements in the SGI run begin to fail and the model becomes unstable a few milliseconds before the PC results. Overall, agreement between the results appears to be acceptable.

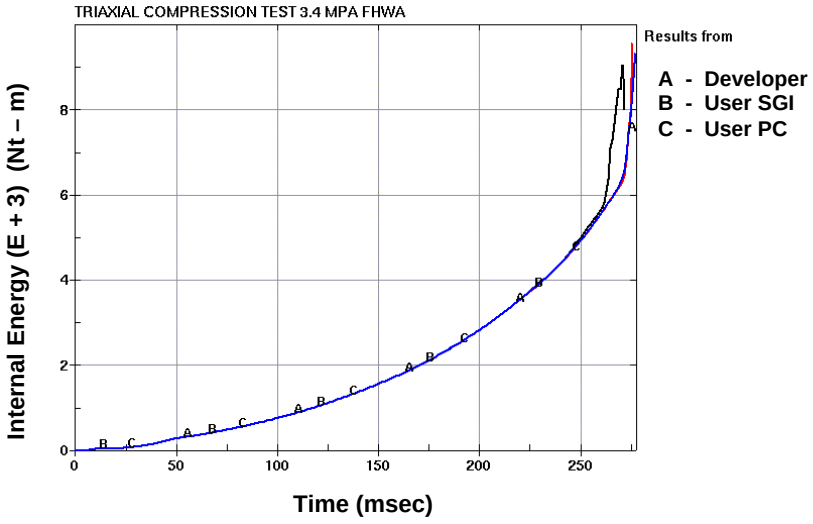

Figure 29. Internal energy.

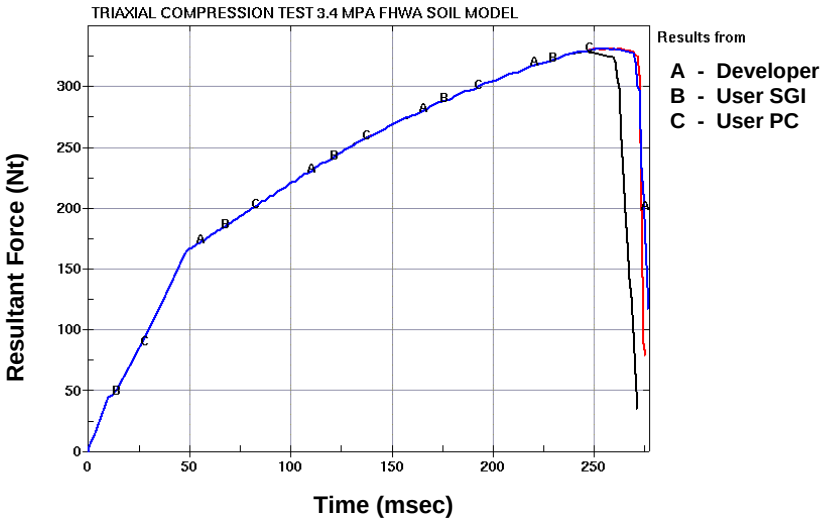

Figure 30. Cross section force through cylinder.

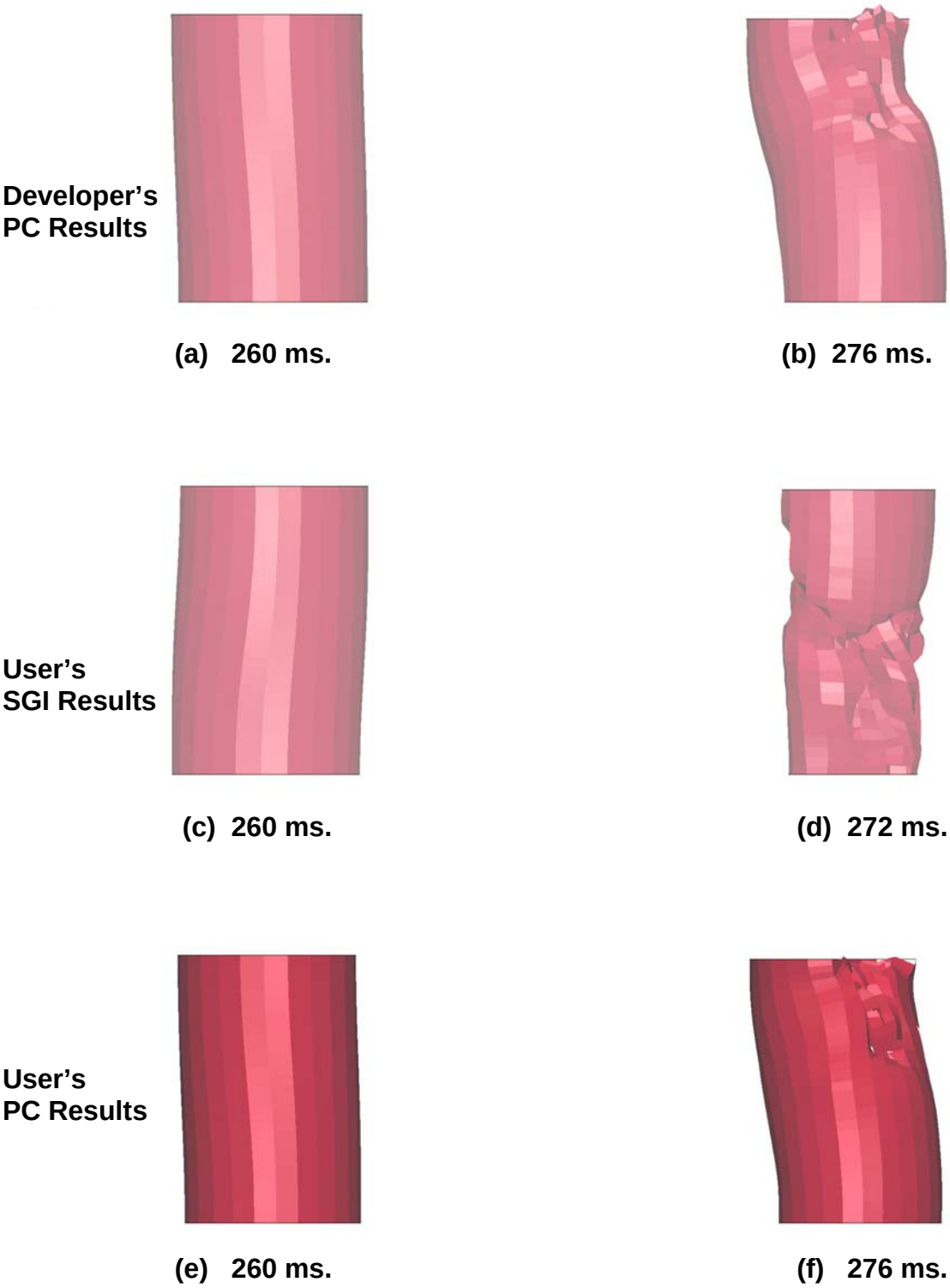

Figure 31. Deformed geometry.

REFERENCES

1. Hallquist, J.O., *LS-DYNA Keyword User's Manual, Version 960*, Livermore Software Technology Corporation, Livermore, CA, March 2001.

2. Lewis, B.A., *Manual for LS-DYNA Soil Material Model 147*, Report No. FHWA-HRT-04-095, Federal Highway Administration, November 2004.

3. Murray, Y.D., *Manual for LS-DYNA Wood Material Model 143*, Report No. FHWA-HRT-04-097, Federal Highway Administration, to be published in 2005

4. Murray, Y.D., and J.D. Reid, *Evaluation of LS-DYNA Wood Material Model 143*, Report No. FHWA-HRT-04-096, Federal Highway Administration, to be published in 2005.

5. Coon, B.A., *Dynamic Testing and Simulation of Guardrail Posts in Soil*, M.S. Thesis, University of Nebraska at Lincoln, 1999.

6. Coon, B.A., J.D. Reid, J.R. Rohde, and J. Herr, "A New Shear Strength Testing Device for NCHRP Report 350 Strong Soil," Transportation Research Board (TRB) Paper 01-0412, 80th Annual Meeting of the Transportation Research Board, January 2001.

7. Ross, H.E., D.E. Sicking, R.A. Zimmer, and J.D. Michie, *Recommended Procedures for the Safety Performance Evaluation of Highway Features*, National Cooperative Highway Research Program (NCHRP) Report No. 350, Transportation Research Board, Washington, DC, 1993.

8. Nicholson, G.A., *Design of Gravity Dams and Rock Foundations: Sliding Stability Assessment by Limit Equilibrium and Selection of Shear Strength Parameters*, Technical Report GL-83-13, U.S. Army Corps of Engineers Waterways Experiment Station, Vicksburg, MS, 1983.

9. U.S. Army Corps of Engineers Waterways Experiment Station, Material Properties Query (MPQ) Database, Vicksburg, MS.

10. Das, B.M., *Principles of Geotechnical Engineering*, Fourth Edition, PWS Publishing, Boston, MA, 1998.

11. Zeevaert, L., *Free Vibration Torsion Tests to Determine the Shear Modulus of Elasticity of Soils*, Universidad Nacional de México, Proceedings Third Panamerican Conference on Soil Mechanics and Foundation Engineering, Paper 1-6, Vol. I, pp. 111-129, Sociedad Venezolana de Mecánica de Suelo e Ingenieria de Fundaciones, Caracas, Venezuela, 1967.

12. Penman, A., J.A. Charles, J.K. Nash, and J.D. Humphreys, "Performance of a Culvert Under Winscar Dam," *Geotechnique*, Vol. 25, No. 4, 1975, pp. 713-730.

13. Trautmann, C.H., and F.H. Kulhawy, *CUFAD—A Computer Program for Compress and Uplift Foundation Analysis and Design*, Report EL-4540-CMM, Vol. 16, Electrical Power and Research Institute, 1987.

14. Das, B.M., *Advanced Soil Mechanics*, Second Edition, Taylor & Francis, Washington, DC, 1997, p. 401.

15. Fiedler, S., C. Nelson, E.F. Berkman, and A. DiMillio, "Soil Stiffness Gauge for Soil Compaction Control," *Public Roads*, March/April 1998.

16. Mohr, O., "Welche Umstände Bedingen die Elastizitätsgrenze und den Bruch eines Materiales? [What Conditions Affect the Yield Surface and Failure of Materials]," *Zeitschrift des Vereines Deutscher Ingenieure* (Journal of the Society of German Engineers), Vol. 44, 1900 pp 1524-1530 and 1572-1577.

17. Coulomb, C.A., "Essai sur une application des regles de Maximums et Minimus á quelques Problèmes de Statique, relatifs á l'Architecture [Test on an Application of Rules of Maxima and Minima for Some Problems in Statics, Relative to Architecture]," *Memoires de Mathematique et de Physique, Présentés, Á l'Academie Royale des Sciences* [Transactions of Mathematics and Physics, Presented at the Royal Academy of Sciences], Paris, France, Vol. 3, 1776.

18. Terzaghi, K., *Theoretical Soil Mechanics*, Wiley, New York, NY, 1942.

19. Heyman, J., "Coulomb's Analysis of Soil Thrust," *Proceedings of the Institution of Civil Engineers, Geotechnical Engineering*, Vol. 131, No. 2, April 1998, pp. 83-88.

20. Schofield, A.N., "Terzaghi's True Cohesion Error," *Geotechnical News*, Vol. 17, No. 4, December 1999.

21. Taylor, D.W., *Fundamentals of Soil Mechanics*, Wiley, New York, NY, 1948.

22. Drucker, D.C., and W. Prager, "Soil Mechanics and Plastic Analysis in Limit Design," *Quarterly Applied Mathematics*, Vol. 10, 1952.

23. Abbo, A.J., and S.W. Sloan, "A Smooth Hyperbolic Approximation to the Mohr-Coulomb Yield Criterion," *Computers and Structures*, Vol. 54, No. 1, 1995.

24. Zimmermann, T., A. Truty, A. Urbanski, S. Commend, and K. Podles, "ZSOIL.PC: A Unified Approach to Stability, Bearing Capacity, Consolidation, Creep, and Flow for Two- and Three-Dimensional Simulations in Geotechnical Practice," White Paper, ZACE Services, Ltd., Lausanne, Switzerland, 2002.

25. Klisinski, M., *Degradation and Plastic Deformation of Concrete*, Ph.D. Dissertation (In Polish), Polish Academy of Sciences, (Institute of Fundamental Technology Research (IFTR) Works) Report 38, 1984.

26. Klisinski, M., and Z. Mroz, "Description of Inelastic Deformation and Degradation of Concrete," *International Journal of Solids and Structures*, Vol. 24, No. 4, 1988, pp. 391-416.

27. Schofield, A.N., and C.P. Wroth, *Critical State Soil Mechanics*, McGraw Hill, London, UK, 1968.

28. LeKarp, Fredrick, U. Isacsson, and A. Dawson, "State of the Art. I: Resilient Response of Unbound Aggregates," *Journal of Transportation Engineering*, January/February 2000, pp. 66-75.

HRDS-04/11-04(1M)E

Manual for LS-DYNA Soil Material Model 147

PUBLICATION NO. FHWA-HRT-04-095

NOVEMBER 2004

U.S. Department of Transportation
Federal Highway Administration

Research, Development, and Technology
Turner-Fairbank Highway Research Center
6300 Georgetown Pike
McLean, VA 22101-2296

Manual for LS-DYNA Soil Material Model 147

FHWA-HRT-04-095

November 2004

Federal Highway Administration
Research and Development
Turner-Fairbank Highway Research Center
6300 Georgetown Pike
McLean, VA 22101-2296

Foreword

This report documents a soil material model that has been implemented into the dynamic finite element code, LS-DYNA, beginning with version 970. This material model was developed specifically to predict the dynamic performance of the foundation soil in which roadside safety structures are mounted when undergoing a collision by a motor vehicle. This model is applicable for all soil types when one surface is exposed to the elements if the appropriate material coefficients are inserted. Default material coefficients for *National Cooperative Highway Research Program (NCHRP) Report 350, Strong Soil*, are stored in the model and can be accessed for use.

This report is one of two that completely documents this material model. This report, *Manual for LS-DYNA Soil Material Model 147* (FHWA-HRT-04-095), completely documents this material model for the user. The second report, *Evaluation of LS-DYNA Soil Material Model 147* (FHWA-HRT-04-094), completely documents the model's performance and the accuracy of the results. This performance evaluation was a collaboration between the model developer and the model evaluator. Regarding the model performance evaluation, the developer and evaluator were unable to come to a final agreement regarding the model's performance and accuracy. (The material coefficients for the default soil result in a soil foundation that may be stiffer than desired.) These disagreements are listed and thoroughly discussed in section 9 of the second report.

This report will be of interest to research engineers associated with the evaluation and crashworthy performance of roadside safety structures, particularly those engineers responsible for the prediction of the crash response of such structures when using the finite element code LS-DYNA.

Michael F. Trentacoste
Director, Office of Safety
Research and Development

Notice

Quality Assurance Statement

The Federal Highway Administration (FHWA) provides high-quality information to serve Government, industry, and the public in a manner that promotes public understanding. Standards and policies are used to ensure and maximize the quality, objectivity, utility, and integrity of its information. FHWA periodically reviews quality issues and adjusts its programs and processes to ensure continuous quality improvement.

Technical Report Documentation Page

1. Report No.	2. Government Accession No.	3. Recipient's Catalog No.
FHWA-HRT-04-095		

4. Title and Subtitle	5. Report Date
MANUAL FOR LS-DYNA SOIL MATERIAL MODEL 147	November 2004
	6. Performing Organization Code

7. Author(s)	8. Performing Organization Report No.
Brett A. Lewis, Ph.D.	

9. Performing Organization Name and Address	10. Work Unit No. (TRAIS)
APTEK, Inc. 1257 Lake Plaza Drive Colorado Springs, CO 80906	
	11. Contract or Grant No. DTFH61-98-C-00071

12. Sponsoring Agency's Name and Address	13. Type of Report and Period Covered
Volpe National Transportation Systems Center 55 Broadway, Kendall Square Cambridge, MA 02142-1093 Federal Highway Administration 6300 Georgetown Pike McLean, VA 22101-2296	Final Report 09-28-1998 through 08-31-2004
	14. Sponsoring Agency's Code

15. Supplementary Notes

Contracting Officer's Technical Representative (COTR): Martin Hargrave, Office of Safety Research and Development, HRDS-04, Turner-Fairbank Highway Research Center

16. Abstract

This is the final report for the development of the Federal Highway Administration's (FHWA's) soil model implemented into LS-DYNA. This report is in three sections: (1) the research plan, which describes the justification and the detailed theory of the model; (2) the user's manual that was submitted to Livermore Software Technology Corporation (LSTC) for inclusion in the LS-DYNA user's manual; and (3) examples that show the expected results of the model.

The companion report to this manual is:

Evaluation of LS-DYNA Soil Material Model 147 (FHWA-HRT-04-094)

17. Key Words	18. Distribution Statement
Soil, LS-DYNA, shear, elastic, plastic, damage roadside safety	No restrictions. This document is available to the public through the National Technical Information Service, Springfield, VA 22161.

19. Security Classif. (of this report)	20. Security Classif. (of this page)	21. No. of Pages	22. Price
Unclassified	Unclassified	68	

Preface

The goal of the work performed under this program, Development of DYNA3D Analysis Tools for Roadside Safety Applications, is to develop soil and wood material models, implement the models into the LS-DYNA finite element code, and evaluate the performance of each model through correlations with available test data.[1]

This work was performed under Federal Highway Administration (FHWA) Contract No. DTFH61-98-C-00071. The FHWA Contracting Officer's Technical Representative (COTR) was Martin Hargrave.

Two reports are available for each material model. One report is a user's manual, *Manual for LS-DYNA Soil Material Model* 147; the second report is a performance evaluation, *Evaluation of LS-DYNA Soil Material Model 147*.[2] The user's manual thoroughly documents the soil model theory, reviews the model input, and provides example problems for use as a learning tool. The performance evaluation for the soil model documents LS-DYNA parametric studies and correlations with test data performed by a potential end user of the soil model, along with commentary from the developer. The reader is urged to review this user's manual before reading the evaluation report. A user's manual[3] and evaluation report[4] are also available for the wood model.

The model developer and evaluator were unable to come to a final agreement regarding several issues associated with the model's performance and accuracy during the second independent evaluation of the soil model. These issues are listed and thoroughly discussed in section 9 of the soil model evaluation report.[2]

SI* (MODERN METRIC) CONVERSION FACTORS

APPROXIMATE CONVERSIONS TO SI UNITS

Symbol	When You Know	Multiply By	To Find	Symbol
		LENGTH		
in	inches	25.4	millimeters	mm
ft	feet	0.305	meters	m
yd	yards	0.914	meters	m
mi	miles	1.61	kilometers	km
		AREA		
in^2	square inches	645.2	square millimeters	mm^2
ft^2	square feet	0.093	square meters	m^2
yd^2	square yard	0.836	square meters	m^2
ac	acres	0.405	hectares	ha
mi^2	square miles	2.59	square kilometers	km^2
		VOLUME		
fl oz	fluid ounces	29.57	milliliters	mL
gal	gallons	3.785	liters	L
ft^3	cubic feet	0.028	cubic meters	m^3
yd^3	cubic yards	0.765	cubic meters	m^3
		NOTE: volumes greater than 1000 L shall be shown in m^3		
		MASS		
oz	ounces	28.35	grams	g
lb	pounds	0.454	kilograms	kg
T	short tons (2000 lb)	0.907	megagrams (or "metric ton")	Mg (or "t")
		TEMPERATURE (exact degrees)		
°F	Fahrenheit	5 (F-32)/9 or (F-32)/1.8	Celsius	°C
		ILLUMINATION		
fc	foot-candles	10.76	lux	lx
fl	foot-Lamberts	3.426	candela/m^2	cd/m^2
		FORCE and PRESSURE or STRESS		
lbf	poundforce	4.45	newtons	N
lbf/in^2	poundforce per square inch	6.89	kilopascals	kPa

APPROXIMATE CONVERSIONS FROM SI UNITS

Symbol	When You Know	Multiply By	To Find	Symbol
		LENGTH		
mm	millimeters	0.039	inches	in
m	meters	3.28	feet	ft
m	meters	1.09	yards	yd
km	kilometers	0.621	miles	mi
		AREA		
mm^2	square millimeters	0.0016	square inches	in^2
m^2	square meters	10.764	square feet	ft^2
m^2	square meters	1.195	square yards	yd^2
ha	hectares	2.47	acres	ac
km^2	square kilometers	0.386	square miles	mi^2
		VOLUME		
mL	milliliters	0.034	fluid ounces	fl oz
L	liters	0.264	gallons	gal
m^3	cubic meters	35.314	cubic feet	ft^3
m^3	cubic meters	1.307	cubic yards	yd^3
		MASS		
g	grams	0.035	ounces	oz
kg	kilograms	2.202	pounds	lb
Mg (or "t")	megagrams (or "metric ton")	1.103	short tons (2000 lb)	T
		TEMPERATURE (exact degrees)		
°C	Celsius	1.8C+32	Fahrenheit	°F
		ILLUMINATION		
lx	lux	0.0929	foot-candles	fc
cd/m^2	candela/m^2	0.2919	foot-Lamberts	fl
		FORCE and PRESSURE or STRESS		
N	newtons	0.225	poundforce	lbf
kPa	kilopascals	0.145	poundforce per square inch	lbf/in^2

*SI is the symbol for the International System of Units. Appropriate rounding should be made to comply with Section 4 of ASTM E380.
(Revised March 2003)

Table of Contents

List of Figures

List of Tables

CHAPTER 1. THEORY MANUAL

INTRODUCTION

This document is the final report for the development of the Federal Highway Administration's (FHWA's) soil model implemented into LS-DYNA. This report is in three sections: (1) a description of the justification and detailed theory of the model, (2) a user's manual that was submitted for inclusion in the LS-DYNA user's manual, and (3) examples that show the expected results of the model.

The original research plan was submitted to Martin Hargrave of FHWA and the FHWA organized Centers of Excellence in Finite Element Crash Analysis in September 1999. The material model was developed and changes requested by the centers of excellence were implemented in 2000. During this time, the user-defined material models in LS-DYNA were used. The model was verified and preliminary validation took place in 2001. The model was implemented as a standard material model in version 970 of LS-DYNA in February 2002. The soil model in the production version was checked against analyses done with the user-defined version in spring 2002. A user ran identical analyses and other analyses to validate the model in summer 2002.

A significant difference between the soil material model discussed in this report and the wood material model discussed in another report is that the wood material model was based on extensive experimental data. In the case of the soil model, there was no material property data available for the applications needed (road-base materials). This lack of data caused the material model to be developed based on the one set of data available and the general behavior of cohesionless soils. In addition, some behaviors could not be validated and default properties for the soils used in road-base testing could not be uniquely defined.

The goal of this research was to develop a soil material model in LS-DYNA that will represent the soils used for National Cooperative Highway Research Program (NCHRP) 350 roadside safety hardware testing. In this section of the report, the theory for the soil material model is presented. Investigative work done prior to development of the model is discussed first. The investigative work was for the purpose of determining the critical behaviors of the material that must be included in a model and establishing whether an existing model could be enhanced to meet these requirements or whether a new material model had to be developed. The critical behaviors and how they can be modeled, followed by details of a review of currently used soil material models, are also discussed. Also in this section, model development areas, including details of the algorithms and implementation, are described.

PRELIMINARY WORK

The investigative work included determining the critical behaviors of NCHRP 350 soil. Material models already in LS-DYNA were investigated to see if one of them, if enhanced, would be suitable, and what enhancements would be necessary for the modeling of soils in roadside safety applications.

Determination of Critical Behaviors

Behaviors that were critical to soil modeling in roadside safety applications were determined through discussions with roadside safety testers and analysts, by performing literature reviews, and by studying road-base laboratory test results. Most soil data that have been used for past soil model development in LS-DYNA are from laboratory tests that have relatively high confinement.[5] For roadside safety applications, the soil will have low or no confinement. Therefore, the laboratory data used to evaluate and develop the model must be at low or no confinement. Maximum pressures will be less than 30 megapascals (MPa).[6]

Most of the basic triaxial shear test data (from the laboratory) used to determine critical behaviors and develop algorithms have been from the U.S. Army Corps of Engineers (USACE) geological database. The specific soil used is a crushed limestone road base that conforms to NCHRP 350 soil, grade B (see table 1). However, the larger aggregate was removed so that uniform stresses/strains could be achieved in standard specimen sizes for triaxial shear tests. Additional data from the roadside safety testing subcontractor were used to verify and validate the new soil model developed for LS-DYNA.

Elastic behavior of soil is isotropic. This requirement is based on the fact that road-base soils are well graded and not stratified. The standard soil is considered to be cohesionless (i.e., it has no tensile strength). This behavior is common to soils that contain little clay. Elastic behavior mainly affects unloading and the isotropic compression (volumetric) behavior because road-base material tends to have very low shear strength at low confinement (< 0.5 MPa). Very little shear stress is needed to initiate nonrecoverable energy dissipation (plasticity and damage).

Soil behavior is greatly affected by void ratio, compaction, and excess pore-water pressure. Experimental data for a standard road base show that undrained conditions (high moisture content) can greatly affect the amount of deformation. Compaction tends to increase the initial yield strength and the ultimate strength. The void ratio is directly related to compaction. Reduction in the void ratio increases the strength and the bulk modulus of the soil.

Figure 1 shows two commonly used models for yield surfaces. The three axes shown are the three principal stress axes. The generator axis for each surface is the pressure axis. The surface on the left is the Mohr-Coulomb model (a typical soil yield surface) and, for comparison, the surface on the right is the standard Von Mises model (a typical metal yield surface). The yield (onset of plasticity) and ultimate (peak) strength of soil

are pressure-dependent. This means that the plasticity surface is dependent on both the pressure and the shear stresses. This behavior differs from metals where the plasticity surface is only a function of the shear stresses. Experimental evidence for cohesionless soil shows that, at low pressures, the yield surface is triangular in the deviatoric plane as shown in figure 2.[3] For the Waterways Experiment Station (WES) road-base soil, the ratio of minimum stress (triaxial extension) to maximum stress (triaxial compression) in the deviatoric plane is 0.70.

Table 1. Gradation data for USACE road-base soil tests.

Sieve Size (mm)	Percent Passing
9.5200	100.0
6.3500	90.0
4.7600	79.0
3.3600	66.0
2.3800	54.0
2.0000	49.0
1.1900	36.0
0.8400	32.0
0.5900	28.0
0.4200	24.0
0.2970	21.0
0.2100	18.0
0.1490	15.0
0.1050	13.0
0.0740	11.0

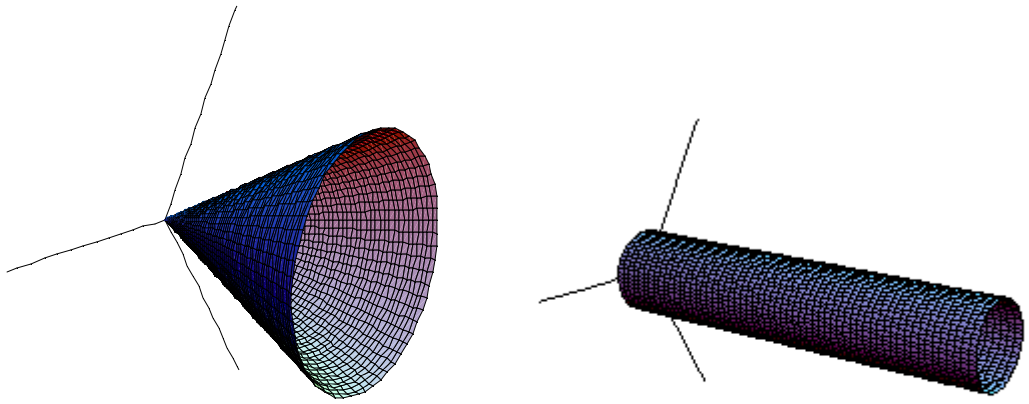

(a) (b)

Figure 1. (a) Pressure-dependent (Mohr-Coulomb) and (b) pressure-independent (Von Mises) yield surfaces.

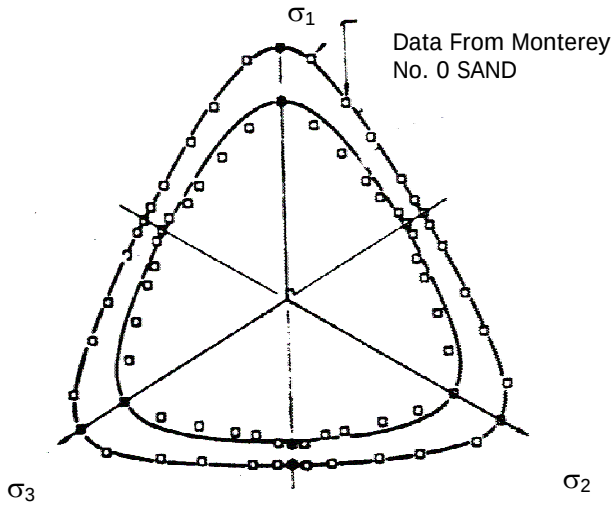

Figure 2. Yield surface in deviatoric plane for cohesionless soils.

Figure 3 shows the peak principal stress difference versus the average normal stress for the crushed limestone road-base material. The peak principal stress difference is

also the maximum shear strength at the given pressure. This plot presents the shear strength as a function of pressure for the road-base material. Notice that for the pressure range indicated in the figure, the shear strength of this soil varies linearly with pressure.

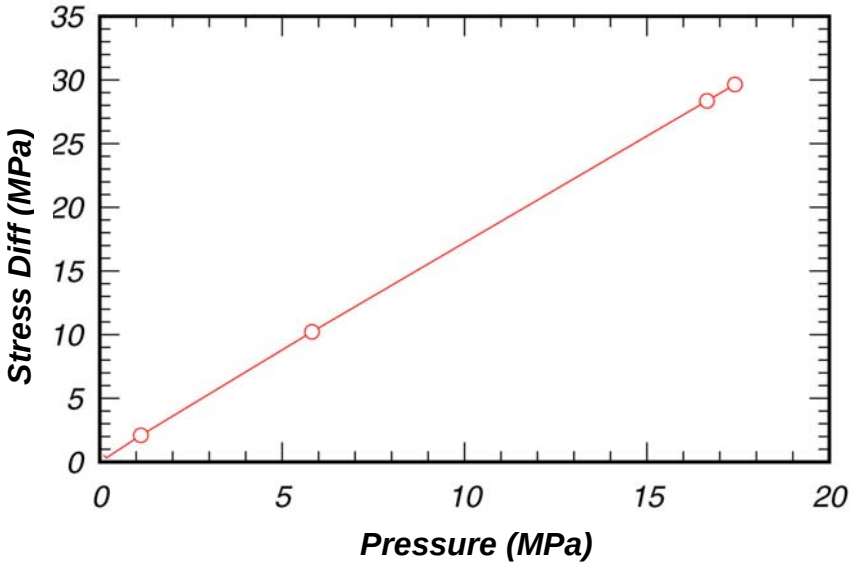

Figure 3. Principal stress difference (peak shear strength) versus pressure (average normal stress) for road-base material.

At high confinement, the road-base soil can have significant peak shear strength (> 120 MPa).

At low confining pressures, the standard soil dilates (expands) near peak shear stresses. At high confining pressures (> 100 MPa), the standard soil will stop expanding. This change in volumetric behavior is one of the reasons for employing a cap model. For roadside safety analysis applications, there are no pressures greater than 30 MPa; thus, it is believed that a cap model is not needed. A fully associative plasticity model predicts dilation of the material after the yield strength is reached.

The standard soil at low confining pressures typically exhibits strain softening. That is, at pressures below 30 MPa, the soil strain hardens from the yield stress to the ultimate stress, then the strain softens. Strain softening can be a major source of energy dissipation; thus, it is believed that it must be included in the material model.

The strength of the soil increases at high strain rates. No experimental strain rate data were found for road-base materials, but data for cohesionless (sandy) soils show significant strain-rate effects. However, we are not convinced that strain-rate behavior is a critical behavior, because applicable rates are relatively low for roadside safety applications.

The moisture content of the soil can affect the elastic moduli, the shear strength, and the softening behavior of the soil.

Figure 4 shows the force-deflection curves measured in two steel posts in NCHRP 350 soil bogie tests.[8] The tests were identical except for the moisture content (5 percent versus 26 percent). The peak force for the relatively dry soil was much higher, and the stiffness was much greater. Figure 5 shows the energy absorbed during the two tests. The amount of energy absorbed at a given deflection was much larger for the low-moisture-content NCHRP 350 soil.

The effects of moisture are complicated and are different for different soil types. For instance, granular soils with low relative densities show little effect on bulk modulus, while clayey soils show significant effects. Fortunately, the NCHRP 350 soil is granular and the test facilities typically run their tests at a low moisture content (3 percent to 7 percent). However, we believe that the ability to simulate actual field conditions is important, so techniques to simulate moisture effects were implemented. The degree of saturation and the void ratio are critical parameters in the determination of moisture effects. Moisture effects on shear strength can be introduced by including an excess pore-water pressure algorithm.

Compaction is the decrease in the void ratio and the increase in the relative density. Compaction in granular soils tends to increase the shear strength slightly and lessen the amount of volumetric strain that causes the onset of excess pore-water pressure effects.

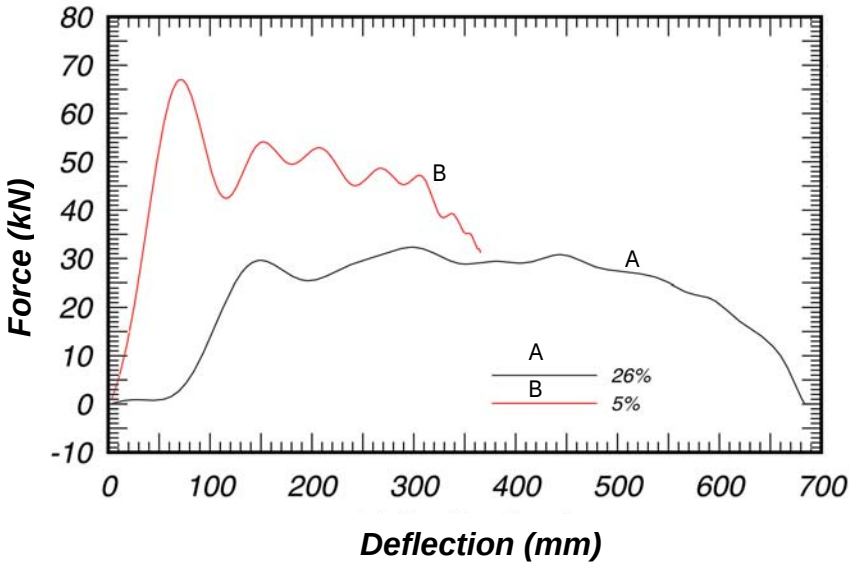

Figure 4. Force deflection for two steel posts in soil tests with different moisture contents (5 percent and 26 percent).

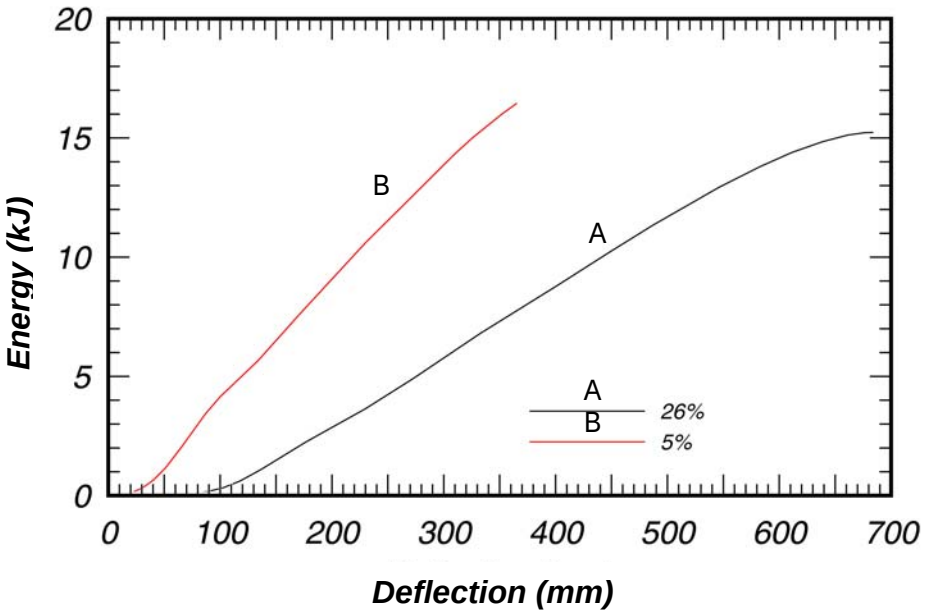

Figure 5. Energy versus deflection for two steel posts in soil bogie tests with different moisture contents.

Evaluation of the Utility of Models Already in LS-DYNA

Several material models available in LS-DYNA were reviewed as possible soil model candidates, from the simplest (material model 5) to the most complex (material model 25). Most of the candidate models in LS-DYNA are extensions of material model 5 (soil and foam). Two of the exceptions to this are model 16 (pseudo-tensor model) and model 25 (geological cap model). Model 5 and its extensions, model 14 (soil and foam with failure), and model 79 (hysteretic soil) are basically an analytical pressure-dependent yield surface. They all must have confinement to be stable (see the LS-DYNA user's manual for model 5). For the roadside application, the top surface of the soil is not confined and is at zero pressure during a significant portion of the analysis. However, both model 5 and model 79 were evaluated with single-element runs. Both of these models were indeed found to be unstable in unconfined states. Material model 14 and model 78 (soil and concrete) are for analyses in high-pressure regions. Model 14 was evaluated previously and it was found that it does not simulate low-/zero-pressure behavior well.

Material model 25 (geological cap model) was also evaluated. This model is complex, but does handle low-confinement behavior well. This model was first evaluated with single-element runs. It performed well, it was stable (see figure 6), and it predicted peak stress level accurately. However, model 25 cannot simulate strain softening. Despite this shortcoming, it is the only existing model that could simulate much of the basic behavior needed for roadside safety applications. However, model 25 is very inefficient for this application since it uses a cap surface. Because of the relatively low confinement that soil has in roadside safety applications, a cap surface is not needed.

Because of the cap/shear surface intersection (non-smooth) in model 25, there are many corners in the yield surface. These corners cause the algorithm to be very complex and inefficient. In addition, model 25 would need extensive enhancements, including:

- Three invariant yield surfaces instead of two invariant surfaces to simulate lower strength in triaxial extension than in triaxial compression and triaxial shear.
- Smooth behavior of the yield surface at very low shear stresses.
- Strain softening behavior.
- Isotropic hardening behavior on the yield surface, instead of kinematic hardening.
- Strain-rate-dependent strength enhancements.
- Pore-water pressure behavior.

Based on these observations, it was concluded that none of the existing models are adequate, and it was decided to develop a new soil material model. The theoretical basis for this new model is presented in the next section.

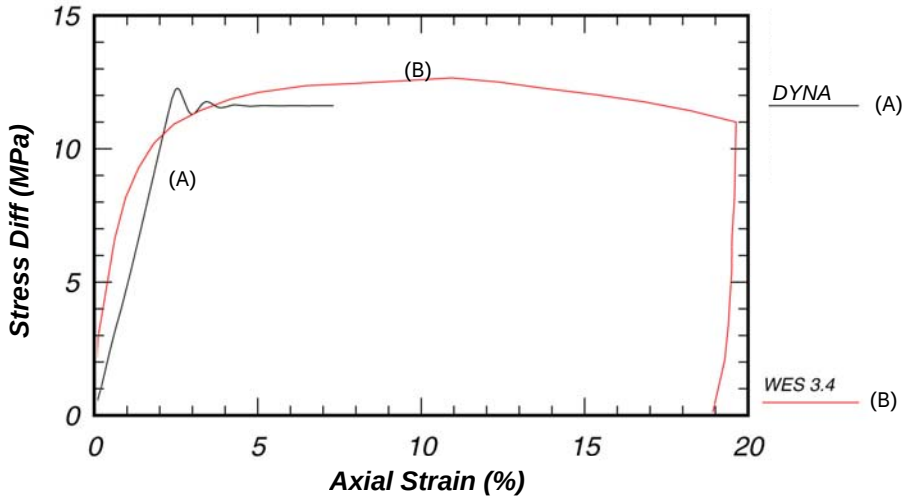

Figure 6. Model 25 single-element run, triaxial compression at 3.4 MPa compared to WES data.

MODEL DEVELOPMENT

The objectives of the material model development effort in order of priority were: accuracy, robustness, efficiency (speed), and ease of use. The choices made in the model are balanced between these objectives. The following subsections describe the characteristics of the algorithms necessary to model soil for roadside safety applications.

Elastic Constitutive Behavior

We assumed that the elastic properties of the soil are isotropic. Bulk and shear moduli were used as input parameters. Standard soil tests (i.e., triaxial shear tests and uniaxial strain tests) produce these parameters directly. To simulate the effects of voids, the bulk modulus was made to be a function of volumetric strain. As the volumetric strain increases, the modulus increases to simulate the collapse of voids and the stiffening of the material.

The effects of moisture content/excess pore pressure were also simulated with changes to the elastic moduli. As the remaining voids of the soil become filled with moisture, the material becomes more incompressible. To simulate the effects of excess pore-water pressure, a function that involves the nonporous bulk modulus (inverse of soil compressibility), the porosity, and the degree of saturation was used:

$$K = \frac{K_i}{1 + K_i D_1 n_{cur}} \tag{1}$$

where:

K_i = nonporous bulk modulus

n_{cur} = current porosity = $Max[0, (w - \varepsilon_v)]$

w = volumetric strain corresponding to the volume of air voids
= $n(1 - S)$

ε_v = total volumetric strain

D_1 = material constant controlling the stiffness before the air voids are collapsed

n = porosity of the soil = $\frac{e}{1+e}$

e = void ratio = $\frac{\gamma_{sp}\rho_w(1+m_c)}{\rho} - 1$

S = degree of saturation = $\frac{\rho m_c}{n\rho_w(1+m_c)}$

$\rho, \gamma_{sp}, m_c, \rho_w$ = soil density, specific gravity, moisture content, and water density.

Figure 7 shows the effect of the D_1 parameter on the pressure-volumetric strain relationship (bulk modulus). The elastic moduli are used to determine the elastic stresses and the elastic trial stresses. The bulk modulus is always a monotonically increasing value (i.e., *j* is the time-step index),

$$K_{j+1} = \begin{cases} \dfrac{K_i}{1 + K_i D_1 n_{cur}} & if\ \varepsilon_{v\ j+1} > \varepsilon_{vj} \\ K_j & if\ \varepsilon_{v\ j+1} \le \varepsilon_{vj} \end{cases} \tag{2}$$

Note that the standard practice of treating compressive stresses and strains as positive quantities is followed.

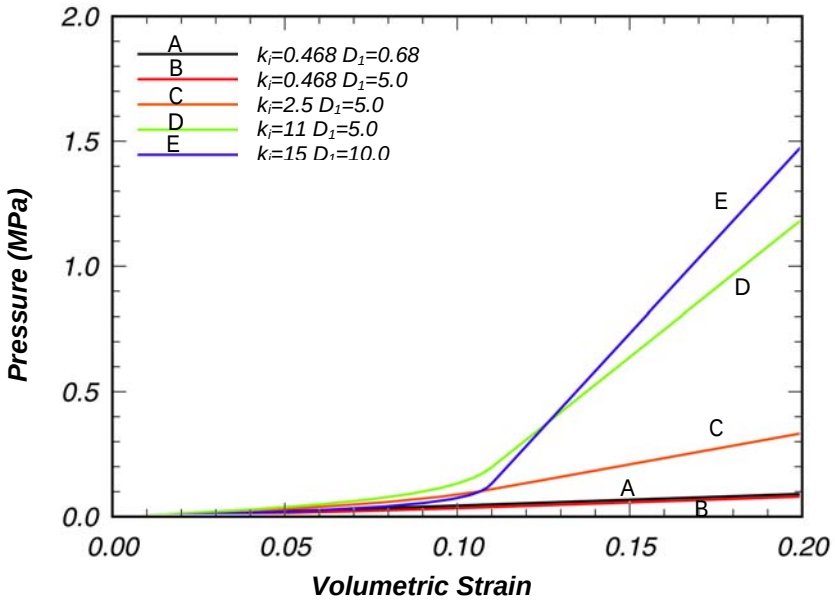

Figure 7. Pressure versus volumetric strain showing the effects of the D_1 parameter.

Yield Surface Behavior

The initial yield surface is where the soil initially starts to dissipate nonrecoverable strain energy. A well-documented yield surface used for soils is the Mohr-Coulomb surface. However, the standard Mohr-Coulomb surface has two significant deficiencies for our use:

The first deficiency is that the surface comes to a point (singularity) at the intersection with the pressure axis (zero shear strength). This region of the yield surface is critical in roadside safety applications because of the low confinement. This type of singularity

can cause both numerical and efficiency problems in the plasticity algorithm. To ensure an accurate, robust, and efficient algorithm, the yield surface needs to be convex and smooth. Second, the Mohr-Coulomb surface is hexagonal or circular in the deviatoric plane (see figure 8). Based on the experimental evidence, the yield surface should be able to become triangular in shape at low confinement pressures.[9]

To correct these deficiencies, a modified Mohr-Coulomb surface was adopted. The yield surface was modified based on the work of Abbo and Sloan.[9] The standard Mohr-Coulomb yield surface, F, is represented as:

$$F = -P\sin\varphi + K(\theta)\sqrt{J_2} - c\cos\varphi = 0 \tag{3}$$

where:

P = pressure

φ = internal friction angle

$K(\theta)$ = function of the angle θ in the deviatoric plane

$\sqrt{J_2}$ = square root of the second invariant of the stress deviator

c = amount of cohesion

The modified yield surface is a hyperbola fitted to the Mohr-Coulomb surface. At the crossing of the pressure axis (zero shear strength), the modified surface is a smooth surface. At this point, it is perpendicular to the pressure axis. The equation for the modified Mohr-Coulomb surface is:

$$F = -P\sin\varphi + \sqrt{J_2 K(\theta)^2 + a^2\sin^2\varphi} - c\cos\varphi = 0 \tag{4}$$

Here, a is a parameter for determining how close the modified surface is fitted to the standard Mohr-Coulomb yield surface. If a is zero, then the standard Mohr-Coulomb surface is recovered. The input parameter a should be set close to zero, based on numerical considerations.

Figure 9 shows the modified Mohr-Coulomb surface in shear stress versus pressure space. It is almost identical to the original surface, except at low shear stresses.

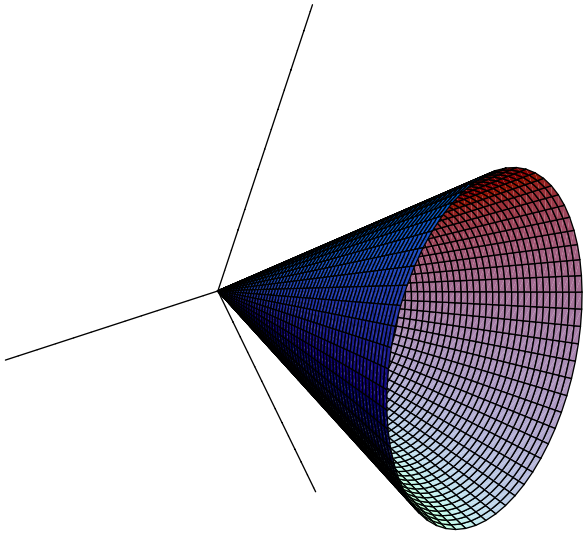

Figure 8. Standard Mohr-Coulomb yield surface in principal stress space.

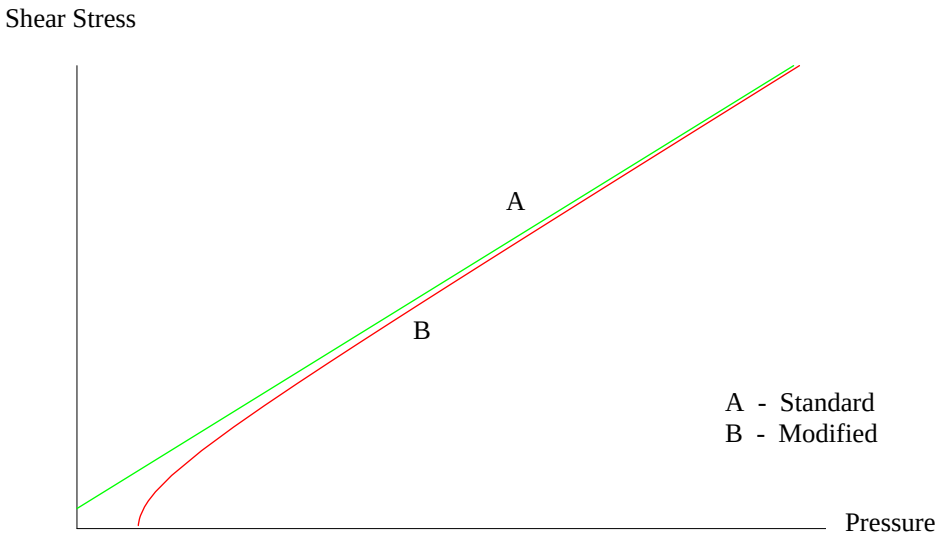

Figure 9. Comparison of Mohr-Coulomb yield surfaces in shear stress—Pressure space (standard—(A)/green, modified—(B)/red).

To remedy the second deficiency, the shape in the deviatoric plane, the standard Mohr-Coulomb $K(\theta)$ function was changed to a function used by Klisinski:[10]

$$K(\theta) = \frac{4(1-e^2)\cos^2\theta + (2e-1)^2}{2(1-e^2)\cos\theta + (2e-1)[4(1-e^2)\cos^2\theta + 5e^2 - 4e]^{\frac{1}{2}}} \quad (5)$$

Here, $\cos 3\theta = \frac{3\sqrt{3}J_3}{2J_2^{3/2}}$, J_3 = third invariant of the stress deviator, and e = material input parameter describing the ratio of triaxial extension strength to triaxial compression strength. If e is set equal to 1, then a circular cone surface is formed (see figure 8). If e is set to 0.55, then a triangular surface is found (see figure 10). $K(\theta)$ is defined for $0.5 < e \leq 1.0$.

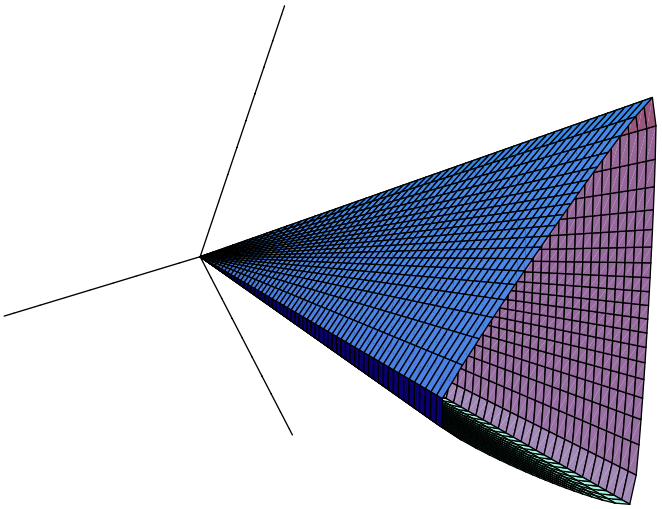

Figure 10. Yield surface with e = 0.55.

Excess Pore-Water Pressure Behavior

For some soils, excess pore-water pressure can make a significant difference on the shear strength of the soil, especially for near-saturated conditions. Because of the loading typical for roadside safety applications (i.e., many soils have low permeability), water in the voids will not have time to flow; therefore, the water will cause an excess pressure increase as the impact load collapses the air voids in the soil. To simulate this behavior, a standard (practical) soil mechanics technique[(11)] is used for reducing the total pressure, P, by the excess pore-water pressure, u, to get an "effective pressure" P':

$$P' = P - u \tag{6}$$

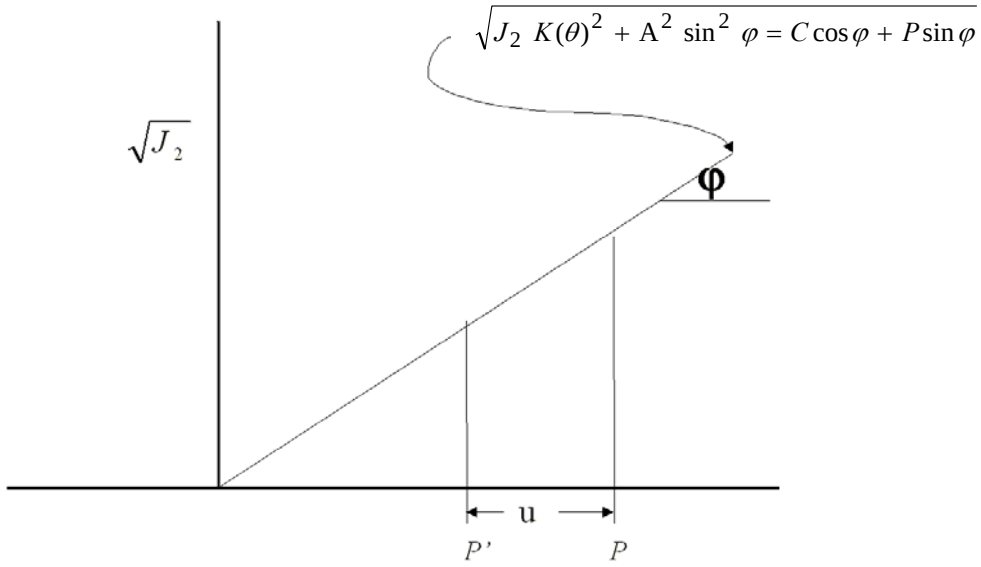

Figure 11. Effects on pressure because of pore-water pressure.

Figure 11 shows how pore-water pressure affects the algorithm for the plasticity surface. The excess pore-water pressure reduces the total pressure, which will lower the shear strength, $\sqrt{J_2}$. A large excess pore-water pressure can cause the shear strength to become zero.

The water in the voids of the soil causes the excess pore-water pressure. As the air void volume is reduced to zero during loading, the pore-water pressure increases. The water in the remaining voids causes the effective load on the soil particles to be reduced.

To calculate the pore-water pressure, u, an expression similar to the equation used for the moisture effects on the bulk modulus was used:

$$u = \frac{K_{sk}}{1 + K_{sk} D_2 n_{cur}} \varepsilon_v \tag{7}$$

where:

K_{sk} = bulk modulus for soil without air voids (skeletal bulk modulus)

n_{cur} = current porosity = $Max[0, (w - \varepsilon_v)]$

w = volumetric strain corresponding to the volume of air voids

= $n(1 - S)$

ε_v = total volumetric strain

D_2 = material constant controlling the pore-water pressure before the air voids are collapsed

n = porosity of the soil = $\frac{e}{1+e}$

e = void ratio = $\frac{\gamma_{sp}(1+m_c)}{\rho} - 1$

S = degree of saturation = $\frac{\rho m_c}{n(1+m_c)}$

ρ, γ_{sp}, m_c = soil density, specific gravity, and moisture content, respectively

Pore-water pressure is not allowed to become negative ($u \geq 0$).

Figure 12 is a plot of the pore pressure versus volumetric strain for different parameter values. With the D_2 parameter set relatively high compared to $K_{sk,}$ there is no pore pressure until the volumetric strain is greater than the strains associated with the air voids. However, as D_2 is lowered, the pore pressure starts to increase before the air voids are totally collapsed. The K_{sk} parameter affects the slope of the post-void collapse pressure-volumetric behavior.

Parameter D_2 can be found from Skempton pore-water pressure parameter B, where B is defined as:[11]

$$B = \frac{1}{1 + n\frac{K_{sk}}{K}} \tag{8}$$

$$\therefore \quad D_2 = \frac{1-B}{B\,K_{sk}[n(1-S)]} \tag{9}$$

where: K_{sk} = bulk modulus of the soil without air voids

This method does not include the dissipation of excess pore-water pressure as a function of time. The rate of dissipation can be a function of the loading rate and soil parameters, such as permeability. However, at this time, the lack of experimental data on road-base material on typical roadside tests would make this type of dissipative model useless. However, if experimental data and the required parameters for roadside tests become available, then a dissipative model could be easily inserted.

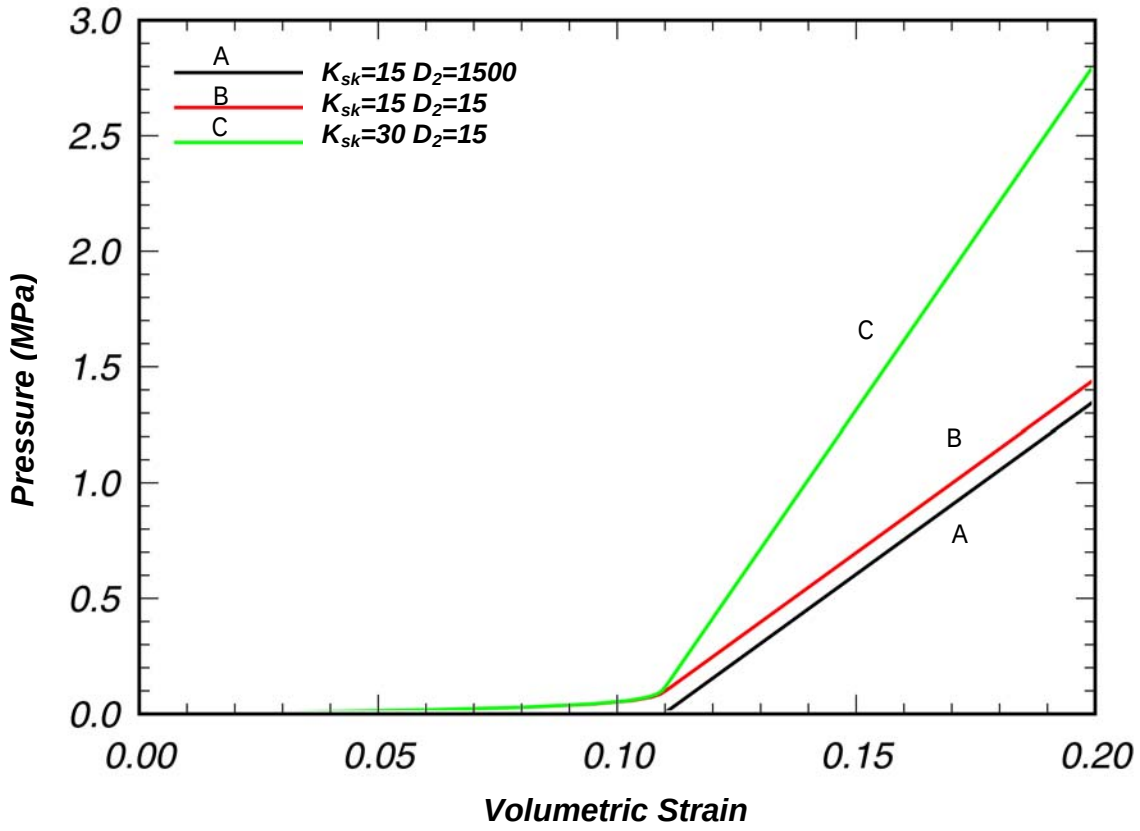

Figure 12. Effects of parameters on pore-water pressure.

Strain Hardening Behavior

Figure 13 shows the principal stress difference versus principal strain difference results of a triaxial compression test at a lateral stress of 6.9 MPa for a standard soil. The unloading portion of the curve shows that there was very little elastic (recoverable) strain in this test. The nonlinear part of the loading portion of the curve is pre-peak (plastic) hardening. The amount of hardening increases as the lateral confinement increases (i.e., there is less hardening at lower confining pressures). To simulate this nonlinear hardening behavior, the friction angle φ was increased as a function of the effective plastic strain:

$$\Delta\phi = H(1-\frac{\phi-\phi_{init}}{N\phi_{\max}})\Delta\varepsilon_{eff\ plas} \tag{10}$$

where:

$\varepsilon_{eff\ plas}$ = effective plastic strain

N = fraction of the peak strength internal friction angle where nonlinear behavior begins ($0 < N \leq 1$)

H (the input parameter) determines the stiffness of the nonlinear hardening

Figure 14 shows the effect on the yield surface of an increase in φ.

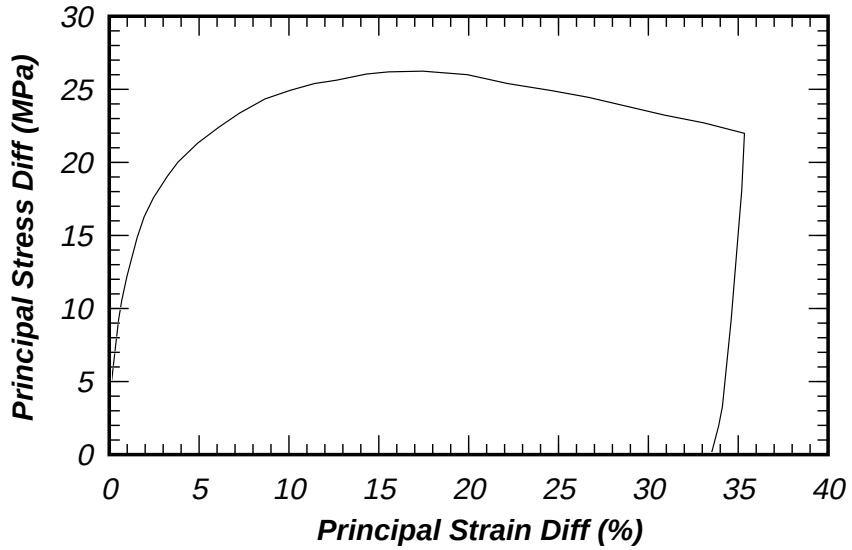

Figure 13. Principal stress difference versus principal strain difference for triaxial compression test at σ_2 = 6.9 MPa of WES road-base material.

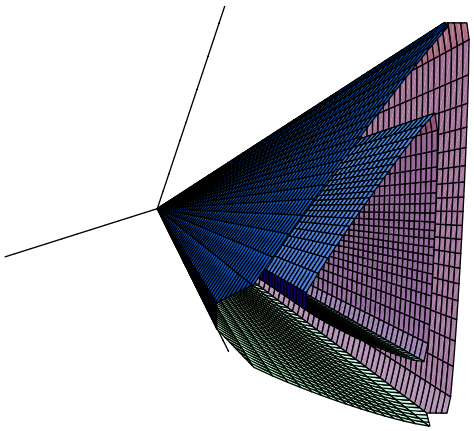

Figure 14. Hardening of yield surface.

Strain Softening Behavior

Figure 15 is a plot of the principal stress difference versus axial strain result for the same experiment as shown in figure 13. The principal stress difference softens (i.e., decreases) after it has reached its peak. The area under the curve in figure 15 after the peak stress is reached is the strain energy dissipated by the material because of strain softening. The strain energy dissipated in this post-peak region is almost as great as the strain energy dissipated in the pre-peak region.

To simulate this behavior, a continuum damage algorithm was implemented. The strain softening (damage) algorithm is based on the work of J.W. Ju and J.C. Simo. They proposed a strain-energy-based damage criteria.[12-13] The major advantage of their method is that the strain softening is uncoupled from the plasticity algorithm. The plasticity algorithm uses undamaged stresses. This means that the plasticity algorithm can be implemented and verified independently of the damage algorithm.

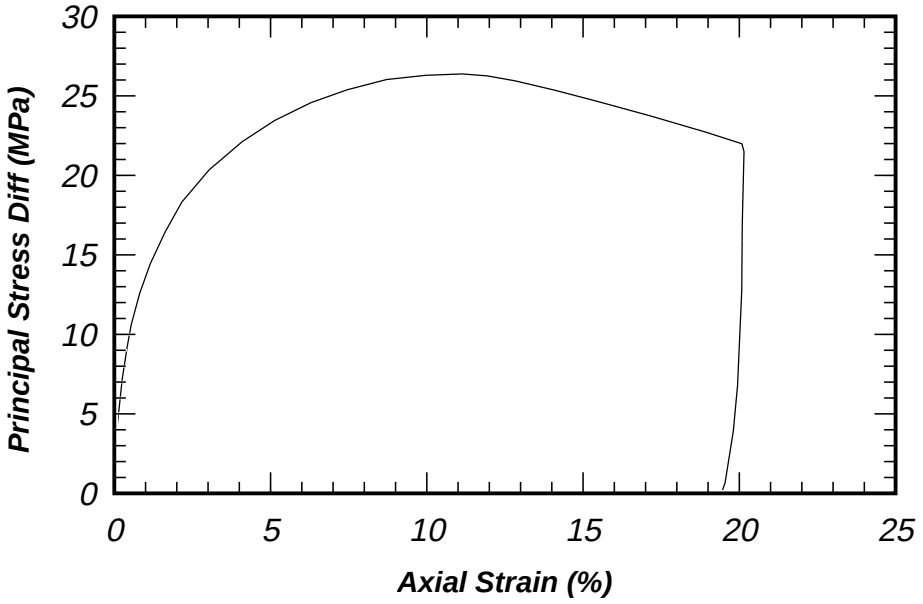

Figure 15. Principal stress difference versus axial strain for triaxial compression test at σ_2 = 6.9 MPa of WES road-base material.

For the damage criterion, ξ, we used:

$$\xi = -\frac{1}{K_i}\int \overline{P} d\varepsilon_{pv} \tag{11}$$

where: $\overline{P}$ = pressure and ε_{pv} = plastic volumetric strain

When $\varepsilon_{pv} < 0$, the soil is dilating. The damaged stress is found from the undamaged stresses, namely:

$$\sigma = (1-d)\overline{\sigma} \tag{12}$$

where: d = isotropic damage parameter and the damage parameter is found at step $j+1$ as:

$$\begin{aligned} d_{j+1} &= d_j \ldots\ldots\ldots\ldots\ldots\ldots\ldots if \quad \xi_{j+1} \le r_j \\ d_{j+1} &= \frac{\xi_{j+1}-\xi_0}{\alpha-\xi_0} \ldots\ldots\ldots\ldots\ldots if \quad \xi_{j+1} > r_j \end{aligned} \tag{13}$$

Here, r_{j+1} is a damage threshold surface, which is updated in this manner:

$$\mathrm{r_{j+1}} = \max\left(\mathrm{r_j}, \xi_{\mathrm{j+1}}\right), \text{ and } \xi_0 = r_0 \tag{14}$$

Typically, the damage, *d*, varies from 0 to a maximum of 1. However, some soils can have residual strength that is pressure-dependent. The residual strength is represented by φ_{res}, an internal friction angle.

The maximum damage allowed is related to the internal friction angle of residual strength by:

$$d_{\max} = \frac{\sin\varphi - \sin\varphi_{res}}{\sin\varphi} \tag{15}$$

If $\varphi_{res} > 0$, then $d_{\max}$, the maximum damage, will not reach 1, and the soil will have residual strength.

The damage parameter is used to reduce the effective internal stress $\sigma = (1-d)\overline{\sigma}$.

If damage parameter *d* is allowed to become 1, then the internal stress is zero, which for a finite element code such as LS-DYNA (explicit) causes the internal forces (element stiffness) to become zero. By not allowing the damage parameter *d* to become 1, this keeps a residual stiffness in the element. Therefore, by setting $\varphi_{res} > 0$, then $d_{\max}$, the maximum damage, will not reach 1, and the soil will have some residual strength. If the strains continue with approximately the same behavior, the effective internal stresses will be almost constant. However, if the strains drastically increase or decrease, then the effective internal stresses can change, because $\overline{\sigma}$, the undamaged stresses, are changing drastically.

When material models include strain softening, special techniques must be used to prevent mesh sensitivity. Mesh sensitivity is the tendency of the finite element model/analysis to produce significantly different results as the element size is reduced. Mesh sensitivity occurs because softening in the model concentrates in one element. As the element size is reduced, the failure becomes localized in smaller volumes; this causes less energy to be dissipated by the softening, leading to instabilities or at least mesh-sensitive behavior.

To eliminate or reduce the effects of strain-softening mesh sensitivity, the softening parameter, α (the strain at full damage), must be modified as the element size changes. Normally, a material property that is independent of the test specimen size is used. For many materials (e.g., metal, concrete, wood, composites), the material property used is the fracture energy. However, for soil, there seems to be no corresponding softening property that is independent of the test specimen size. Therefore, we assume a property—void formation—and use it as an input parameter. Figure 16 shows graphically the definition of the void formation parameter, G_f. The void formation parameter is the area under the softening region of the pressure-volumetric strain curve times the cube root of the element volume, $V^{1/3}$. For the linear softening model, $G_f / V^{1/3}$ is just the area of the shaded triangle:

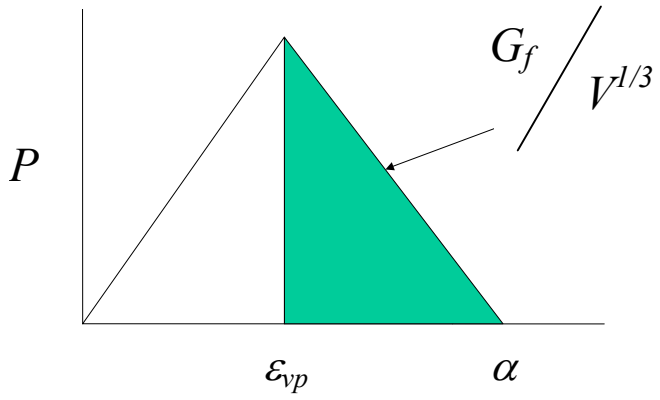

Figure 16. Definition of the void formation parameter.

$$G_f = V^{\frac{1}{3}} \int_{\varepsilon_{\mathrm{vp}}}^{\alpha} P \mathrm{d}\varepsilon_{\mathrm{v}} = \frac{P_{\mathrm{peak}} (\alpha - \varepsilon_{\mathrm{vp}}) V^{\frac{1}{3}}}{2} \tag{16}$$

where: ε_{vp} = volumetric strain at peak pressure

Then, α can be found as a function of the volume of the element V:

$$\alpha = \frac{2G_f}{K\varepsilon_{vp}V^{1/3}} + \varepsilon_{vp} \qquad (17)$$

where: ε_{vp} = an input parameter

If G_f is made very small relative to $K\varepsilon_{vp}V^{1/3}$, then the softening behavior will be brittle.

Strain-Rate Behavior

There are some experimental data that suggest that soil strength is strain-rate-dependent.[11] Based on the earlier evaluation of a steel post in soil experiments,[14] strength enhancements caused by high strain rates may not be needed for roadside safety applications. However, since the development and implementation of strain-rate-dependent effects are relatively easy and will not affect the overall efficiency if they are not used, strain-rate effects were implemented into the soil model.

The two-parameter Devaut-Lions viscoplastic update algorithm developed by Y. Murray was used.[15] This algorithm interpolates between the elastic trial stress and the inviscid stress. The inviscid stresses are on the plasticity surface $\overline{\sigma}_{vp} = (1-\varsigma)\overline{\sigma} + \varsigma\overline{\sigma}_{trial}$, with $\varsigma = \frac{1}{\Delta t/\eta + 1}$ and $\eta = (\frac{\gamma}{\dot{\varepsilon}})^{(n-1)/n}$.

Figure 17 shows the behavior of ζ. As ζ becomes 1, then the viscoplastic stress becomes the elastic trial stress.

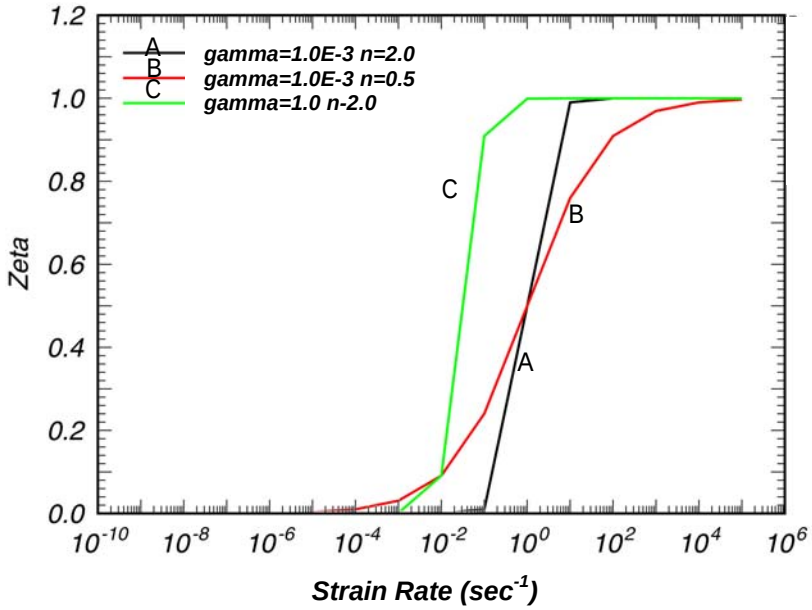

Figure 17. Zeta versus strain rate for different parameters.

INCORPORATION INTO LS-DYNA

The above discussion describes the equations and the form of the soil model. In this section, the implementation of the model into LS-DYNA is discussed. The intermediate equations were determined using the symbolic algebra program Mathematica®.

First, the elastic moduli and undamaged stresses are found (see figure 18). The bulk modulus function needs the current total volumetric strain. The undamaged stresses are recovered from the damaged stresses based on the current value of the damage variable d.

Next, the elastic trial stresses are determined (see figure 19**Error! Reference source not found.**) and it is determined whether the state of stress is within the current yield surface. If it is, the routine bypasses the plasticity algorithm.

Enter routine with:

σ_j

$\Delta\varepsilon_{j+1}$

Get undamaged stresses:

$$\overline{\sigma} = \frac{\sigma_j}{1-d_j}$$

Determine elastic moduli:

$$\varepsilon_{v\,j+1} = \varepsilon_{v\,j} + \Delta\varepsilon_{v\,j+1}$$

$$K_{j+1} = K_i/(1+K_i D_1 n_{cur})$$

$$G_{j+1} = G_j$$

Figure 18. Elastic moduli and undamaged stresses.

Compute elastic trial stress:

$$\Delta\overline{p} = (K - \frac{K_{sk}}{1+K_{sk}D_2 n_{cur}})\Delta\varepsilon_{v\,j+1}$$

$$\overline{p}_{j+1} = \overline{p}_j + \Delta\overline{p}$$

$$\overline{\sigma}_e = \overline{\sigma}_j + \Delta\overline{p} + 2G(\Delta\varepsilon_{j+1} - \Delta\varepsilon_{v\,j+1})$$

Determine if elastic trial stress is within the yield surface:

If $F(\overline{p}, J_2, \theta, \varepsilon_{ep}) \le 0$, go to figure 23

> 0, go to figure 20

Figure 19. Elastic trial stresses.

The total strains are split into elastic and plastic strains:

$$\varepsilon = \varepsilon_e + \varepsilon_p \tag{18}$$

The stress increment at step $j+1$ is then:

$$\Delta\sigma_{j+1} = C(\Delta\varepsilon_{j+1} - \Delta\varepsilon_{p\,j+1}) \tag{19}$$

To compute the stress increments, it is first necessary to determine the plastic strain increments. The latter are determined by assuming an associated flow rule (see figure 20). Note that the gradient of the yield function is taken at the stress state of the previous time step; this is consistent with the explicit algorithm used in LS-DYNA. The explicit form of the gradients is presented in appendix A. The increment in the hardening parameter φ is assumed to have a form similar to the flow rule. *C* is the elasticity tensor. The function *h* will be determined later (see figure 21). For the determination of the increment of the scale parameter, the gradients of the yield function are again evaluated at step *j*. Once the plasticity scale parameter is determined, the stresses and history variables can be updated (see figure 21).

The plastic strain increment is found from the associated flow rule:

$$\Delta\,\varepsilon_{p\;\;j+1} = \Delta\,\lambda\,\left.\frac{\partial F}{\partial\,\sigma}\right|_j$$

The increment in the hardening parameter φ is:

$$\Delta\varphi = \Delta\lambda h(\varepsilon_{ep})$$

Employing standard techniques, the increment of the scalar parameter λ is:

$$\Delta\lambda = \left.\frac{\frac{\partial F}{\partial\sigma}C\Delta\varepsilon}{\frac{\partial F}{\partial\sigma}C\frac{\partial F}{\partial\sigma} - \frac{\partial F}{\partial\varphi}h}\right|$$

Figure 20. Determination of plastic strains.

Now we can update the stresses and plasticity variables:

$$\bar{\sigma}_{j+1} = \bar{\sigma}_e - K\Delta\varepsilon_{pv} - 2G(\Delta\varepsilon_p - \Delta\varepsilon_{pv})$$

$$\Delta\varphi = \Delta\lambda h(\varepsilon_{ep})$$

where: $h(\varepsilon_{ep}) = \dfrac{\partial\varphi}{\partial\varepsilon_{ep}}\sqrt{\dfrac{2}{3}}\sqrt{\dfrac{\partial F}{\partial\sigma}\dfrac{\partial F}{\partial\sigma}}$

Determine if stress is on the yield surface:

If $F(\bar{p}, J_2, \theta, \varepsilon_{ep}) \le 0$, go to figure 22

> 0, go to figure 20

Figure 21. Update of stresses and history variables.

Determine effective strain rate:

$$\dot{\varepsilon}_e = \Delta\varepsilon_t \Big/ \Delta t$$

If $\dot{\varepsilon}_e \le$ tolerance, then skip viscoplasticity update

$$\eta = \left(\frac{\gamma}{\dot{\varepsilon}_e}\right)^{(n-1)/n}$$

$$\zeta = \frac{1}{\Delta t/\eta + 1}$$

$$\bar{\sigma}_{v-p} = (1-\zeta)\bar{\sigma} - \zeta\bar{\sigma}_e$$

Figure 22. Viscoplasticity update.

Next, the effect of the strain rates on the strength of the material is determined. The effective strain rate must be found and used to determine the viscoplasticity scale factor. If the effective strain rate is less than 0.00001, the step is assumed to be static and the algorithm is skipped. The viscoplasticity scale factor interpolates between the elastic trial stress and the inviscid stress (see figure 22).

The strain softening algorithm transforms the effective (undamaged) stresses to the damaged stresses (see figure 23). The damage is assumed to be isotropic. The damage scale factor is determined based on total volumetric strain energy. It is desirable for strain to soften based on tensile volumetric (dilation) strain energy. In this routine, compressive strain values are considered to be positive and, therefore, the increment of volumetric strain energy is subtracted. When the element starts to dilate, the volumetric strain energy starts to increase. The initial damage threshold r_n (a user input parameter) is input with a value close to zero.

Finally, the history variable to be plotted is updated, erosion (failure) is determined, and the routine is exited.

Once the model was verified and preliminarily validated, the material model source code was implemented into the production version of LS-DYNA in February 2002. We next checked that the soil model was correctly implemented into LS-DYNA. An independent evaluator then began the investigation of the validity of the soil model.

Update total volumetric strain energy:

$$\xi_{j+1} = \xi_j - \frac{1}{2}(\bar{p}_{j+1} - \bar{p}_j)\Delta\varepsilon_{v\,j+1}$$

If $\xi_{j+1} < r_j$, then skip to end

$$d_{j+1} = \frac{\xi_{j+1} - \xi_0}{\alpha - \xi_0}$$

$$\sigma = (1 - d_{j+1})\bar{\sigma}$$

$$r_{j+1} = \max(r_j, \xi_{j+1})$$

end

Figure 23. Damage update.

CHAPTER 2. USER'S MANUAL

The user's manual was written as the model was being implemented, verified, and validated. The user's manual consists of a user input guide (much like material model sections in the LS-DYNA user's manual); a brief theory manual (LSTC theory manual), which is a condensed version of the first section of this report; and a discussion of the use of the model. Both manuals will be added to an updated LS-DYNA manual. The user's manual addresses the basics of the model, input parameters, and basic equations.

Table 2 contains a brief description of the user input variables for the soil model, along with the corresponding symbols used in the LSTC theory manual. The bold text is the LSTC theory manual symbol, which is typically followed by a brief description and then the user input value symbol. The parameters that need to be specified are dependent on the soil and the specific application.

Table 2. Input parameters for soil model.

Elastic and Soil Characteristics	**K** (bulk modulus or nonporous bulk modulus if pore-water effects are used, K) **G** (shear modulus, G) γ_{sp} (specific gravity, Spgrav) $\mathbf{m_c}$ (moisture content, 0.0-1.00, Mcont) ρ (density of soil, RO)
Plasticity	ϕ (friction angle, radians, Phimax) **c** (cohesion, units of stress, Coh) **ahyp** (coefficient for modified Drucker-Prager surface, units of stress, Ahyp) **e** (eccentricity parameter for third invariant effects, Eccen)
Pore-Water Effects	$\mathbf{D_1}$ (parameter for pore-water effects on bulk modulus, Pwd1) $\mathbf{K_{sk}}$ (skeleton bulk modulus pore-water parameter, PwKsk) $\mathbf{D_2}$ (parameter for pore-water effects on effective pressure, Pwd2)
Strain Hardening	$\mathbf{A_n}$ (strain hardening, percent of phimax where nonlinear effects start, A_n) $\mathbf{E_t}$ (strain hardening, amount of nonlinear effects, E_t)
Strain Softening	ξ_0 (volumetric strain at initial damage threshold, Dint) $\mathbf{G_f}$ (void formation energy, Vdfm) φ_{res} (minimum internal friction angle used for residual strength, radians, Phires)
Strength Enhancement Caused by Strain-rate Effects	γ (viscoplasticity parameter, strain-rate-enhanced strength, Gammar) **n** (viscoplasticity parameter, strain-rate-enhanced strength, V_n)
Element Deletion	**Damlev:** Level of damage that will cause element deletion (0.0-1.0) **Epsmax:** Maximum principal failure strain
Miscellaneous	**Nplot:** Element plotting variable to put into effective plastic strain variable **Rhowat:** Density of water in model units, used to determine air void strain (saturation) **Itermax:** Maximum number of iterations used in plasticity iterations

FHWA Soil Material Model Input

MAT_FHWA_SOIL_*OPTION

Available options include:
NEBRASKA
<BLANK>
such that the keyword cards appear as
*MAT_FHWA_SOIL
*MAT_FHWA_SOIL_NEBRASKA

This is material type 147. This is an isotropic material with damage and is available for solid elements in LS-DYNA. The model has a modified Mohr-Coulomb surface to determine the pressure-dependent peak shear strength. It was developed for applications involving road-base soils.

*MAT_FHWA_SOIL_NEBRASKA
It is an option to use the default properties determined for soils used at the University of Nebraska at Lincoln. The default units used for this material are millimeter (mm), millisecond (ms), and kilogram (kg). If different units are desired, the conversion factors must be input.

Card Format

Card 1	1	2	3	4	5	6	7	8
Variable	MID	FCTIM	FCTMAS	FCTLEN				
Type	I	F	F	F				
Default	None	1.0	1.0	1.0				

Variable	Description
MID	Material identification (a unique number has to be chosen)
FCTIM	Factor by which to multiply milliseconds to get desired time units
FCTMAS	Factor by which to multiply kilograms to get desired mass units
FCTLEN	Factor by which to multiply millimeters to get desired length units

MAT_NCHRP_SOIL_*blank
Define the following cards:

Card Format

Card 1	1	2	3	4	5	6	7	8
Variable	MID	RO	Nplot	Spgrav	Rhowat	V_n	Gammar	Itermax
Type	I	F	I	F	F	F	F	I
Default	None	None	1	None	1.0	0.0	0.0	1
Card 2	1	2	3	4	5	6	7	8
Variable	K	G	Phimax	Ahyp	Coh	Eccen	A_n	E_t
Type	F	F	F	F	F	F	F	F
Default	None	None	None	None	None	None	None	None
Card 3	1	2	3	4	5	6	7	8
Variable	Mcont	Pwd1	PwKsk	Pwd2	Phires	Dint	Vdfm	Damlev
Type	F	F	F	F	F	F	F	F
Default	None	None	None	None	0.0	None	None	None
Card 4	1	2	3	4	5	6	7	8
Variable	Epsmax							
Type	F							
Default	None							

Variable	Description
MID	Material identification (a unique number has to be chosen)
RO	Mass density
Nplot	Plotting options: 1 Effective strain 2 Damage criterion threshold 3 Damage (diso) 4 Current damage criterion 5 Not used 6 Current friction angle (phi)
Spgrav	Specific gravity of soil used to get porosity
Rhowat	Density of water in model units, used to determine air void strain (saturation)
V_n	Viscoplasticity parameter (strain-rate-enhanced strength)
Gammar	Viscoplasticity parameter (strain-rate-enhanced strength)
Itermax	Maximum number of plasticity iterations (default 1)
K	Initial bulk modulus or nonporous bulk modulus if pore-water effects are used (non-zero)
G	Shear modulus (non-zero)
Phimax	Peak shear strength angle (friction angle) (radians)
Ahyp	Coefficient for modified Drucker-Prager surface
Coh	Cohesion, shear strength at zero confinement (overburden)
Eccen	Eccentricity parameter for third invariant effects
A_n	Strain hardening percent of phimax where nonlinear effects start

E_t	Strain hardening amount of nonlinear effects
Mcont	Moisture content of soil (determines amount of air voids) (0-1.00)
Pwd1	Parameter for pore-water effects on bulk modulus
PwKsk	Skeleton bulk modulus, pore-water parameter, set to zero to eliminate effects
Pwd2	Parameter for pore-water effects on effective pressure (confinement)
Phires	Minimum internal friction angle (radians) (residual shear strength)
Dint	Volumetric strain at initial damage threshold (ξ_0)
Vdfm	Void formation energy (like fracture energy)
Damlev	Level of damage that will cause element deletion (0.0-1.0)
Epsmax	Maximum principal failure strain

THEORY MANUAL

MAT_FHWA_SOIL
A brief discussion of the FHWA soil model is given. The elastic properties of the soil are isotropic. The implementation of the modified Mohr-Coulomb plasticity surface is based on the work of Abbo and Sloan.[9] The model is extended to include excess pore-water effects, strain softening, kinematic hardening, strain-rate effects, and element deletion.

The modified yield surface is a hyperbola fitted to the Mohr-Coulomb surface. At the crossing of the pressure axis (zero shear strength), the modified surface is a smooth surface and it is perpendicular to the pressure axis. The yield surface is given as:

$$F = -P\sin\varphi + \sqrt{J_2 K(\theta)^2 + ahyp^2 \sin^2\varphi} - c\cos\varphi = 0 \tag{20}$$

where:

P = pressure

φ = internal friction angle

$K(\theta)$ = function of the angle in deviatoric plane

$\sqrt{J_2}$ = square root of the second invariant of the stress deviator

c = amount of cohesion, $\cos 3\theta = \dfrac{3\sqrt{3}J_3}{2J_2^{\frac{3}{2}}}$

J_3 = third invariant of the stress deviator

ahyp = parameter for determining how close to the standard Mohr-Coulomb yield surface the modified surface is fitted

If *ahyp* is input as zero, the standard Mohr-Coulomb surface is recovered. The input parameter *ahyp* should be set close to zero, based on numerical considerations, but always less than $c \cot \varphi$. It is best not to set the cohesion, *c*, to very small values since this causes excessive iterations in the plasticity routines.

To generalize the shape in the deviatoric plane, the standard Mohr-Coulomb $K(\theta)$ function was changed to a function used by Klisinski:(10)

$$K(\theta) = \frac{4(1-e^2)\cos^2\theta + (2e-1)^2}{2(1-e^2)\cos\theta + (2e-1)[4(1-e^2)\cos^2\theta + 5e^2 - 4e]^{\frac{1}{2}}} \tag{21}$$

where:

$$\cos 3\theta = \frac{3\sqrt{3}J_3}{2J_2^{\frac{3}{2}}}$$

J_3 = third invariant of the stress deviator

e = material parameter describing the ratio of triaxial extension strength to triaxial compression strength

If e is set to 1, then a circular cone surface is formed. If e is set to 0.55, then a triangular surface is formed. $K(\theta)$ is defined for $0.5 < e \le 1.0$.

To simulate nonlinear strain hardening behavior, the friction angle φ is increased as a function of the effective plastic strain:

$$\Delta\phi = E_t\left(1 - \frac{\phi - \phi_{init}}{A_n \phi_{\max}}\right)\Delta\varepsilon_{eff\ plas} \tag{22}$$

where:

$\varepsilon_{eff\ plas}$ = effective plastic strain

A_n = fraction of the peak strength internal friction angle where nonlinear behavior begins, $0 < A_n \le 1$

The input parameter E_t determines the rate of the nonlinear hardening. If there is no strain hardening, then $\varphi_{\max} = \varphi_{\text{init}} = \varphi$.

To simulate the effects of moisture and air voids, including excess pore-water pressure, both the elastic and plastic behaviors can be modified. The bulk modulus is:

$$K = \frac{K_i}{1 + K_i D_1 n_{cur}} \tag{23}$$

where:

K_i = nonporous bulk modulus

n_{cur} = current porosity = $Max[0, (w - \varepsilon_v)]$

w = volumetric strain corresponding to the volume of air voids
= $n(1 - S)$

ε_v = total volumetric strain

D_1 = material constant controlling the stiffness before the air voids are collapsed

n = porosity of the soil = $\frac{e}{1+e}$

e = void ratio = $\frac{\gamma_{sp}\rho_w(1+m_c)}{\rho} - 1$

S = degree of saturation = $\frac{\rho m_c}{n\rho_w(1+m_c)}$

$\rho, \gamma_{sp}, m_c, \rho_w$ = soil density, specific gravity, moisture content, and water density.

Figure 24 shows the effect of the D_1 parameter on the pressure-volumetric strain relationship (bulk modulus). The bulk modulus will always be a monotonically increasing value, that is:

$$K_{j+1} = \begin{cases} \frac{K_i}{1 + K_i D_1 n_{cur}} & if\ \varepsilon_{v\ j+1} > \varepsilon_{vj} \\ K_j & if\ \varepsilon_{v\ j+1} \le \varepsilon_{vj} \end{cases} \tag{24}$$

Note that the model is following the standard practice of assuming that compressive stresses and strains are positive. If the input parameter D_1 is zero, then the standard linear elastic bulk modulus behavior is used.

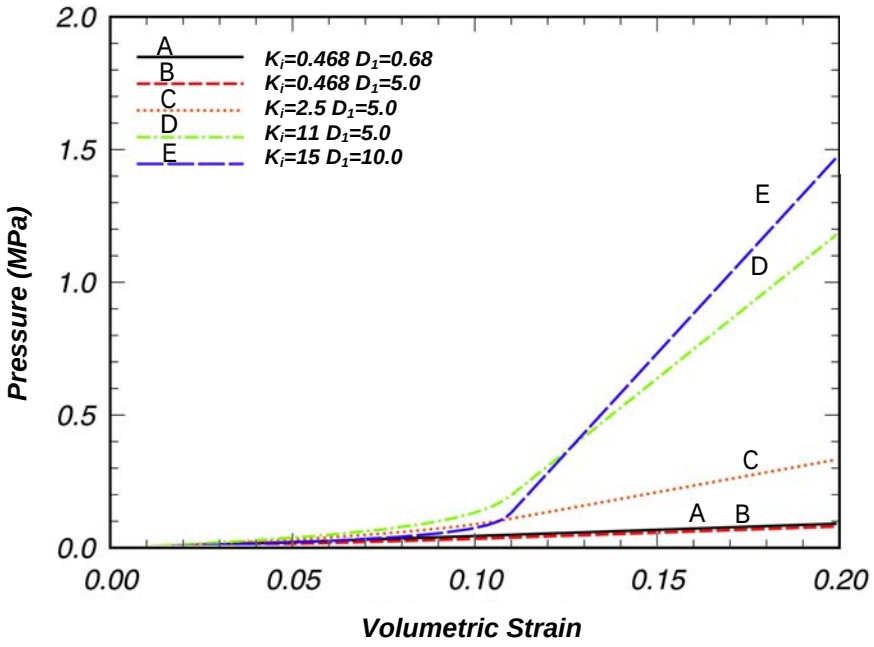

Figure 24. Pressure versus volumetric strain showing the effects of the D_1 parameter.

If D_1 is not set to zero, the bulk modulus input should be the fully collapsed bulk modulus.

To simulate the loss of shear strength caused by excess pore-water effects, the model uses a standard soil mechanics technique[11] of reducing the total pressure, P, by the excess pore-water pressure, u, to get an "effective pressure," P':

$$P' = P - u \tag{25}$$

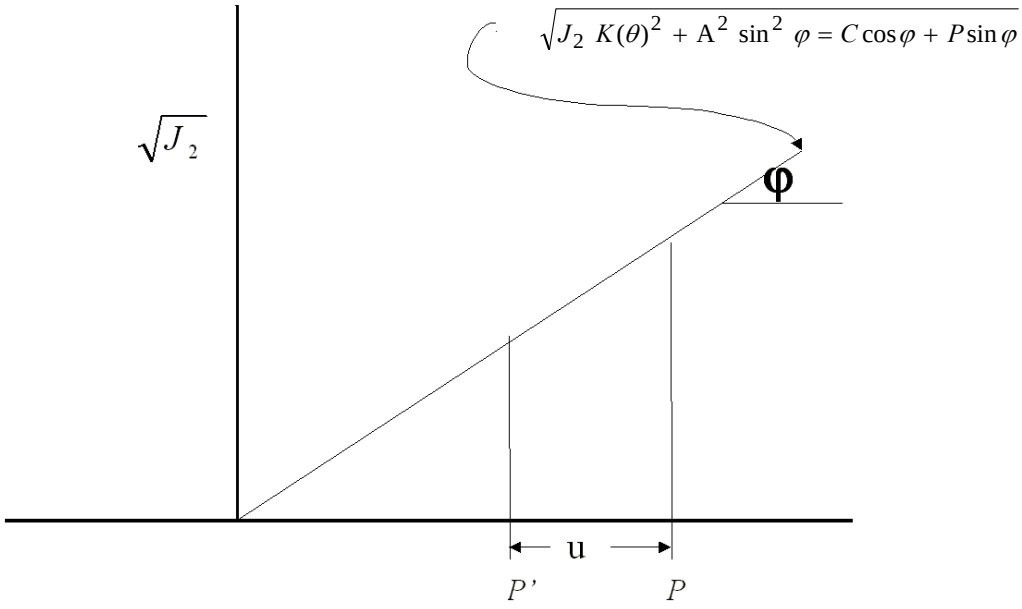

Figure 25. Effects on pressure caused by pore-water pressure.

Figure 25 shows how pore-water pressure affects the algorithm for the plasticity surface. The excess pore-water pressure reduces the total pressure, which lowers the shear strength, $\sqrt{J_2}$. Significant excess pore-water pressure can cause the effective pressure to become zero. To calculate the pore-water pressure, u, the model uses an equation similar to the equation used for the moisture effects on the bulk modulus:

$$u = \frac{K_{sk}}{1 + K_{sk} D_2 n_{cur}} \varepsilon_v \tag{26}$$

where:

K_{sk} = bulk modulus for soil without air voids (skeletal bulk modulus)

n_{cur} = current porosity = $Max[0, (w - \varepsilon_v)]$

w = volumetric strain corresponding to the volume of air voids
= $n(1 - S)$

ε_v = total volumetric strain

D_2 = material constant controlling the pore-water pressure before the air voids are collapsed $D_2 \geq 0$

n = porosity of the soil = $\frac{e}{1 + e}$

e = void ratio = $\frac{\gamma_{sp}(1+m_c)}{\rho} - 1$

S = degree of saturation = $\frac{\rho m_c}{n(1+m_c)}$

ρ, γ_{sp}, m_c = soil density, specific gravity, and moisture content, respectively

The increment pore-water pressure is zero if the incremental mean strain is negative (tensile).

Figure 26 is a plot of the pore pressure versus volumetric strain for different parameter values. With the D_2 parameter set relatively high compared to K_{sk}, there is no pore pressure until the volumetric strain is greater than the strains associated with the air voids. However, as D_2 is lowered, the pore pressure starts to increase before the air voids are totally collapsed. The K_{sk} parameter affects the slope of the post-void collapse pressure-volumetric strain behavior.

The parameter D_2 is found from Skempton pore-water pressure parameter B, where B is defined as:[7]

$$B = \frac{1}{1 + n\frac{K_{sk}}{K}} \tag{27}$$

$$\therefore \quad D_2 = \frac{1-B}{B\,K_{sk}[n(1-S)]} \tag{28}$$

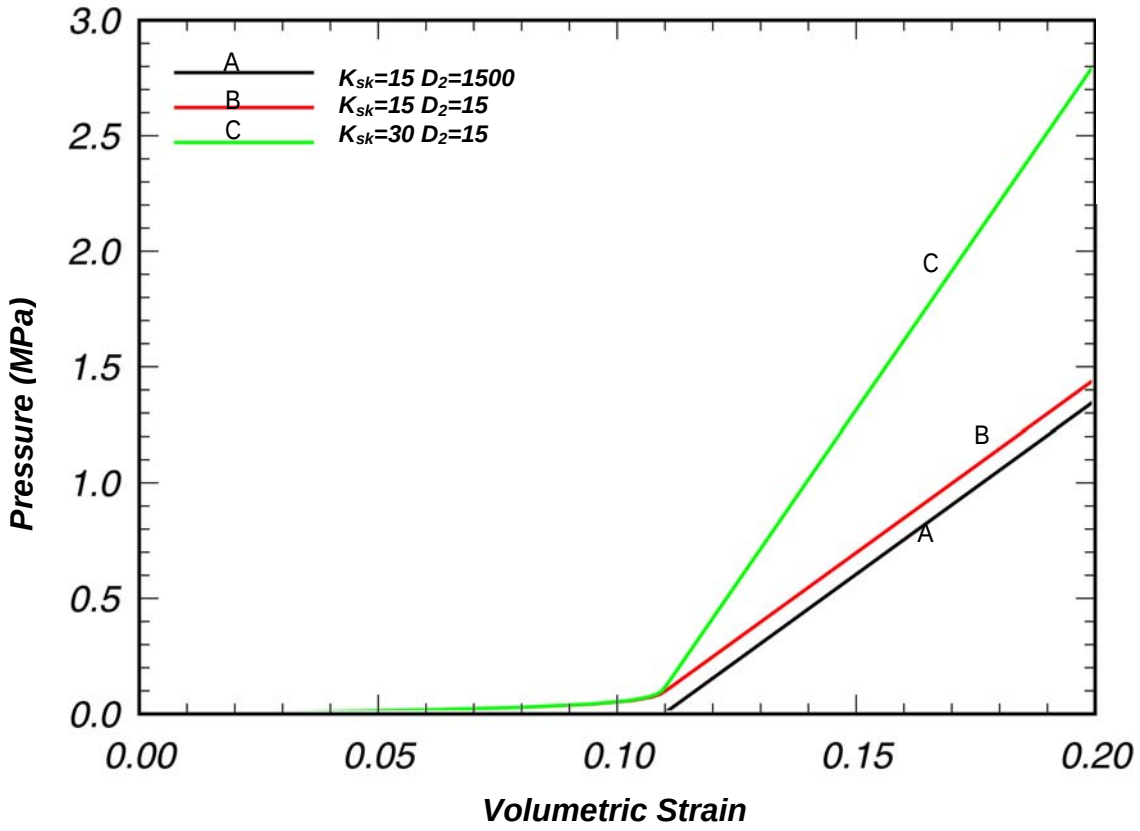

Figure 26. Effects of D_2 and K_{sk} parameters on pore-water pressure.

To simulate strain softening behavior, the FHWA soil model uses a continuum damage algorithm. The strain-based damage algorithm is based on the work of J.W. Ju and J.C. Simo. They proposed a strain-based damage criterionthat is uncoupled from the plasticity algorithm.[12,13]

For the damage criterion $\xi = -\frac{1}{K_i}\int \overline{P} d\varepsilon_{pv}$, where $\overline{P}$ = pressure and ε_{pv} = plastic volumetric strain, the damaged stress is found from the undamaged stresses:

$$\sigma = (1-d)\overline{\sigma} \tag{29}$$

where: d = isotropic damage parameter (diso)

The damage parameter is found at step $j+1$ as:

$$\begin{aligned} d_{j+1} &= d_j \ldots\ldots\ldots\ldots\ldots\ldots\ldots\ldots if \quad \xi_{j+1} \le r_j \\ d_{j+1} &= \frac{\xi_{j+1}-\xi_0}{\alpha-\xi_0} \ldots\ldots\ldots\ldots\ldots if \quad \xi_{j+1} > r_j \end{aligned} \tag{30}$$

where:
r_{j+1} = damage threshold surface

$$r_{j+1} = \max(r_j, \xi_{j+1})$$

$\xi_0 = r_0$ (Dint)

The mesh-sensitivity parameter, α, is described below.

Typically, the damage, *d*, varies from 0 to a maximum of 1. However, some soils can have a residual strength that is pressure-dependent. The residual strength is represented by φ_{res}, the minimum internal friction angle.

The maximum damage allowed is related to the internal friction angle of residual strength by:

$$d_{\max} = \frac{\sin\varphi - \sin\varphi_{res}}{\sin\varphi} \tag{31}$$

If $\varphi_{res} > 0$, then $d_{\max}$, the maximum damage, will not reach 1 and the soil will have residual strength.

When material models include strain softening, special techniques must be used to prevent mesh sensitivity. Mesh sensitivity is the tendency of the finite element model/analysis to produce significantly different results as the element size is reduced. Mesh sensitivity occurs because the softening in the model is concentrated in one element. As the element size is reduced, the failure becomes localized in smaller volumes, which causes less energy to be dissipated by the softening. This can lead to instabilities or, at least, mesh-sensitive behavior.

To eliminate or reduce the effects of strain softening mesh sensitivity, the softening parameter, α (the strain at full damage), must be modified as the element size changes. The FHWA soil model uses an input parameter, "void formation," G_f, that is like the fracture energy material property for metals. The void formation parameter is the area under the softening region of the pressure-volumetric strain curve times the cube root of the element volume, $V^{1/3}$:

$$G_f = V^{1/3}\int_{\xi_0}^{\alpha} P\,\mathrm{d}\varepsilon_{\mathrm{v}} = \frac{P_{\mathrm{peak}}(\alpha - \xi_0)V^{1/3}}{2} \tag{32}$$

with ξ_0 as the volumetric strain at peak pressure (strain at initial damage (Dint)). Then, α can be found as a function of the volume of the element V:

$$\alpha = \frac{2G_{\mathrm{f}}}{K\xi_0 V^{1/3}} + \xi_0 \tag{33}$$

If G_f is made very small relative to $K\xi_0 V^{1/3}$, then the softening behavior will be brittle.

Strain-rate-enhanced strength is simulated by a two-parameter Devaut-Lions viscoplastic update algorithm developed by Y. Murray.[15] This algorithm interpolates between the elastic trial stress (beyond the plasticity surface) and the inviscid stress. The inviscid stresses ($\overline{\sigma}$) are on the plasticity surface $\overline{\sigma}_{vp} = (1-\varsigma)\overline{\sigma} + \varsigma\overline{\sigma}_{trial}$, with $\varsigma = \frac{\eta}{\Delta t + \eta}$ and $\eta = (\frac{\gamma_r}{\dot{\varepsilon}})^{(vn-1)/vn}$.

As ζ becomes 1, then the viscoplastic stress becomes the elastic trial stress. Setting the input value $\gamma_r = 0$ (gamma) eliminates any strain-rate-enhanced strength effects.

The model allows element deletion if needed. As the strain softening (damage) increases, the effective stiffness of the element can become very small, causing severe element distortion and "hourglassing." The element can be "deleted" to remedy this behavior. There are two input parameters that affect the point of element deletion. Damlev is the damage threshold where element deletion will be considered. Epsmax is the maximum principal strain where the element will be deleted. Both $d \geq$ Damlev and $\varepsilon_{pr\max} >$ Epsmax are required for element deletion to occur. If Damlev is set to zero, there is no element deletion. Care must be taken when employing element deletion to ensure that the internal forces are very small (element stiffness is zero) or significant errors may be introduced into the analysis.

MAT_FHWA_SOIL_NEBRASKA
This option gives the soil parameters that were used to validate the material model with experiments performed at the University of Nebraska at Lincoln. The units of these default inputs are milliseconds, kilograms, and millimeters. There are no required input parameters except for material ID (MID). If different units are desired, the appropriate unit conversion factors can be input.

DISCUSSION OF SOIL MODEL USE

Material models for geomaterials (soils, concrete, rock, etc.) tend to be complex. The determination of the input parameters for the models is complicated. In addition, modeling different loading conditions and accurate simulation of boundary conditions add to the complexity involved in using these material models.

There are two methods that are typically used to determine the material input variables for soils. The most accurate method is to perform laboratory tests that include both triaxial compression and uniaxial strain tests. These tests can be used to determine the

elastic moduli, yield surface parameters, and softening parameters. Typically, these tests use drained soil conditions. Laboratory tests with undrained soil conditions can be used to determine the pore-water effects.

A second method is to use full-scale testing of the specific application (e.g., a bogie impacting a steel post) to fit the parameters in a trial-and-error method. This method requires more time by the analyst. Since the soil model is nonlinear, there may not be a set of unique input parameters that can be determined.

Compaction of the soil is typically used to remove some of the air voids that exist in disturbed soils. However, the density, pore-water effects, stiffness, and strength are also changed upon compacting the soil. To simulate compaction in highway safety applications where the soil is exposed, we recommend that the values for the soil density, pore-water effects, stiffness, and strength be modified. Applying pressure to the ground surface to account for the effects of compaction is a less accurate method that will incorrectly simulate how the soil is deformed at the surface.

In full-scale testing or applications, the soil typically extends to infinity. Analyses typically do not extend to infinity, so some type of boundary condition must be applied to the exterior surfaces of a soil analysis model (except for soil surfaces exposed to atmospheric pressure). Standard boundaries reflect dynamic disturbances (stress waves), which does not happen in the real applications. Such reflections can cause serious contamination of the analysis results. Exterior boundaries for analyses involving soil need a nonreflecting boundary. A partial nonreflecting boundary exists in LS-DYNA. This boundary is an impedance-matching boundary, which is only good for high-frequency (highly transient) behavior. At this time, there is no nonreflecting boundary that matches both low- (quasi-static) and high- (highly transient) frequency behaviors. Also, only linear behavior is assumed. Thus, to use the current nonreflecting boundary, the material near the boundaries must only behave linearly. Also, the nonreflecting boundary should only experience high-frequency behavior.

CHAPTER 3. EXAMPLES MANUAL

This section presents some examples of simulations that were used during the verification phase of the development of the FHWA soil material model. The first example can be used to check the model accuracy and to familiarize the user with the material model. It consists of a single-element simulation of a triaxial compression experiment. Appendix B contains an example of the input for the triaxial compression single-element simulation. Figure 27 shows the results of the single-element simulation of a triaxial compression test at 3.4 MPa.

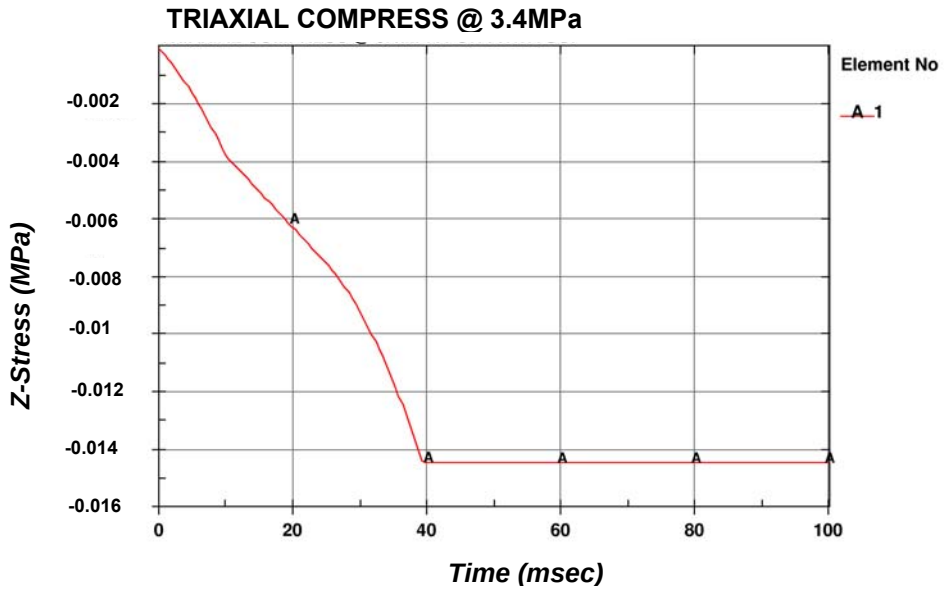

Figure 27. Z-stress versus time for single-element 3.4-MPa triaxial **compression simulation.**

The peak strains in this example reach 80 percent. This shows that the material model will successfully analyze problems with large strains (deformations).

A second example of the use of the FHWA soil material model is a simulation of a direct shear test. The goal of the tests was to determine the soil properties for the NCHRP Report 350 strong soil using large test specimens. The analysis is of direct shear test 4 (DS-4).[16] Contractors developed the model (see figure 28). The material model input for this simulation is shown in appendix B. Figure 29 shows the comparison between the test and the analysis of shear force versus deflection. The early time test data exhibit questionable trends and the analysis results show the expected trend (i.e., positive stiffness). Figure 30 shows the deformed shape of the cylinder at the end of

the analysis. The analysis was terminated at approximately 47 millimeters (mm) of deflection because of the current failure criteria in LS-DYNA. An element fails (i.e., is eliminated from the simulation) when *one of the gauss points* reaches the failure criteria. For selective reduced integrated elements (8 gauss points), this causes premature failure. This premature failure does not let the internal forces go to zero in the failed elements. In turn, this leads to very large unbalanced forces at the nodes, causing unstable behavior (shooting nodes).

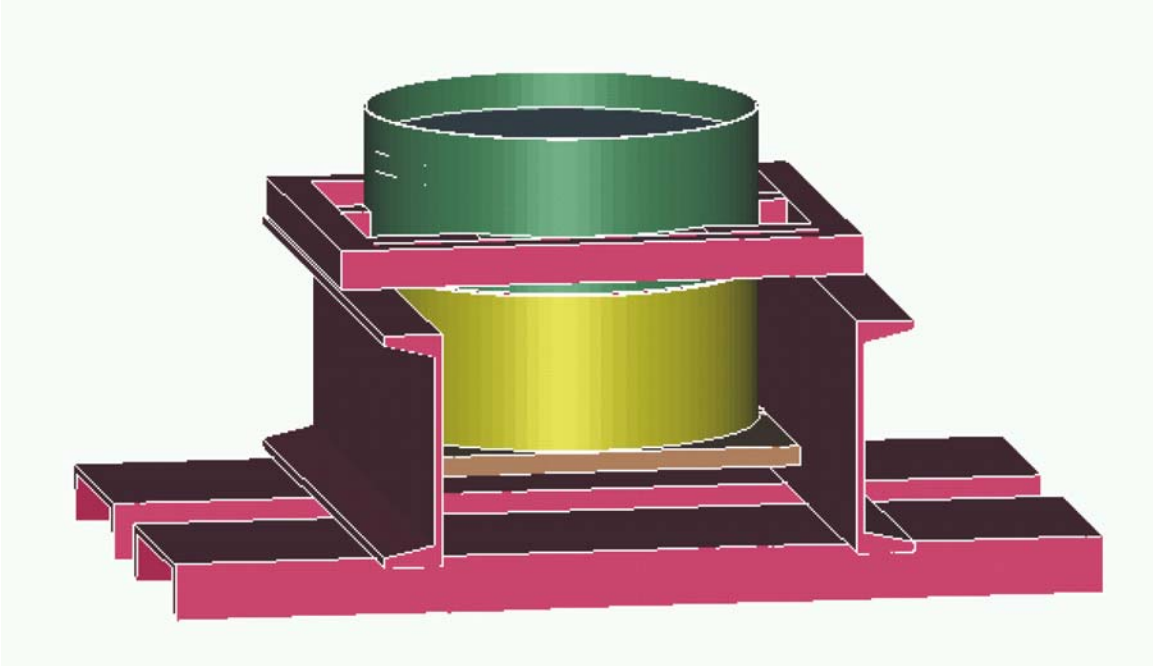

Figure 28. LS-DYNA model of direct shear test DS-4.

The element formulation for this model is selective-reduced (S/R) elements. It is well known (see note 5 in the *SECTION input of the LS-DYNA manual) that poor aspect ratios (highly distorted elements) will cause shear locking. Elements along the shearing surface of the direct shear test simulation experience very large distortions, approximately equal to the element dimensions. Therefore, if severely distorted elements are not eliminated by erosion, the simulation will produce excessively stiff response (shear locking). An obvious way to overcome these problems is to use the standard constant stress (1 gauss point) element. However, time and funding did not allow the exploration of this option. A second option would be to refine the element mesh in the vicinity of the shearing surface to reduce the large deformations of the individual elements. A third option would be to use the Arbitrary Langrangian-Eulerian (ALE) formulation and the constant stress element. However, at this time, the FHWA material model is not available for use with ALE (although the capability of the FHWA soil material model to be used in conjunction with ALE was successfully tested during the early phase of this development effort with the model implemented as a user-defined material model).

As shown in figure 30, there are surfaces of the soil, which at the time of the analysis, are in contact with the metal or air. Also, the interface between the two cylinder halves has become a noncontinuous surface (i.e., a slide surface). This behavior cannot be accurately modeled by the continuum mechanics material model; it must be modeled by slide surfaces.

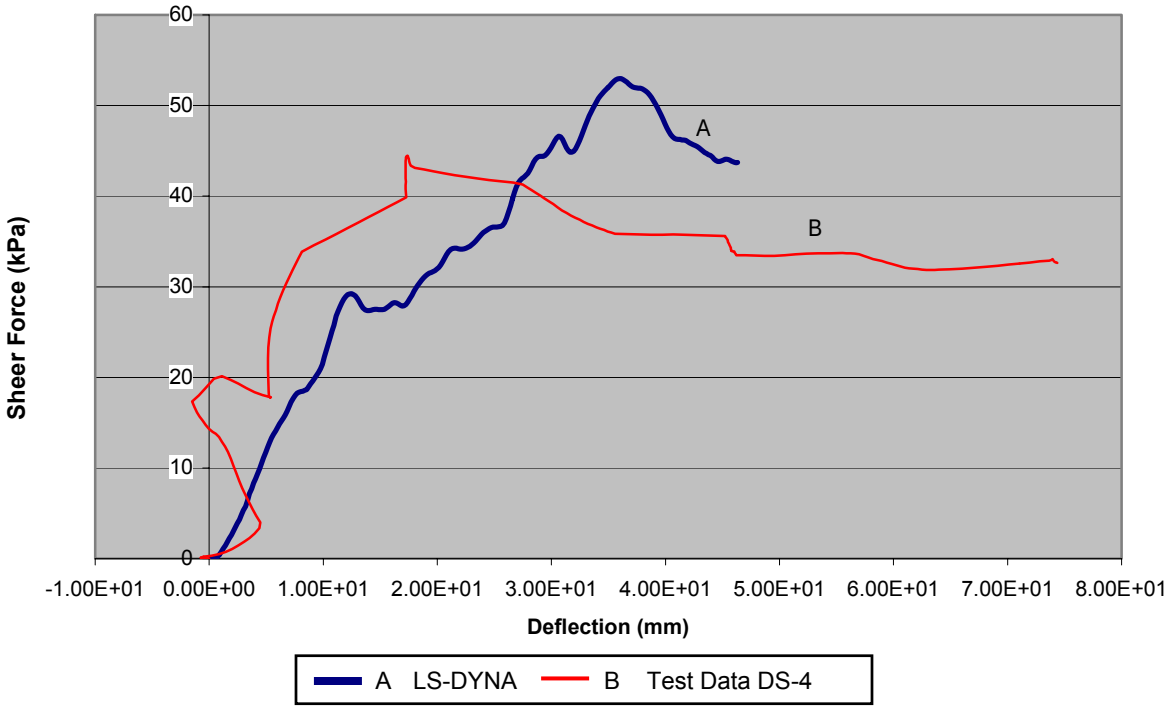

Figure 29. Shear stress versus deflection comparison for DS-4.

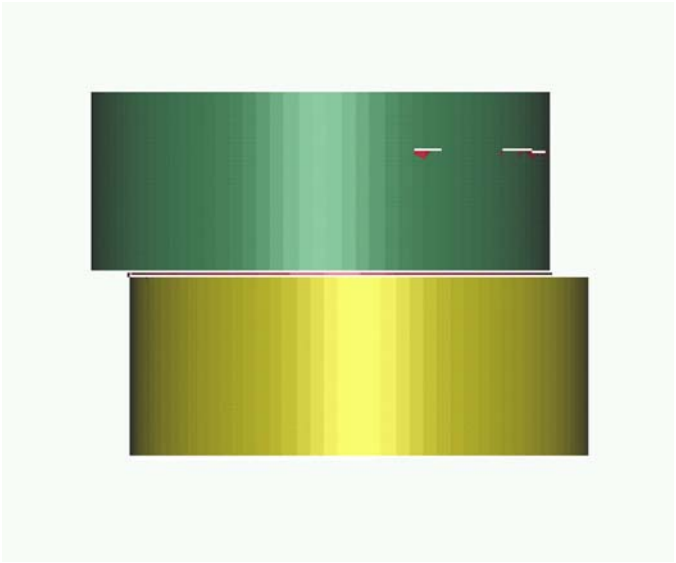

Figure 30. Analysis results for DS-4 deformation.

To further investigate the behavior of the soil model in shear stress, a model used in the development of the model was run with both 1 gauss point (elform = 1) and 8 gauss point (elform = 2) elements. Figure 31 shows the model, which consists of two materials (the material on the left is the FHWA soil material and the material on the right is a relatively stiff elastic material). A velocity boundary condition is applied to the free soil surface in the vertical position.

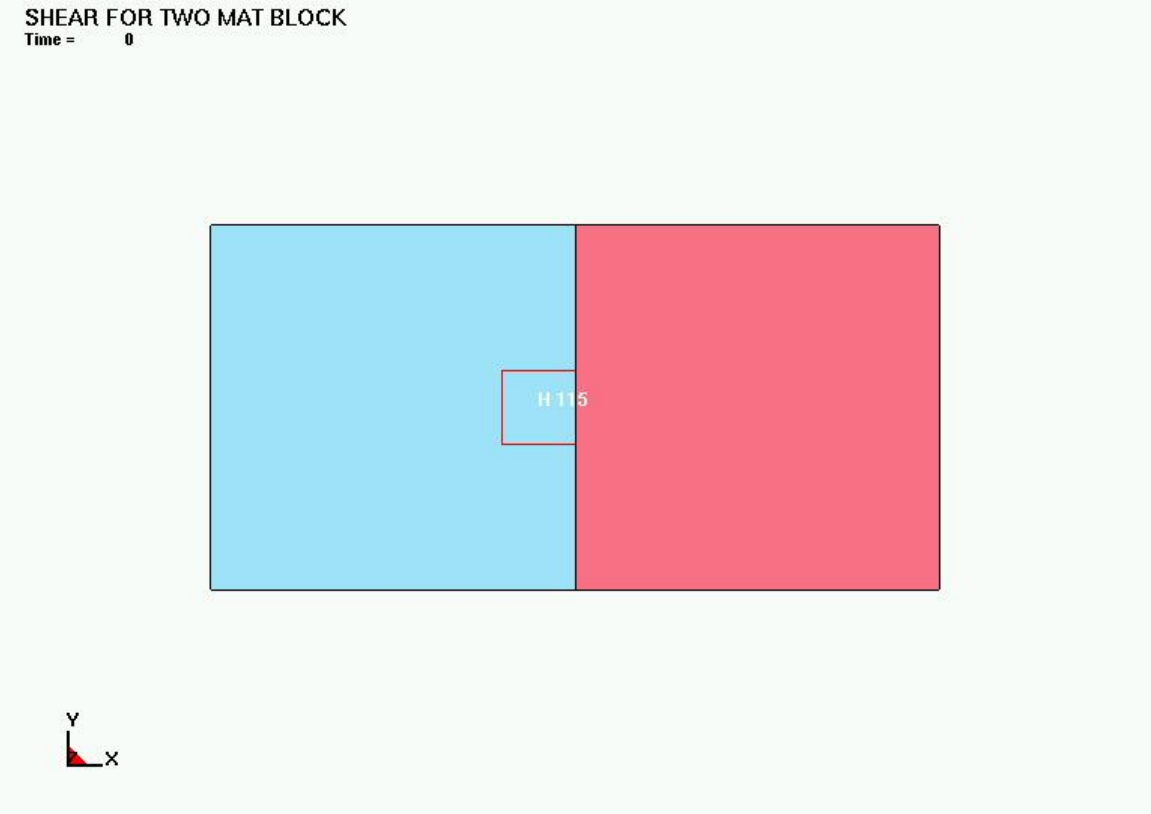

Figure 31. Simple two-material shear model.

The input parameters for the soil material were from the direct shear analysis. Figure 32 shows the deformed shape of the 1 gauss point element analysis at 1.75 milliseconds (ms), and figure 33 shows the deformed shape of the 8 gauss point element analysis at 1.75 ms. The analyses were stopped just before the 8 gauss point element becomes unstable because of the failure criteria error in the 8 gauss point element (outside the material subroutine).

Figure 34 shows the x-y shear stress in element 115 (shown in the previous figures). Since the soil material has a low cohesion (shear strength at zero normal force) of 6.2×10^{-6} gigapascals (GPa) (6.2 kilopascals (KPa)), the x-y shear stress should not get very large. The 8 gauss point element shows an immediate increase in the x-y shear stress to more than 0.03 GPa (30 MPa); this type of behavior is known as “shear locking.” It is caused by the formulation of the 8 gauss point element outside of the material routine. As mentioned previously, this inaccurate behavior is mentioned in the

LS-DYNA manual. **The 8 gauss point element should not be used for any analysis that involves shearing or failure.**

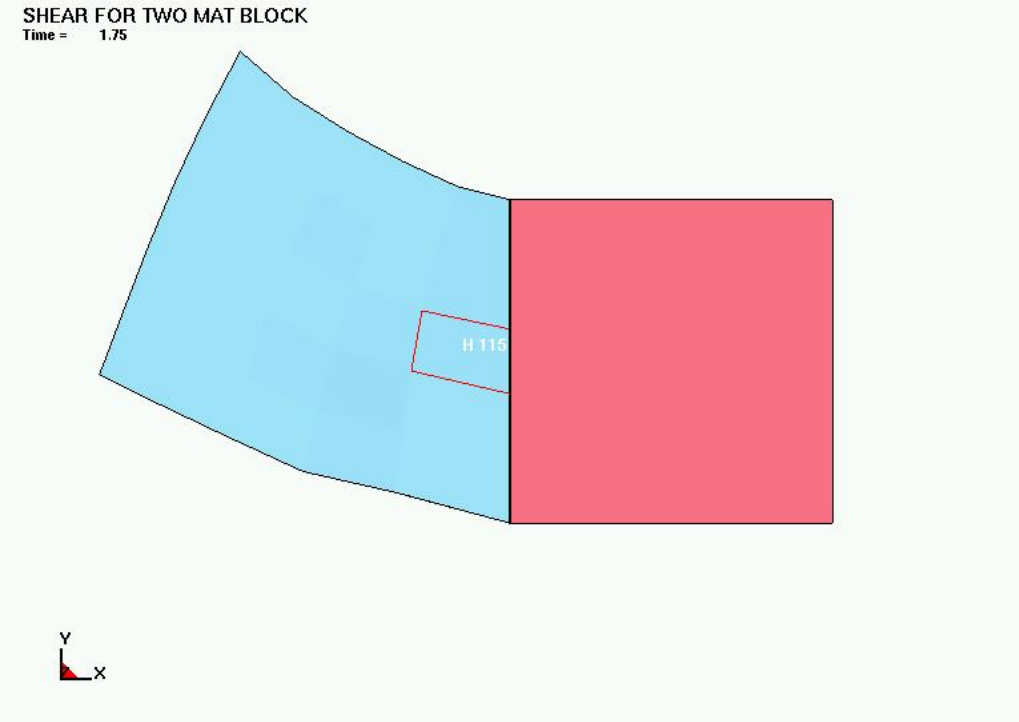

Figure 32. Deformed shape of 1 gauss point element analysis.

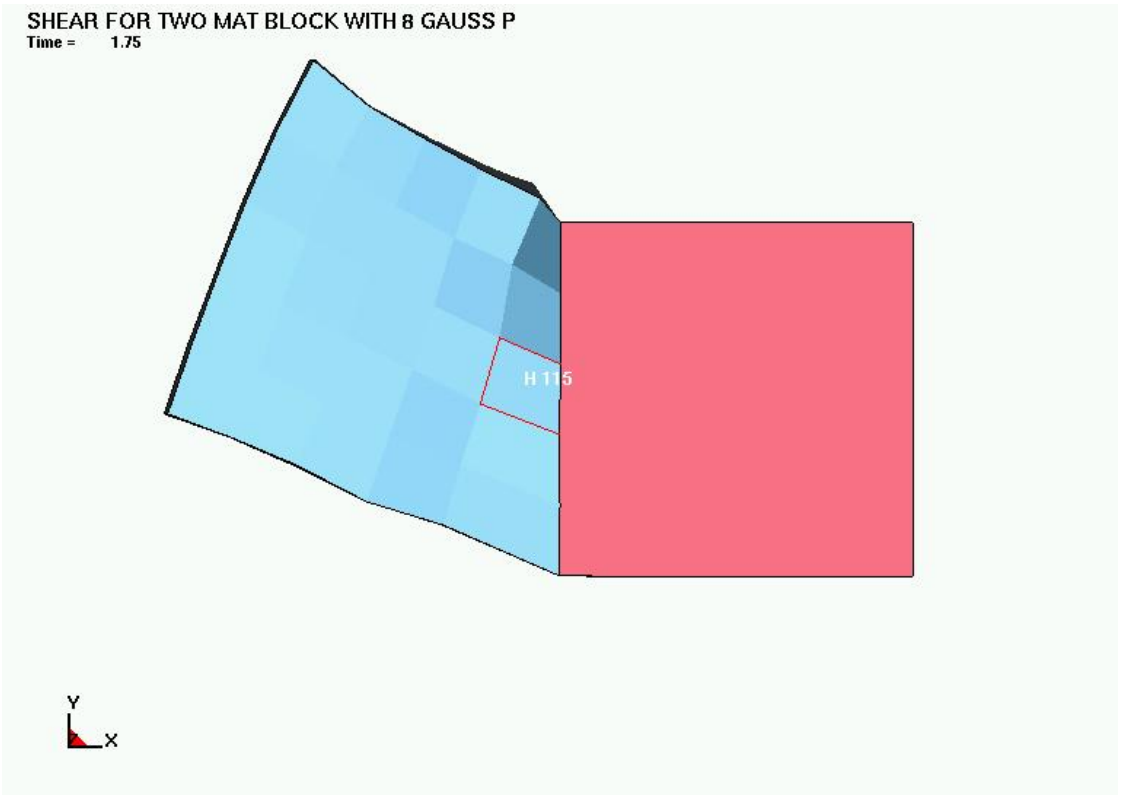

Figure 33. Deformed shape of 8 gauss point element analysis.

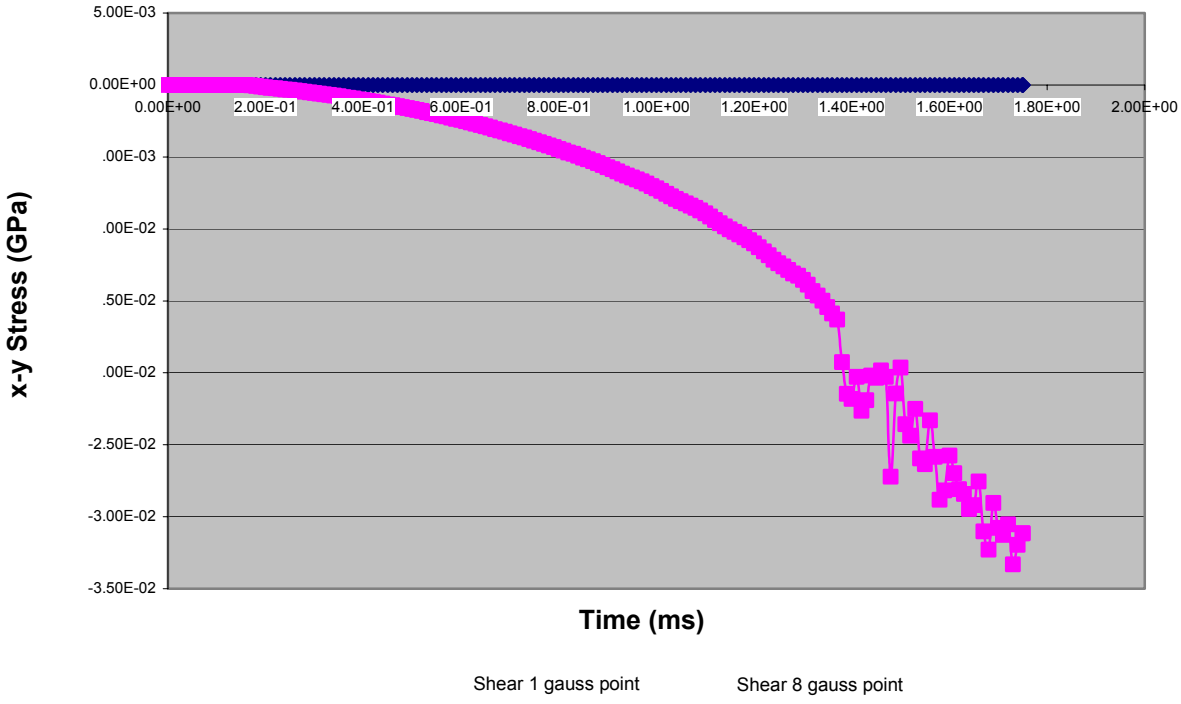

Figure 34. Comparison of x-y stress at element 115 for 1 gauss point and 8 gauss point elements.

The material properties used in the simulations/examples described above were not determined from actual material property test data, but were found by trial and error. Obviously, actual material property data would probably lead to more confident results.

CHAPTER 4. SUMMARY

This report presents the theory manual, user's manual, and typical examples for the FHWA soil material model implemented into LS-DYNA. This model was developed for use in roadside safety applications. The model is a modified Drucker-Prager plasticity model. In addition to the plasticity model, the FHWA soil material model includes pre-peak hardening, post-peak strain softening (damage), strain-rate effects (strength enhancement), pore-water effects (moisture effects), and erosion capability. These enhancements to the standard soil material models were made to increase the accuracy, robustness, and ease of use for roadside safety applications.

The theory manual gives a detailed description of the model, including the justification, equations, and methods of implementation of the equations. Developers should be able to use the theory manual to make modifications to, or maintain, the FHWA soil material model. Appendix A presents the details of the determination of the plasticity gradients.

The user's manual is a contractor's user's manual for the FHWA soil material model. Also included is a table that shows the correspondence between the symbols used in the theory manual and the input variables in the user's manual. A brief discussion of the use of the model in roadside safety applications is also included in this section.

Finally, typical examples are presented. These examples should help the user prepare the input and check out the model for their versions of LS-DYNA. The direct shear test simulation was stopped at approximately 46 ms because of shear locking and premature erosion (deletion) of the selectively reduced integration (8 gauss integration point) elements. The problem of shear locking is well known for this type of element when the element is subjected to large distortions. Premature erosion of this element type is a deficiency of the current version of LS-DYNA (version 970 Beta) and is not ascribable to improper functioning of the FHWA soil material model. The use of ALE with constant stress elements (1 gauss integration point) may produce results with greater simulation times.

Presently, the FHWA soil material model has been shown to be accurate for small soil samples at all levels of deformation and for large simulations that involve small to intermediate deformations. This restriction is caused by limitations in the current version of LS-DYNA.

Additional work is recommended to provide a more robust FHWA soil material model. This work includes investigation of the use of ALE for simulations involving large distortions, investigation/development of nonreflecting boundaries, and further simulations investigating moisture and strain-rate effects. Additional testing would be advantageous for the determination of accurate material properties (soil material model input).

APPENDIX A. DETERMINATION OF PLASTICITY GRADIENTS

In the following, the gradient of the yield surface in stress space is determined. The yield function is:

$$F = -P\sin\varphi + \sqrt{J_2 K(\theta)^2 + \mathrm{a}^2\sin^2\varphi} - \mathrm{c}\cos\varphi \tag{34}$$

where:

$$K(\theta) = \frac{4(1-e^2)\cos^2\theta + (2e-1)^2}{2(1-e^2)\cos\theta + (2e-1)[4(1-e^2)\cos^2\theta + 5e^2 - 4e]^{\frac{1}{2}}}$$

$$\cos 3\theta = \frac{3\sqrt{3}J_3}{2J_2^{3/2}}$$

J_3 = third invariant of the stress deviator

e = material parameter describing the ratio of triaxial extension strength to triaxial compression strength

We need to find $\frac{\partial F}{\partial \sigma}$. A convenient method is:

$$\frac{\partial F}{\partial \sigma} = C_1\frac{\partial p}{\sigma} + C_2\frac{\partial\sqrt{J_2}}{\partial\sigma} + C_3\frac{\partial J_3}{\sigma} \tag{35}$$

where:

$$C_1 = \frac{\partial F}{\partial p}, \quad C_2 = \frac{\partial F}{\partial \sqrt{J_2}} - \frac{\tan 3\theta}{\sqrt{J_2}} \frac{\partial F}{\partial \theta}, \quad C_3 = \frac{\sqrt{3}}{2\cos 3\theta \, {J_2}^{3/2}} \frac{\partial F}{\partial \theta}$$

$$\frac{\partial p}{\partial \sigma} = \frac{1}{3} \begin{Bmatrix} 1 \\ 1 \\ 1 \\ 0 \\ 0 \\ 0 \end{Bmatrix} \qquad \frac{\partial \sqrt{J_2}}{\partial \sigma} = \frac{1}{2\sqrt{J_2}} \begin{Bmatrix} s_{11} \\ s_{22} \\ s_{33} \\ 2\sigma_{12} \\ 2\sigma_{23} \\ 2\sigma_{31} \end{Bmatrix}$$

$$\frac{\partial J_3}{\partial \sigma} = \begin{Bmatrix} s_{22}s_{33} - {\sigma_{23}}^2 \\ s_{11}s_{33} - {\sigma_{31}}^2 \\ s_{11}s_{22} - {\sigma_{12}}^2 \\ 2(\sigma_{23}\sigma_{13} - s_{33}\sigma_{12}) \\ 2(\sigma_{31}\sigma_{12} - s_{11}\sigma_{23}) \\ 2(\sigma_{12}\sigma_{23} - s_{22}\sigma_{31}) \end{Bmatrix} + \frac{J_2}{3} \begin{Bmatrix} 1 \\ 1 \\ 1 \\ 0 \\ 0 \\ 0 \end{Bmatrix}$$

Here, s_i is the stress deviator. Now, we just need to determine the coefficients C_1, C_2, and C_3:

$$C_1 = -\sin\varphi \tag{36}$$

$$C_2 = \frac{\sqrt{J_2}K(\theta)}{\sqrt{J_2 K(\theta)^2 + a^2 \sin^2\varphi}} \left(K(\theta) - \tan 3\theta \frac{\partial K(\theta)}{\partial \theta}\right) \tag{37}$$

$$C_3 = \frac{\sqrt{J_2}K(\theta)}{\sqrt{J_2 K(\theta)^2 + a^2 \sin^2\varphi}} \frac{\sqrt{3}}{2\cos 3\theta J_2} \frac{\partial K(\theta)}{\partial \theta} \tag{38}$$

$$\frac{\partial K(\theta)}{\partial \theta} = \frac{8(1-e^2)\cos\theta\sin\theta}{2(1-e^2)\cos\theta + (-1+2e)(-4e+5e^2+4(1-e^2)\cos^2\theta)^{\frac{1}{2}}} - \frac{((-1+2e)^2 + 4(1-e^2)\cos^2\theta)(-2(1-e^2)\sin\theta - \left(\frac{4(-1+2e)(1-e^2)\cos\theta\sin\theta}{(-4e+5e^2+4(1-e^2)\cos^2\theta)^{\frac{1}{2}}}\right)}{(2(1-e^2)\cos\theta + (-1+2e)(-4e+5e^2+4(1-e^2)\cos^2\theta)^{\frac{1}{2}})^2} \tag{39}$$

Note that $\frac{\partial K(\theta)}{\partial \theta}$ is not defined at e = 0.5 and $\theta = \frac{\pi}{2}$.

For the hardening functions, see equations 40 and 41.

$$\frac{\partial F}{\partial \varphi} = p\cos\varphi + c\sin\varphi + \frac{a^2\cos\varphi\sin\varphi}{\sqrt{J_2 K(\theta)^2 + a^2\sin^2\varphi}} \tag{40}$$

$$\frac{\partial \varphi}{\partial \varepsilon_{ep}} = H(1 - \frac{\varphi - \varphi_{init}}{N\varphi_{\max}}) \tag{41}$$

From Chen and Han, p. 223, see equation 42 below:

$$h = \frac{\partial f}{\partial \sigma} C \frac{\partial f}{\partial \sigma} = (9KB_0^2 + 4GB_1^2 J_2 + \frac{4}{3}GB_2^2 J_2^2 + 12GB_1 B_2 J_2) \tag{42}$$

where: $\frac{\partial f}{\partial \sigma} = B_0 \frac{\partial I_1}{\partial \sigma} + B_1 \frac{\partial J_2}{\partial \sigma} + B_2 \frac{\partial J_3}{\partial \sigma}$

In comparison with Abbo and Sloan:

$$B_0 = \frac{\sin\phi}{3} \tag{43}$$

$$B_1 = \frac{C_2}{2\sqrt{J_2}} \tag{44}$$

$$B_2 = C_3 \tag{45}$$

Therefore,

$$h = K\sin\phi^2 + GC_2^2 + \frac{4}{3}GC_3^2 J_2^2 + \frac{6GC_2 C_3 J_3}{\sqrt{J_2}} \tag{46}$$

$$\Delta\sigma_{ij} = \Delta\lambda C_{ijkl} \frac{\partial f}{\partial \sigma_{kl}} = \Delta\lambda(K\sin\phi\delta_{ij} + \frac{GC_2}{\sqrt{J_2}} s_{ij} + 2GC_3 t_{ij}) \tag{47}$$

where:

$s_{ij} = \sigma_{ij} - p\delta_{ij}$

$t_{ij} = \frac{\partial J_3}{\partial \sigma_{ij}} = s_{ik}s_{kj} - \frac{2J_2\delta_{ij}}{3}$

APPENDIX B. EXAMPLES OF INPUT

INPUT FOR SINGLE-ELEMENT SIMULATION OF 3.4-MPA TRIAXIAL COMPRESSION TEST

```
*KEYWORD
*TITLE
TRIAXIAL COMPRESS @ 3.4MPa for FHWA soil model
$
$ Check out/debug model with research plan changes
$      Look at effects of changing Ksk and pwd2
$      Look at effects of changing moisture content with Ksk and pwd2 fixed
$      Use Nebraska soil parameters
$
$ Last Modified: March 27, 2002 by Brett Lewis
$
$ Units: kg, mm, msecs
$
$$$$$$$$$$$$$$$$$$$$$$$$$$$$$$$$$$$$$$$$$$$$$$$$$$$$$$$$$$$$$$$$$$$$$$$$$$$$$$$$
$
$$$$ Control Output
$
$$$$$$$$$$$$$$$$$$$$$$$$$$$$$$$$$$$$$$$$$$$$$$$$$$$$$$$$$$$$$$$$$$$$$$$$$$$$$$$$
$
*CONTROL_TERMINATION
$   endtim    endcyc     dtmin    endneg    endmas
    100.00
$
*CONTROL_TIMESTEP
$   dtinit      scft      isdo    tslimt      dtms      lctm     erode     ms1st
                                                           3
*DEFINE_CURVE
$     lcid      sidr      scla      sclo      offa      offo
         3
$           abscissa            ordinate
               0.000            1.54E-04
             10.0000            1.54E-04
          50.000                1.54E-03
        1000000.                1.54E-03
$
*CONTROL_ENERGY
$     hgen      rwen    slnten     rylen
         2         1
$
*CONTROL_OUTPUT
$    npopt    neecho    nrefup    iaccop     opifs    ipnint    ikedit
         0         3
$
$
*DATABASE_BINARY_D3PLOT
$       dt      lcdt
    0.5000
$   1.0000
$
*DATABASE_EXTENT_BINARY
```

```
$    neiph    neips    maxint    strflg    sigflg    epsflg   rltflg    engflg
$   cmpflg   ieverp    beamip
                  0
$
*DATABASE_BINARY_D3THDT
$       dt      lcdt
    999999
$
*DATABASE_GLSTAT
$       dt
   .500000
$
*DATABASE_MATSUM
$       dt
   .500000
$
$
$
$
$
$$$$$$$$$$$$$$$$$$$$$$$$$$$$$$$$$$$$$$$$$$$$$$$$$$$$$$$$$$$$$$$$$$$$$$$$$$$$$$$$
$
$$$$ Define Parts and Materials
$
$$$$$$$$$$$$$$$$$$$$$$$$$$$$$$$$$$$$$$$$$$$$$$$$$$$$$$$$$$$$$$$$$$$$$$$$$$$$$$$$
$
$$$ Part   1   solid: SINGLE ELEMENT
$
*PART
$      pid       sid       mid     eosid      hgid      adpopt
cube - Material 147 HRCL soil
         1         1         1
$$$$  materials
$...>....1....>....2....>....3....>....4....>....5....>....6....>....7....>....8
*MAT_147
$      mid        ro     NPLOT    SPGRAV    RHOWAT        VN    GAMMAR   ITERMAX
         1  2.350E-6         3      2.79    1.0E-6       1.1      000.        10
$        K         G    PHIMAX      AHYP       COH    ECCEN        AN        ET
   .465000   .186000       1.1    1.0E-7    1.0E-6       0.7       0.0       10.
$    MCONT      PWD1     PWKSK      PWD2    PHIRES      DINT      VDFM    DAMLEV
     0.034    000.00   0.0E-05       0.0       0.0    .00005   1.0E-09       .80
$ EPSMAX
      .030
*NODE
$...>....1....>....2....>....3....>....4....>....5....>....6....>....7....>....8
$   node               x               y               z      tc      rc
       1    0.000000E+00    0.000000E+00    0.000000E+00       7       7
       2    1.0000000000    0.000000E+00    0.000000E+00       3       7
       3    1.0000000000    1.000000E+00    0.000000E+00       3       7
       4    0.0000000000    1.000000E+00    0.000000E+00       3       7
       5    0.0000000000    0.000000E+00    1.000000E+00       0       7
       6    1.0000000000    0.000000E+00    1.000000E+00       0       7
       7    1.0000000000    1.000000E+00    1.000000E+00       0       7
       8    0.0000000000    1.000000E+00    1.000000E+00       0       7
$$$$  sections
$
```

```
*SECTION_SOLID
$     sid    elform
        1         0
$
$$$$$$$$$ elements solid
*ELEMENT_SOLID
$...>....1....>....2....>....3....>....4....>....5....>....6....>....7....>....8
$   eid      pid      n1      n2      n3      n4      n5      n6      n7      n8
      1        1       1       2       3       4       5       6       7       8
$$$$$$$$$$$$$$$$$$$$$$$$$$$$$$$$$$$$$$$$$$$$$$$$$$$$$$$$$$$$$$$$$$$$$$$$$$$$$$$
$
$$$$ Loading - PRESCRIBED_MOTION_RIGID
$
$$$$$$$$$$$$$$$$$$$$$$$$$$$$$$$$$$$$$$$$$$$$$$$$$$$$$$$$$$$$$$$$$$$$$$$$$$$$$$$
$
*BOUNDARY_PRESCRIBED_MOTION_NODE
$      nid       dof       vad       lcid        sf       vid
         5         3         0          1 1.000E+00
         6         3         0          1 1.000E+00
         7         3         0          1 1.000E+00
         8         3         0          1 1.000E+00
$
*DEFINE_CURVE
$     lcid      sidr      scla       sclo      offa       offo
         1
$           abscissa             ordinate
              0.000            -0.00E-04
             10.0000           -4.94E-04
             25.0000           -4.94E-04
             50.0000           -20.00E-04
            500.00000          -40.00E-04
$$$$$$$$$$$$$$$$$$$$$$$$$$$
$ PRESSURE LOADING ON SIDES
*LOAD_SEGMENT
$...>....1....>....2....>....3....>....4....>....5....>....6....>....7....>....8
         2      0.0       0.0         1         2         6         5
         2      0.0       0.0         2         3         7         6
         2      0.0       0.0         3         4         8         7
         2      0.0       0.0         4         1         5         8
*DEFINE_CURVE
$     lcid      sidr      scla      sclo      offa      offo
         2
$           abscissa            ordinate
              0.000           .000000000
             10.0000          .003450000
            500.00000         .003450000
*END
```

FHWA MATERIAL MODEL INPUT FOR DIRECT SHEAR EXAMPLE

```
$$$$ Input for FHWA soil Units mm, kg, msecs
$
*MAT_FHWA_SOIL
$      mid        ro     NPLOT    SPGRAV    RHOWAT       V_N    GAMMAR    ITERMAX
         1  2.350E-6         3      2.79    1.0E-6       1.1     0000.         10
$        K         G    PHIMAX      AHYP       COH     ECCEN       A_N       E_T
   .003250   .001300       1.1    1.0E-7    6.2E-6       0.7       0.0        0.
$     MCONT      PWD1     PWKSK      PWD2    PHIRES      DINT      VDFM     DAMLEV
     0.034    000.00  0.0E-05       0.0      .001    1.0E-5    6.0E-08     .99000
$ EPSPRMAX
        .8
```

REFERENCES

1. Hallquist, J.O., *LS-DYNA Keyword User's Manual, Version 960*, Livermore Software Technology Corporation, Livermore, CA, March 2001.

2. Reid, J.D., B.A. Coon, B.A. Lewis, S.H. Sutherland, and Y.D. Murray, *Evaluation of LS-DYNA Soil Material Model 147*, Report No. FHWA-HRT-04-094, Federal Highway Administration, November 2004.

3. Murray, Y.D., *Manual for LS-DYNA Wood Material Model 143*, Report No. FHWA-HRT-04-097, Federal Highway Administration, to be published in 2005.

4. Murray, Y.D., and J.D. Reid, *Evaluation of LS-DYNA Wood Material Model 143*, Report No. FHWA-HRT-04-096, Federal Highway Administration, to be published in 2005.

5. Chen, W.F., and G.Y. Baladi, *Soil Plasticity Theory and Implementation*, Elsevier Science LTD, 1985. ISBN 0444424555.

6. U.S. Army Corps of Engineers, Waterways Experiment Station, "DNA Hardened Runway Studies for Crushed Limestone," *User's Guide for Material Properties Database Search and Retrieval Program*, Vicksburg, MS, 1993.

7. Lade, P.V., and J.M. Duncan, "Elastoplastic Stress-Strain Theory for Cohesionless Soil," *Journal of the Geotechnical Engineering Division*, American Society of Civil Engineers, Vol. 101, No. 10, October 1975, pp. 1037-1053.

8. Coon, B.A., J.D. Reid, and J.R. Rohde, "Dynamic Impact Testing of Guardrail Posts Embedded in Soil," Federal Highway Administration, Midwest Roadside Safety Facility, University of Nebraska at Lincoln, TRP-03-77-98, July 21, 1999.

9. Abbo, A.J., and S.W. Sloan, "A Smooth Hyperbolic Approximation to the Mohr-Coulomb Yield Criterion," *Computers and Structures*, Vol. 54, No. 1, 1995.

10. Klisinski, M., *Degradation and Plastic Deformation of Concrete*, Ph.D. Dissertation, Polish Academy of Sciences, 1985, Institute of Fundamental Technology Research (IFTR) Report 38.

11. Holtz, R.D., and W.D. Kovacs, *An Introduction to Geotechnical Engineering*, Prentice Hall, Inc., 1981. ISBN 0134843940.

12. Simo, J.C., and J.W. Ju, “Stress- and Strain-Based Continuum Damage Models, Parts I and II,” *International Journal of Solids and Structures*, Vol. 23, No. 7, 1987.

13. Ju, J.W., “Energy-Based Coupled Elastoplastic Damage Models at Finite Strains,” *Journal of Engineering Mechanics*, Vol. 115, No. 11, November 1989.

14. Coon, B.A., J.D. Reid, and J.R. Rohde, *Dynamic Impact Testing of Guardrail Posts Embedded in Soil,* Federal Highway Administration, Midwest Roadside Safety Facility, University of Nebraska, TRP-03-77-98, July 21, 1999.

15. Murray, Y.D., “Modeling Rate Effects in Rock and Concrete,” *Proceedings of the 8th International Symposium on the Interaction of the Effects of Munitions With Structures*, Defense Special Weapons Agency, McLean, VA, April 1997.

16. Coon, B.A., J.D. Reid, J.R. Rohde, and J. Herr, “A New Shear Strength Testing Device for NCHRP Report 350 Strong Soil,” Paper 01-0412, Annual Meeting of the Transportation Research Board, January 2001.

17. Nayak, G.C., and O.C. Zienkiewicz, “Convenient Form of Stress Invariants for Plasticity,” *Journal of the Structural Division*, American Society of Civil Engineers, Vol. 98, ST4, 1972, pp. 949-953.

18. Lewis, B.A., *Evaluation of LS-DYNA Soil Material Model 147*, Report No. FHWA-HRT-04-094, Federal Highway Administration, August 2004.

19. Chen, Y.F. and D.J. Han, *Plasticity for Structural Engineers,* Springer-Verlag, New York Inc., 1988.

HRDI-04/11-04(1M)E